NSF/ENG-85087
PB87-234308

CALIFORNIA INSTITUTE OF TECHNOLOGY

EARTHQUAKE ENGINEERING RESEARCH LABORATORY

Earthquakes, Natural Hazards
clays, plasticity

A SIMPLE STRAIN-SPACE PLASTICITY MODEL FOR CLAYS

By

Kasivisvanathan Chelvakumar

Report No. EERL 85-05

A Report on Research Conducted under a Grant from the
National Science Foundation and the
Earthquake Research Affiliates Program at the
California Institute of Technology

Pasadena, California

1985

This investigation was sponsored by Grant No. CEE81-19962 from the National Science Foundation under the supervision of W. D. Iwan. Any opinions, findings, conclusions or recommendations expressed in this publication are those of the author and do not necessarily reflect the views of the National Science Foundation.

50272-101

REPORT DOCUMENTATION PAGE	1. REPORT NO. NSF/ENG-85087	2.	3. Recipient's Accession No. PB87 234308/AS
4. Title and Subtitle: Simple Strain-Space Plasticity Model for Clays			5. Report Date: 1985
7. Author(s): K. Chelvakumar			8. Performing Organization Rept. No. EERL 85-05
9. Performing Organization Name and Address: California Institute of Technology, Pasadena, CA 91126			10. Project/Task/Work Unit No.
			11. Contract(C) or Grant(G) No. (C) (G) CEE8119962
12. Sponsoring Organization Name and Address: Directorate for Engineering (ENG), National Science Foundation, 1800 G Street, N.W., Washington, DC 20550			13. Type of Report & Period Covered: PhD Thesis
			14.

15. Supplementary Notes

16. Abstract (Limit: 200 words)

This thesis develops and demonstrates a simple strain-space constitutive model for wet clays. The model is based on the experimentally observed physical behavior of soil. Initially developed for triaxial load systems, its predictions are tested against other model predictions and experimental data. The model is then generalized, rendering it capable of handling general stress-strain states and finite deformations. The generalized model is used to solve an idealization of a practical problem and the solution predicted by the strain-space model is compared with other model predictions and test results.

17. Document Analysis a. Descriptors

Earthquakes
Deformation
Plastic properties
Mathematical models
Clays
Strains
Loads (forces)

b. Identifiers/Open-Ended Terms

c. COSATI Field/Group

18. Availability Statement: NTIS	19. Security Class (This Report)	21. No. of Pages: 209
	20. Security Class (This Page)	22. Price

(See ANSI-Z39.18) See Instructions on Reverse OPTIONAL FORM 272 (4-77) (Formerly NTIS-35) Department of Commerce

A SIMPLE STRAIN-SPACE PLASTICITY MODEL FOR CLAYS

Thesis by

Kasivisvanathan Chelvakumar

In Partial Fulfillment of the Requirements
for the Degree of
Doctor of Philosophy

California Institute of Technology
Pasadena, California

1985

(Submitted December 5, 1984)

ACKNOWLEDGMENTS

I sincerely extend my thanks and gratitude to my advisor, Professor W. D. Iwan, for his most valuable advice during the course of this study. If not for his encouragement, understanding, availability, friendship and unwavering support, I may never have produced this thesis. I am also thankful to Professor R. F. Scott for his expert advice and for the several useful discussions we had.

This investigation was supported by the National Science Foundation, Earthquake Hazard Mitigation Program under Grant No. CEE-81-19962, whose financial support is hereby gratefully acknowledged. The financial support through the teaching and research assistantships as well as the tuition scholarships provided by the California Institute of Technology are also gratefully acknowledged.

Special thanks are due to Mrs. Gloria Jackson and Mrs. Sharon Beckenbach for their skillful typing of the manuscript and their cheerful cooperation throughout the typing, and to Miss Cecilia Lin for providing life to the illustrations. Thanks are also due to all those friends who made my life so full and happy by their warm friendships and to my colleagues at California Institute of Technology for their pleasant company.

Finally, I wish to dedicate this thesis to my ammah and appah, who always gave me their best, to my wife Latha, who stood by me through all the troubles and tribulations of my graduate study and gave me the joys

of my life, Gayathri and Meenadchi, and to my advisor Professor Iwan, who made my study so enjoyable.

ABSTRACT

This thesis develops and demonstrates a simple strain-space constitutive model for wet clays. It has been seen that a strain-space formulation of the constitutive behavior of engineering materials facilitates the solution of boundary value problems involving these materials. Soil, because of its multi-phase granular constitution poses challenging problems in constitutive modeling. Although several stress-space plasticity models exist for soils, they are not used commonly in engineering practice due to their complexity. It is attempted herein to develop and test a simple model which could result in simplified solutions for some soil problems.

The model is based on the experimentally observed physical behavior of soil. Certain approaches alien to conventional plasticity are employed so that the material behavior is closely predicted without sacrificing the simplicity of the model.

The model is initially developed for triaxial load systems. Its predictions are then tested against other model predictions and experimental data. The model is then generalized. The generalization renders the model capable of handling general stress-strain states and finite deformations.

Finally, the generalized model is used to solve an idealization of a practical problem. The problem of a pile driven into a soil medium is idealized as an expanding cavity in a homogeneous infinite medium. The

solution predicted by the strain-space model is compared with other model predictions and test results.

TABLE OF CONTENTS

PAGE

ACKNOWLEDGMENTS ii

ABSTRACT iv

CHAPTER I: INTRODUCTION 1

1.1 MOTIVATION 1

1.2 PAST WORK 4

1.2.1 Strain-Space Plasticity 4
1.2.2 Soil Plasticity 6

1.3 OUTLINE OF PRESENT WORK 7

CHAPTER II: SOME FUNDAMENTAL CONSIDERATIONS IN SOIL MODELING . . 10

2.1 INTRODUCTION 10

2.2 REVIEW OF MODELS BASED ON CRITICAL STATE CONCEPT 11

2.2.1 Background 11
2.2.2 Definition of Basic Variables 13
2.2.3 Fundamental Physical Concepts 17
2.2.4 The Development of Stress-Space Constitutive Equations 24
2.2.5 Summary of the Constitutive Equations for the Elliptic Yield Surface Model. 28

2.3 STRAIN-SPACE IMPLICATIONS OF CRITICAL STATE MODELS 30

2.3.1 Isotropic Behavior 30
2.3.2 Critical State Behavior 31
2.3.3 General Behavior 35
2.3.4 Loading Surface in Strain-Space 37

2.4 SUMMARY 39

TABLE OF CONTENTS (CONTINUED)

PAGE

CHAPTER III: DEVELOPMENT OF THE MODEL 40

3.1 INTRODUCTION 40

3.2 BASIC CONCEPTS 41

3.2.1 A New Approach to Constitutive Modeling of Soils . . 41
3.2.2 Over Compression Ratio 47

3.3 DEVELOPMENT OF THE MODEL 49

3.3.1 Undrained Behavior 49
3.3.2 General Monotonic Loading 54
3.3.3 Load Reversals 56

3.4 MODEL EQUATIONS 61

3.5 SUMMARY AND CONCLUSIONS 62

CHAPTER IV: MODEL CALIBRATION AND PREDICTIONS 65

4.1 INTRODUCTION 65

4.2 EXPERIMENTAL DATA 65

4.2.1 Cambridge Test Data 65
4.2.2 Grenoble Test Data 66

4.3 UNDRAINED TRIAXIAL TESTS 69

4.3.1 Model Equations 69
4.3.2 Model Calibration Using Cambridge Test Data 71
4.3.3 Comparison with Grenoble Test Data 77
4.3.4 Model Constants 80

4.4 CONSTANT PRESSURE TRIAXIAL TESTS 80

4.4.1 Model Equations 80
4.4.2 Comparison with Cambridge Test Data 83

4.5 CYCLIC LOADING TESTS 87

4.5.1 Model Equations 88
4.5.2 Comparison with Cambridge Test Data 89

TABLE OF CONTENTS (CONTINUED)

PAGE

4.5.3 Comparison with Grenoble Test Data 91
4.5.4 Comparison with Other Models 96
4.5.5 Comparison for Cyclic Loading Between Constant Stress Limits 103

4.6 SUMMARY AND CONCLUSIONS 109

CHAPTER V: GENERALIZATION OF THE INFINITESIMAL STRAIN AXISYMMETRIC MODEL 112

5.1 INTRODUCTION 112

5.2 DEFINITION OF THE BASIC VARIABLES 113

5.2.1 Deformation and Strain During a General Admissible Motion 113
5.2.2 Traction and Stress 116
5.2.3 The Existence and Coincidence of the Principal Frames of the Stress and Strain Tensors 120
5.2.4 Effective Stresses 123
5.2.5 Stress and Strain Variables 128

5.3 THREE-DIMENSIONAL CONSTITUTIVE MODELING 130

5.3.1 Basic Assumptions 130
5.3.2 Implications of the Basic Assumptions 132
5.3.3 The Loading Surface 133

5.4 SUMMARY 134

CHAPTER VI: APPLICATION OF THE MODEL TO THE EXPANSION OF A CYLINDRICAL CAVITY 137

6.1 INTRODUCTION 137

6.2 MATHEMATICAL MODELING 138

6.2.1 Deformation and Strain 138
6.2.2 Stress and Equilibrium 141
6.2.3 Simplifying Assumptions 144
6.2.4 Formulation Associated with the Rapid Expansion . . . 146

TABLE OF CONTENTS (CONCLUDED)

PAGE

6.3 THE SOLUTION 150

6.3.1 Numerical Implementation 150
6.3.2 Model Predictions 155

6.4 COMPARISON WITH OTHER RESULTS 164

6.4.1 Experimental Results 164
6.4.2 Ladanyi's Calculations 166
6.4.3 Predictions of a Rate Type Model 170
6.4.4 Elastic Solution 173

6.5 SUMMARY AND CONCLUSIONS 173

CHAPTER VII: SUMMARY AND CONCLUSIONS 177

REFERENCES 182

BIBLIOGRAPHY 186

CHAPTER I

INTRODUCTION

1.1 MOTIVATION

The term engineering is defined in Webster's dictionary as "the application of science and mathematics by which the properties of matter and sources of energy in nature are made useful to man in structures, machines, products, systems and processes." One of the properties of matter, specifically that of solids, that is of great relevance to this study is its constitutive behavior. In designing and constructing engineering systems it is necessary to understand their mechanical behavior. In order to understand mechanical behavior, it is necessary to know the local and global relationships between forces and displacements. From past work in engineering mechanics it has been established that it is more appropriate to relate stresses and strains for solids rather than forces and displacements. The stress-strain relationships define the constitutive behavior of the solid.

The purpose of developing constitutive equations for engineering materials is to aid the study of the mechanical behavior of systems made up of these materials. Therefore, before developing the constitutive models it is useful to understand their role in such studies. In order to achieve such an understanding it is helpful to consider the common equations governing the mechanical behavior of solids.

The equation describing the evolution of the deformation of a solid may be written as

$$\operatorname{div}_{\underset{\sim}{y}}[\underset{\sim}{\sigma}(\underset{\sim}{x},t)] + \underset{\sim}{b} = \rho \frac{\partial^2 \underset{\sim}{u}(\underset{\sim}{x},t)}{\partial t^2} \tag{1.1}$$

where,

$\underset{\sim}{x}$ is the coordinate vector of an element of the solid in the reference state,

$\underset{\sim}{y}$ is the coordinate vector of an element of solid in any general deformed state,

$\underset{\sim}{\sigma}(\underset{\sim}{x},t)$ is the Cauchy stress tensor corresponding to a particle at $\underset{\sim}{x}, t$,

$\underset{\sim}{b}$ is the body force per unit volume acting on the particle,

ρ is the local density of the element in the deformed state,

$\underset{\sim}{u}$ is the displacement vector describing the relative displacement of the particle from its reference position, and

t is time.

Equation (1.1) must be solved along with a set of initial and/or boundary conditions which may be expressed in the form

$$f_c(\underset{\sim}{u},\underset{\sim}{\sigma},\underset{\sim}{x},t) = 0 \tag{1.2}$$

In order to solve equation (1.1), it is necessary to know the relationship between $\underset{\sim}{\sigma}$ and $\underset{\sim}{u}$. As mentioned previously, it is known that $\underset{\sim}{\sigma}$ can be related to the strain tensor $\underset{\sim}{\varepsilon}$ more readily than to $\underset{\sim}{u}$. The

strain tensor $\underline{\varepsilon}$ is then related to $\underline{u}$, by the strain displacement equations

$$\underline{\varepsilon} = \underline{\varepsilon}(\underline{u}) \quad . \tag{1.3}$$

It is clear at this stage that the constitutive equation can be in one of the following forms:

$$\underline{\sigma} = \underline{\sigma}(\underline{\varepsilon}, \underline{M}^{\varepsilon}) \tag{1.4}$$

or,

$$\underline{\varepsilon} = \underline{\varepsilon}(\underline{\sigma}, \underline{M}^{\sigma}) \tag{1.5}$$

where $\underline{M}^{\varepsilon}$ and $\underline{M}^{\sigma}$ are vectors which may contain memory variables. If equation (1.4) is used to relate the stress and strain tensors, $\underline{\sigma}$ can be obtained as a function of $\underline{u}$ as follows:

$$\underline{\sigma} = \underline{\sigma}[\underline{\varepsilon}(\underline{u}), \underline{M}^{\varepsilon}] \quad .$$

However, if the relationship is expressed by equation (1.5), then to express $\underline{\sigma}$ as a function of $\underline{u}$ or $\underline{u}$ as a function of $\underline{\sigma}$, an inversion is necessary. That is,

$$\underline{\sigma} = \underline{\varepsilon}^{-1}(\underline{\sigma}, \underline{M}^{\sigma}) \quad \text{and} \quad \underline{\varepsilon} = \underline{\varepsilon}(\underline{u})$$

or,

$$\underline{u} = \underline{\varepsilon}^{-1}(\underline{u}) \quad \text{and} \quad \underline{\varepsilon} = \underline{\varepsilon}(\underline{\sigma}, \underline{M}^{\sigma}) \quad .$$

Both the constitutive equation (1.5) and the strain displacement equation (1.3) are very complex for general cases and hence make inversion very difficult if not impossible. There are many cases for which an analytic inversion is not possible, and it is therefore necessary to resort to numerical inversion.

From the outline presented hereto, it is evident that the constitutive equations formulated in the form described by equation (1.4) are preferable in comparison to their alternative described by equation (1.5). The constitutive equations given by equation (1.4) are termed strain-space constitutive equations since the independent variable is strain. Similarly, equations of the form given by equation (1.5) are termed stress-space constitutive equations. Traditionally, constitutive equations modeling soil plasticity are in stress-space, which makes the solution process complicated. For this reason, it is attempted herein to develop a strain-space constitutive model for clays.

1.2 PAST WORK

1.2.1 Strain-Space Plasticity

Many of the recent advances in strain-space plasticity can be traced to work done by Naghdi, Trapp and Casey on the one hand and Iwan and Yoder on the other. Naghdi and Trapp (1975) described the significance of a strain-space plasticity theory and proposed a model in strain-space. Subsequently Casey and Naghdi (1981) developed this concept. Also Yoder (1981) and Yoder and Iwan (1981) developed a

strain-space plasticity model exploiting the similarities between the stress-space and the strain-space formulations. Although the work done by the two groups show some minor differences, the basic concepts behind the models are similar. In a recent paper, Mroz and Norris (1982) have also looked into the strain-space formulations of plasticity.

Some of the advantages found to arise from the strain-space formulation are:

1) In the case of the stress-space formulation of strain softening materials, the loading conditions must be defined separately for the stable and the unstable regions, whereas in the strain-space formulation a single loading condition is sufficient. Although strain softening produces unstable behavior, such instabilities are only local. In some recent work done by Abeyaratne and Knowles in nonlinear elasticity, it has been shown that global stability can be obtained even while local instabilities exist. Hence the unstable case is certainly one of interest.

2) In the case of multiple yield surface models in stress-space plasticity, the surfaces are not allowed to intersect. Intersection is excluded based on the argument that such intersections destroy the uniqueness of the solution. But it can be shown (Yoder, 1981) that the lack of uniqueness arises purely because the formulation is performed in stress-space.

In the strain-space formulation, unique solutions may be obtained for intersecting yield surfaces.

1.2.2 Soil Plasticity

Soils must be modeled as distinctively different from metals. The reason for such treatment stems from the following observations made on soils.

i) Volume preserving deformations produce hydrostatic stresses.

ii) Pure volume changes produce shear stresses.

iii) There is plastic behavior under both shear and isotropic loadings.

iv) No significant elastic region is observed.

Plasticity theory was basically developed for metals. The mechanics of soil was carried out as an art until about 1925. Terzaghi, based on his knowledge of the heat flow theory and the experience he obtained from consolidation tests on clay, published the mathematical theory of consolidation (Terzaghi, 1923). This is considered by many as a landmark in soil mechanics (Glossop, 1968). From 1925 onwards, simple problems in soils were solved using simple solid mechanics. The solutions were often borrowed from elasticity theory.

Based on the experiments performed at Cambridge University, Roscoe, Schofield and Wroth (1958) published their findings on the existence of a critical void ratio. From these findings and the subsequent work done by Roscoe, Schofield, Wroth, Poorooshasb and Thurairajah (Roscoe, et

al., 1958, 1963a, 1963b) , Roscoe, et al. (1968) published an elasto-plastic constitutive model for soils. Also in this paper, the Cambridge constitutive model was presented within the conventional framework of plasticity.

There are other models used to predict soil behavior. These evolved basically from metal plasticity ideas. Dafalias (1976), Dafalias and Herrmann (1980, 1982) developed a model based on the concept of a bounding surface, while Prevost (1978) adapted a metal plasticity model to soils. However, all the models used to describe soil behavior are formulated in the stress-space.

Despite all these constitutive models available for soil problems, most practicing engineers still use linear elastic solutions, the reason being attributed to the complexity of the more sophisticated constitutive models.

1.3 OUTLINE OF PRESENT WORK

The main purpose of this work is to develop a constitutive model for wet clays which is simple enough to be used by practicing engineers. For this purpose, the physical behavior of clay is studied from past experimental observations. The Cambridge elliptic yield surface model is considered as a guideline for two reasons. First, the model has a minimum number of constants and secondly the model is developed based on experimental observations of soil behavior. In Chapter II the elliptic yield surface model is briefly outlined. From the fundamental concepts

used in the development of the elliptic model, certain deductions of the soil behavior are made in strain-space.

Using the strain-space implications of soil behavior a simple constitutive model is developed in Chapter III. The model is limited at this stage to triaxial stress-strain systems. The model is developed starting from a simple undrained monotonic loading situation. It is progressively generalized to handle all triaxial loadings including load reversals. The model is developed through these stages without losing its simplicity.

The axisymmetric model thus developed is applied to some triaxial tests with and without load reversals. The model predictions are presented in Chapter IV and are compared there with the predictions of the elliptic yield surface model and some experimental data.

Having established the validity of the axisymmetric model, it is then extended to general three-dimensional stress-strain states with finite deformations. The stress and strain tensors are defined formally for general admissible motions. The question of the existence and coincidence of the principal frames of the stress and strain tensors is also addressed in detail in Chapter V.

The generalized model is applied to the problem of an expanding cylindrical cavity in an infinite medium. The solution of the strain-space model is compared with other predictions and some experimental results obtained from pile tests. The strain-space prediction is also

compared with the linear elastic solution for small deformations. These results and comparisons are presented in Chapter VI.

Finally, certain conclusions regarding the strain-space model are summarized in Chapter VII.

CHAPTER II

SOME FUNDAMENTAL CONSIDERATIONS IN SOIL MODELING

2.1 INTRODUCTION

Several constitutive models have been developed to study the behavior of soils in the past two to three decades. They include (i) single yield surface models (Roscoe, et al., 1958, Burland 1965, 1967, DiMaggio and Sandler 1971, Lade 1975, 1977, Pender 1978), (ii) multiple yield surface models (Mroz 1982, Prevost 1978), (iii) bounding surface models (Dafalias and Herrmann 1980), (iv) endochronic models (Valanis and Read 1982), and (v) other models (Davis and Mullenger 1978). Of these models, the single yield surface models developed by Roscoe, et al., and Burland based on critical state theory have the least number of model parameters. These models are chosen to be reviewed in this section. Based on the fundamental concepts used in these models, a constitutive model will be developed using strains instead of stresses as the independent variables. These models, thus chosen as guides, will require only a few parameters for the strain-space formulation. Since such a strain-space formulation is new, having fewer model parameters enhances the understanding of the formulation.

In section 2.2 soil models developed using the critical state concept are reviewed. The development of these models in stress-space is briefly outlined. The purpose of this section is to study the basic concepts used in these stress-space constitutive models so as to develop

the foundation for strain-space constitutive modeling of soils. Section 2.3 lays out the implications of these concepts in strain-space. Some basic equations and properties necessary for the development of the strain-space model are deduced in this section.

2.2 REVIEW OF MODELS BASED ON CRITICAL STATE CONCEPT

2.2.1 Background

The critical state concept was developed at Cambridge University during the late 1950's. Roscoe, Schofield and Wroth (1958) postulated the existence of a critical voids ratio line and verified this postulate by means of test results on Weald clay. They also found confirmation for their concepts in tests performed on silt and sand. Although the critical state concept and its experimental confirmation were debated at the time it was proposed, the concept is now well accepted as being capable of predicting the behavior of clay. Subsequent tests on Kaolin and London clay further reinforced the validity of the critical state concept.

Based on the critical state concept and few other basic concepts on soils, Roscoe, Schofield and Thurairajah developed a constitutive model (Roscoe, et al., 1963). One of the basic assumptions used to determine the shape of the yield surface was based on incremental dissipative energy. Roscoe, et al., assumed that the incremental energy dissipated per unit volume of soil during a general incremental load would be the same as the incremental dissipative shear energy at a corresponding

critical state. This assumption is explained in greater detail in section 2.2.4. The model so developed was subsequently termed the Cam-Clay model and will be thus referred herein.

The Cam-Clay model enabled the solution of simple boundary value problems of soils. However, the non-uniqueness of the normal to the yield surface at the hydrostatic axis led to considerable controversy.

Subsequently, Roscoe and Burland (1968) suggested a different form for the incremental dissipative energy. He assumed that the incremental dissipative energy during a general incremental deformation is same as the square root of the sum of squares of the incremental dissipative energy considered in the Cam-Clay model and the incremental dissipative energy due to purely isotropic deformation. This assumption is further explained in section 2.2.4. The yield surface thus deduced was of elliptic shape and this model will hereto be referred to as the elliptic yield surface model.

The elliptic yield surface model has a unique normal everywhere in the axisymmetric stress-space. It also predicts triaxial results more closely than the Cam-Clay model. But there are several possible assumptions that can be made about the incremental dissipative energy. Each of these assumptions would lead to a different yield surface. Only by checking with experimental observations can it be determined which of these are more suited for soils.

2.2.2 Definition of Basic Variables

In this section the basic stress and strain variables are defined. Using a series of simplifying assumptions described below, the number of such basic variables is reduced from twelve to four. These simplifying assumptions are based on the stress and strain states encountered during common triaxial soil tests, and some postulates on the form of constitutive equations.

Since most tests are done under triaxial load-deformation conditions, it is first assumed that the stress and strain tensors correspond to triaxial states of stress and deformation. Both the Cam-Clay and elliptic yield surface models were developed initially for this simple case. However, the constitutive equations are then generalized to relate a general stress state to a general strain state.

The second assumption is that there exist principal frames for the stress and strain tensors, and that these frames coincide. The existence can be proved for stress and strain tensors defined to be symmetric. The coincidence assumption is motivated by the conventional constitutive laws. In metal plasticity the components of the incremental plastic strain tensor are defined to be proportional to the gradient of a scalar valued function with respect to the corresponding components of the stress tensor. This can be stated as

$$d\varepsilon^{p}_{ij} \propto \frac{\partial g}{\partial \sigma_{ij}} \qquad (2.1)$$

where $d\varepsilon^{p}_{ij}$ and σ_{ij} are the components of the incremental plastic strain tensor and the stress tensor, respectively, in any one given frame. The scalar function g, defined as the plastic potential function may or may not coincide with the scalar function f which specifies the yield surface. However, it is common in plasticity to define the function g as a function of the stress invariants rather than a function of the components of the stress tensor in a particular frame. This can be written as

$$g = g(I_1(\underline{\sigma}), I_2(\underline{\sigma}), I_3(\underline{\sigma})) \tag{2.2}$$

where $I_1(\underline{\sigma})$, $I_2(\underline{\sigma})$ and $I_3(\underline{\sigma})$ are the three invariants of the stress tensor. It can be shown that if the frame is chosen to be the principal frame of the stress tensor, then, the components of the plastic incremental strain tensor in that frame would form a diagonal matrix. This observation motivates the assumption that the principal frames of the stress and strain tensors coincide.

Finally, it is assumed that one of the principal axes coincides with the axis of symmetry.

Under these assumptions, the components of the stress tensor in the principal frame e' can be written as

$$(\underline{\sigma})^{e'} = \begin{pmatrix} \sigma_I & 0 & 0 \\ 0 & \sigma_{II} & 0 \\ 0 & 0 & \sigma_{III} \end{pmatrix} \tag{2.3}$$

Let $\underline{e}'_I$ coincide with the axis of symmetry. Then, $\sigma_{II} = \sigma_{III}$. As in all soil theories, the compressive stresses are taken to be positive.

Since soils are three-phase media with sand grains and pore fluid, the stress at any region of the material is induced by

i) the stress on the solid lattice, and

ii) the pore fluid pressure.

This observation motivates a decomposition of the stress tensor. The total stress tensor is decomposed into an 'effective stress tensor' and a pore pressure as

$$\underline{\sigma} = \underline{\sigma}' + p_f \underline{1} \tag{2.4}$$

where $\underline{\sigma}$ total stress tensor

$\underline{\sigma}'$ effective stress tensor (stress on solids)

p_f pore fluid pressure.

It has been verified that constitutive equations relating the effective stress to soil deformation predict soil behavior more accurately than those using the total stress. Hence, only the effective stresses will be used herein.

Let the first invariant of the effective stress tensor be termed the effective pressure and be denoted by p. Then

$$p = \frac{1}{3} (\sigma_I' + 2\sigma_{II}') \quad . \tag{2.5}$$

Let a measure of shear stress be denoted by q and defined as

$$q = (\sigma_I' - \sigma_{II}') \quad . \tag{2.6}$$

Any symmetric stress state with one of the principal axes coinciding with the axis of symmetry can thus be completely described by the variables p and q. The two-dimensional space defined by the variables p and q will be referred to as the 'Cambridge stress space.'

By the assumptions made in this section, it is implied that the strain tensor is also axisymmetric and $\underline{\varepsilon}'_I$ coincides with the axis of symmetry. This results in the principal components of the strain tensor being given by

$$(\underline{\varepsilon})^{e'} = \begin{pmatrix} \varepsilon_I & 0 & 0 \\ 0 & \varepsilon_{II} & 0 \\ 0 & 0 & \varepsilon_{III} \end{pmatrix} \tag{2.7}$$

where

$$\varepsilon_{II} = \varepsilon_{III} \quad .$$

Let the incremental volumetric and shear strains be denoted by δv and $\delta\varepsilon$. These variables are defined in terms of the incremental principal components of $\underline{\varepsilon}$ as

$$\delta v = \delta\varepsilon_I + 2\delta\varepsilon_{II} \quad ; \quad \delta\varepsilon = \frac{2}{3}(\delta\varepsilon_I - \delta\varepsilon_{II}) \quad . \tag{2.8}$$

The sign convention used for strains is such that the compressive strains are taken to be positive.

The void ratio e is defined as the ratio of the volume of voids in the soil to the volume of solid particles in the soil. Further, the solid soil particles are assumed to be incompressible. If V and δV denote the total volume of soil and its corresponding increment, then

$$V = V_s(1 + e) \quad , \tag{2.9}$$

where V_s is the volume of the solid components. It follows from equation (2.9) and the definition of δv that

$$\delta v = -\frac{\delta V}{V} = -\frac{\delta e}{1+e} \quad . \tag{2.10}$$

The ratio of effective shear stress to effective pressure is customarily denoted by η

$$\eta = q/p \quad . \tag{2.11}$$

The incremental strain variables δv and $\delta \varepsilon$ are assumed to linearly decompose into recoverable and plastic components according to the form

$$\begin{aligned} \delta v &= \delta v^r + \delta v^p \\ \delta \varepsilon &= \delta \varepsilon^r + \delta \varepsilon^p \end{aligned} \quad . \tag{2.12}$$

2.2.3 Fundamental Physical Concepts

The Cam-Clay model and the elliptic yield surface model are developed based upon four fundamental physical concepts related to soils.

i) Normal consolidation and elastic swelling.

ii) The critical state concept.

iii) The boundary surface concept.

iv) Zero elastic shear strains.

i) The behavior of soils during isotropic consolidation is as shown in Figure (2.1a). The plastic compressive loading is termed as 'normal consolidation' and will be referred to by that phrase herein. When the material is allowed to expand or swell, the path it takes is referred to as 'elastic swelling.' The word elastic is used because the forward and reverse paths are very close together and hence can be treated as one.

Terzaghi observed that both the normal consolidation and the swelling lines can be well modeled by logarithmic relationships. He proposed that for normal consolidation,

$$\hat{e} = e_r - \lambda \log_e(\hat{p}/p_r) \tag{2.13}$$

and for elastic swelling

$$e = e_r - \lambda \log_e(\hat{p}/p_r) - \kappa \log_e(p/\hat{p}) \quad . \tag{2.14}$$

The hat and the suffix r denote the values of the corresponding variables along the normal consolidation line and at reference state, respectively. This idealized relationship is shown in Figure (2.1b).

ii) The critical state concept proposed by Roscoe, Schofield and Wroth was motivated by the following observations:

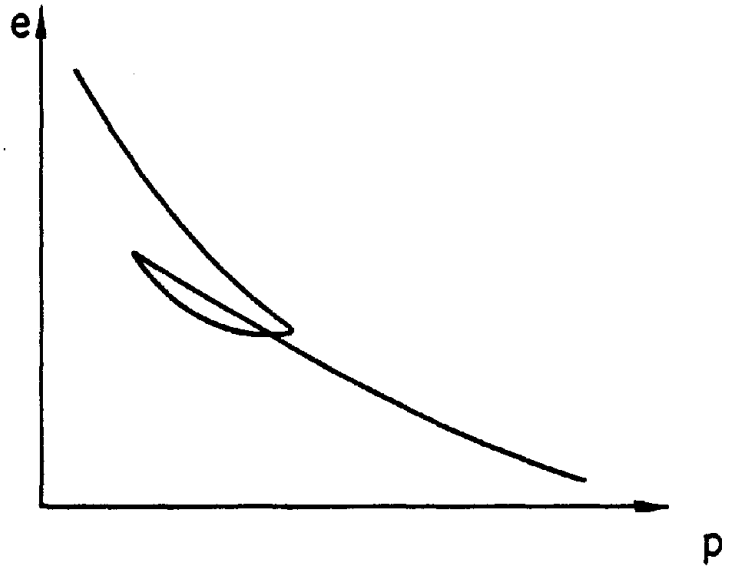

(a) ACTUAL

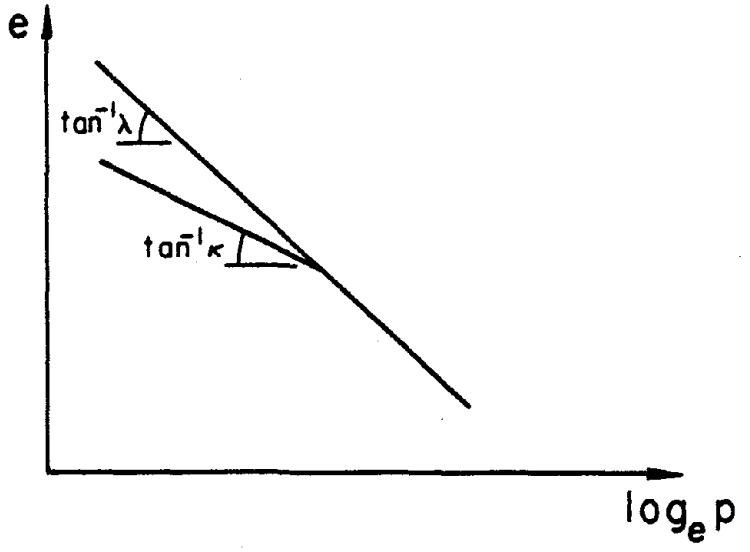

(b) IDEALIZED

FIGURE 2.1 SOIL BEHAVIOR UNDER ISOTROPIC LOADING

a) Soil is a granular medium exhibiting sticking and tearing at the solid-solid contacts. Thus, its behavior would resemble that of a friction material. This would mean that when the effective shear stress to effective pressure ratio, η, reaches a particular value the material would undergo internal slipping. Such internal slipping will produce an overall flow behavior. This state where the soil sample continuously deforms as a frictional material while p, q and e remain constant is defined as the critical state. This implies that at critical state

$$q = M p \tag{2.15}$$

where M, the critical state constant, is analogous to the frictional constant.

b) All soils are three-phase mixtures of solid and pore fluid. As the void ratio increases, the ratio of pore fluid to solids increases as well. At large void ratios it is thus possible for the mixture to behave more like a fluid. It was postulated by Roscoe, et al. (1958) that there exists a finite value of void ratio, depending upon the pressure, at which the material begins to flow as a frictional fluid. From experiments performed on Weald clay, London clay and Kaolin at Cambridge University, it was found that the relationship between the critical void ratio and critical pressure can be given by

$$e_c = e_{rc} - \lambda \log_e(p_c/p_{rc}) \tag{2.16}$$

where the suffices c and rc indicate the values of the corresponding variables at the critical state and at a reference critical state, respectively.

It should be noted here that the projection of the critical state line on the $\log_e p$-e plane is parallel to the normal consolidation line. Figures (2.2a) and (2.2b) show the projections of the critical state line on the p-q and $\log_e p$-e planes, respectively.

iii) Roscoe, et al. (1958), motivated by Hvorslev's (1937) work on shear stress at failure, plotted in p, q, e space, all the states reached by normally consolidated saturated remoulded clay under a very broad range of loading. They found a limiting surface within which lay all these states. This surface was hence termed the 'state boundary surface.' All states plotted lay either on or within the state boundary surface. Thus, this surface defines the limit of the states that can be realized by the clay. A portion of this surface is shown in Figure (2.3). The intersection of this limiting surface with the p-e plane satisfies Terzaghi's equation (2.13).

iv) Finally, it is assumed in both the Cam-Clay and elliptic yield surface models that there are no recoverable shear strains. However, the models assume that recoverable shear stresses exist. These assumptions imply that the material is rigid-plastic in shear. Roscoe and Burland (1968) propose a method of predicting plastic shear strains for load paths within the yield surface, thereby producing plastic shear

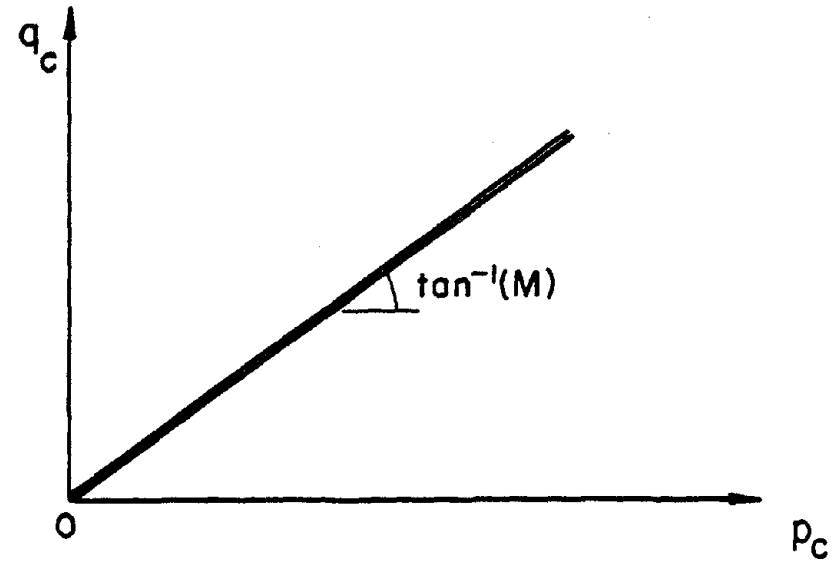

(a) ON p − q PLANE

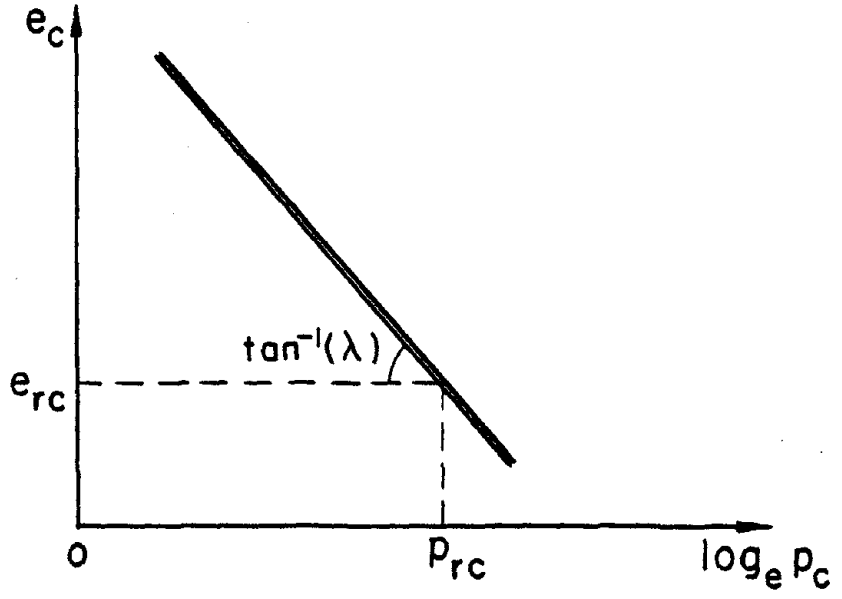

(b) ON $\log_e p - e$ PLANE

FIGURE 2.2 PROJECTIONS OF THE CRITICAL STATE CURVE

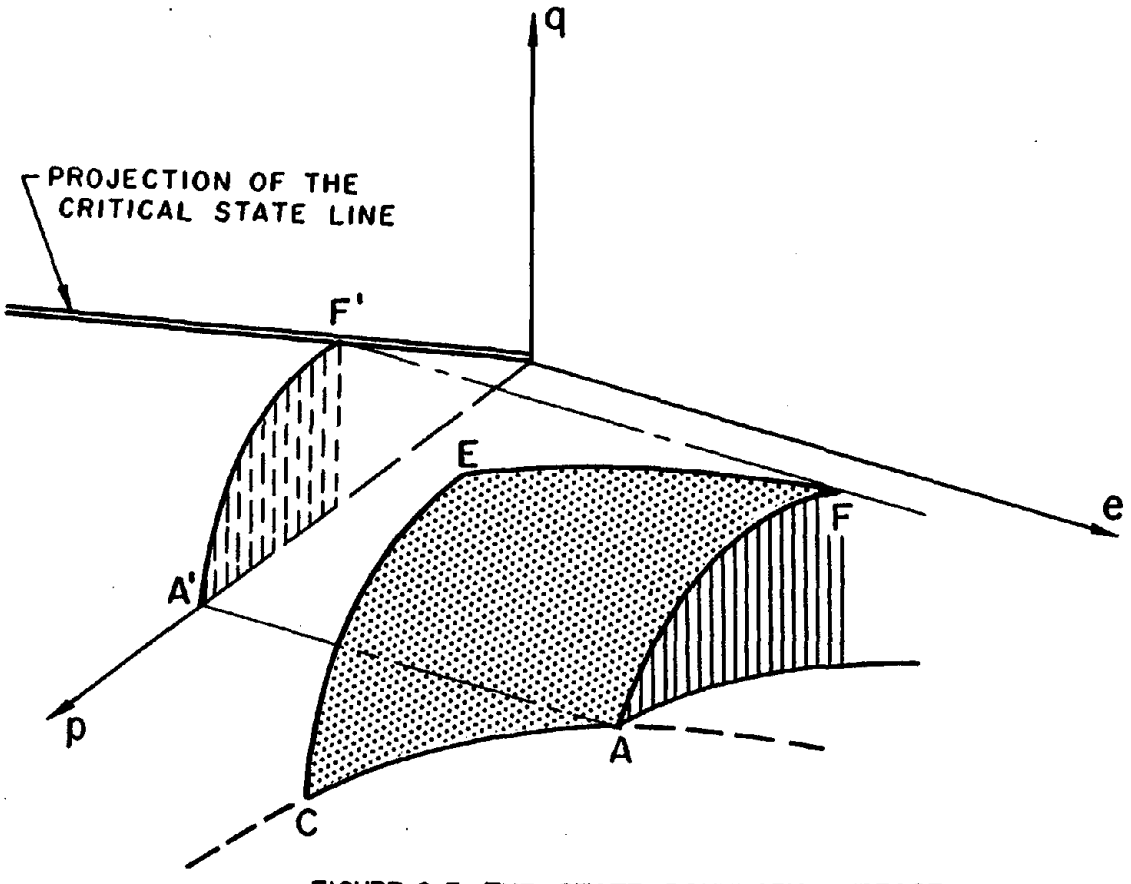

FIGURE 2.3 THE STATE BOUNDARY SURFACE

strains for shear stresses less than the corresponding yield value. But this method does not follow directly from the model, and is rather involved.

2.2.4 The Development of Stress-Space Constitutive Equations

From Terzaghi's equations (2.13) and (2.14) and void ratio-volumetric strain equation (2.10), the recoverable and plastic incremental volumetric strains can be given as

$$\delta v^r = \frac{K}{1+e} \frac{\delta p}{p}$$

and,

$$\delta v^p = \frac{\lambda - K}{1+e} \frac{\delta \hat{p}}{\hat{p}} \quad . \tag{2.17}$$

The ratio of incremental plastic volumetric strain to incremental plastic shear strain is denoted by the variable φ. From the assumption of zero recoverable shear strain and the definition of φ it follows that,

$$\delta \varepsilon^r = 0$$

and,

$$\delta \varepsilon^p = \frac{1}{\varphi} \frac{\lambda - K}{1+e} \frac{\delta \hat{p}}{\hat{p}} \quad . \tag{2.18}$$

The yield surface, described by the scalar function f, is dependent on p, q and $\hat{p}$. This dependence is implied by the boundary surface concept. Hence, f can be written as

$$f = f(p, q, \hat{p}) \tag{2.19}$$

Consistency implies that,

$$\delta f = \frac{\partial f}{\partial p}\delta p + \frac{\partial f}{\partial q}\delta q + \frac{\partial f}{\partial \hat{p}}\delta \hat{p} = 0 \quad . \tag{2.20}$$

Assuming associative flow

$$\frac{\frac{\partial f}{\partial p}}{\frac{\partial f}{\partial q}} = \frac{\delta v^p}{\delta \varepsilon^p} \quad . \tag{2.21}$$

From the definition of the variables φ and η and equations (2.20) and (2.21) it follows that

$$\frac{\delta \hat{p}}{\hat{p}} = \frac{\delta p}{p} + \frac{\delta \eta}{\varphi + \eta} \quad . \tag{2.22}$$

Since φ denotes, by the associative flow rule, the slope of the yield surface, the determination of φ determines the yield function f. Both the Cam-Clay model and the elliptic yield surface model assume that φ is a function of η. The functional form of φ is determined in both models from energy arguments. This derivation will be briefly outlined below, first for the Cam-Clay model and then for the elliptic yield surface model.

During the incremental deformation of a soil continuum, the energy transferred to a unit volume of the soil lattice by the forces acting on the continuum can be given by

$$\delta E' = \mathrm{Tr}(\underline{\sigma}'\delta\underline{\varepsilon}^T) \quad . \tag{2.23}$$

For a triaxial load deformation system, equation (2.23) can be re-written in terms of the components in the principal frame as

$$\delta E' = \sigma'_I\delta\varepsilon_I + 2\sigma'_{II}\delta\varepsilon_{II} \quad . \tag{2.24}$$

In terms of the variables used herein, $\delta E'$ can be expressed as

$$\delta E' = p\delta v + q\delta\varepsilon \quad . \tag{2.25}$$

Further, the incremental energy $\delta E'$ is decomposed into recoverable and dissipated incremental energies, denoted by δU and δW, respectively.

$$\delta E' = \delta U + \delta W \tag{2.26}$$

The recoverable energy can be given by

$$\delta U = p\delta v^r + q\delta\varepsilon^r \tag{2.27}$$

and the dissipated incremental energy by

$$\delta W = p\delta v^p + q\delta\varepsilon^p \quad . \tag{2.28}$$

Both the Cam-Clay and elliptic yield surface models assume certain properties of δW and use them to derive the function ψ.

The Cam-Clay model assumes that the incremental dissipative energy for a general increment is the same as the total shear energy transferred at the critical state having the same shear stress. This assumption leads to

$$\delta W = M p \delta\varepsilon \quad . \tag{2.29}$$

Equation (2.29) results in a φ given by

$$\varphi = M - \eta \tag{2.30}$$

which in turn corresponds to a yield surface described by

$$q - M p \log_e (\hat{p}/p) = f(p,q,\hat{p}) = 0 \quad . \tag{2.31}$$

Roscoe and Burland (1968) proposed that the incremental dissipative energy during a general incremental load can be given by the square root of the sum of squares of the incremental energy at the critical state used in Cam-Clay theory and the incremental dissipative energy due to the isotropic deformation. This assumption led to

$$\delta W = p \sqrt{(\delta v^p)^2 + M^2 (\delta\varepsilon^p)^2} \quad . \tag{2.32}$$

Equation (2.32) results in a φ and corresponding yield surface given by,

$$\varphi = \frac{M^2 - \eta^2}{2\eta} \tag{2.33}$$

$$M^2 p^2 + q^2 - M^2 p \hat{p} = f(p,q,\hat{p}) = 0 \quad . \tag{2.34}$$

This elliptic yield surface model resulted in prediction that fitted the triaxial experimental results better than the Cam-Clay model. Of the two critical state models, the elliptic model is used more commonly. The model equations for the elliptic yield surface model are summarized in the next section. It is the elliptic yield surface model that will be used for comparisons hereafter. The yield surfaces for the

Cam-Clay and elliptic yield surface models are shown in Figure (2.4a) and (2.4b), respectively.

It is worthwhile noting at this point that the intersection of the yield surface and the critical state line in the p-q plane takes place for values of $\hat{p}/p$ equal to 2 and exp(1) for the elliptic yield surface model and the Cam-Clay model, respectively.

2.2.5 Summary of the Constitutive Equations for the Elliptic Yield Surface Model

The yield surface is given by

$$f(p,q,\hat{p}) = M^2 p^2 + q^2 - M\, p\, \hat{p}$$

$$f(p,q,\hat{p}) \leq 0 \quad \text{always.}$$

a.) If $f(p,q,\hat{p}) < 0$ Then, elastic loading, and

$$\begin{aligned} \delta v &= \delta v^r = \frac{K}{1+e}\frac{\delta p}{p} \\ \delta \varepsilon &= 0 \quad . \end{aligned} \tag{2.35a}$$

b.) If $f(p,q,\hat{p}) = 0$ and

$$\frac{\partial f}{\partial p}\delta p + \frac{\partial f}{\partial q}\delta q < 0 \quad ,$$

then, unloading and δv and $\delta \varepsilon$ are the same as in a). (2.35b)

c.) If $f(p,q,\hat{p}) = 0$ and

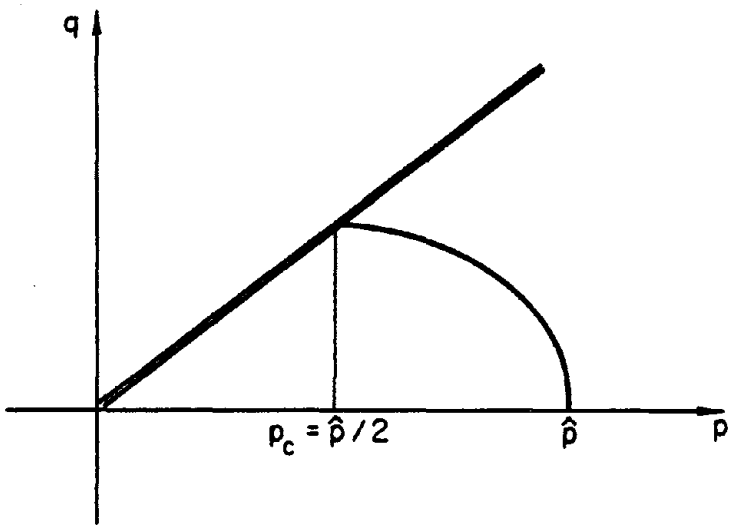

(a) ELLIPTIC MODEL

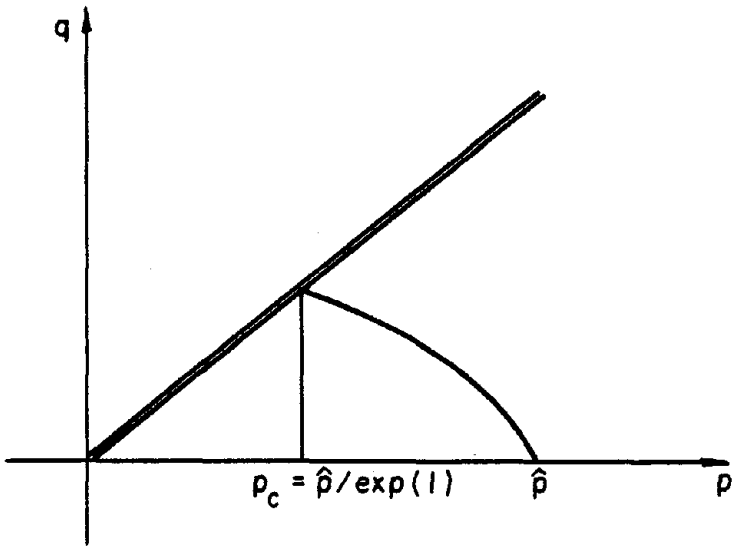

(b) CAM-CLAY MODEL

FIGURE 2.4 STRESS-SPACE YIELD SURFACES

$$\frac{\partial f}{\partial p}\,\delta p + \frac{\partial f}{\partial q}\,\delta q = 0 \quad ,$$

then, neutral loading and δv and $\delta \varepsilon$ are the same as in a). (2.35c)

d.) If $f(p,q,\hat{p}) = 0$ and

$$\frac{\partial f}{\partial p}\,\delta p + \frac{\partial f}{\partial q}\,\delta q > 0 \quad ,$$

then

$$\delta v = \delta v^r + \delta v^p$$

$$\delta v^r = \frac{\kappa}{1+e}\,\frac{\delta p}{p}$$

$$\delta v^p = \frac{\lambda-\kappa}{1+e}\left[\frac{\delta p}{p} + \frac{2\eta\delta\eta}{M^2+\eta^2}\right]$$

$$\delta \varepsilon = \delta \varepsilon^p = \frac{\lambda-\kappa}{1+e}\,\frac{2\eta}{M^2-\eta^2}\left[\frac{\delta p}{p} + \frac{2\eta\delta\eta}{M^2+\eta^2}\right] \quad . \qquad (2.35d)$$

2.3 STRAIN-SPACE IMPLICATIONS OF CRITICAL STATE MODELS

2.3.1 Isotropic Behavior

The isotropic behavior of soils is given by Terzaghi's equations (2.13) and (2.14). Since the equations only relate the void ratio and the pressure, they can easily be inverted to give

$$\hat{p} = p_r \exp \frac{e_r - \hat{e}}{\lambda}$$

$$p = p_r \exp\left[-\frac{(e - e_r)}{K} + \left(\frac{1}{K} - \frac{1}{\lambda}\right)(\hat{e}-e_r)\right] \quad . \qquad (2.36)$$

Equation (2.36) expresses the pressure for both normally consolidated and overconsolidated states in terms of the current void ratio, e, the void ratio at normal consolidation $\hat{e}$ and the reference values p_r, e_r.

2.3.2 Critical State Behavior

The stress-space model uses stresses as its independent variables along with some variables that act as memory variables in order to produce plastic behavior. The elliptic yield surface model uses p, q and $\hat{p}$ as the independent variables. At critical state, this set fails to determine the dependent variable epsilon, uniquely. At this point, p, q and $\hat{p}$ are fixed at their critical state value and ε changes indefinitely while e is fixed.

If the strains are considered as the independent variables instead of the stresses, e and ε along with a memory variable $\hat{e}$ become the independent variables. Hence, p and q will be defined by e, ε and $\hat{e}$. Such a specification defines the material deformation and stresses completely through each stage of a critical state. This is made possible because p and q are uniquely defined by e and $\hat{e}$ at critical state and ε varies independently. For this reason, a strain-space formulation specifies critical state completely. Figure (2.5) illustrates the argument presented above in both the p-q and e-ε planes.

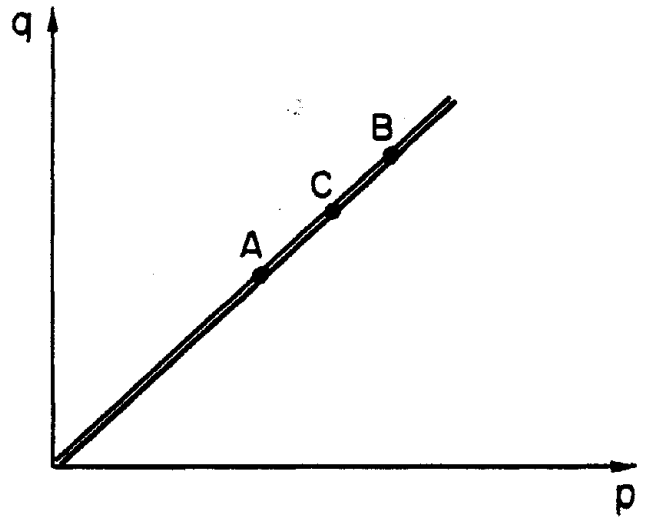

(a) STRESS-SPACE

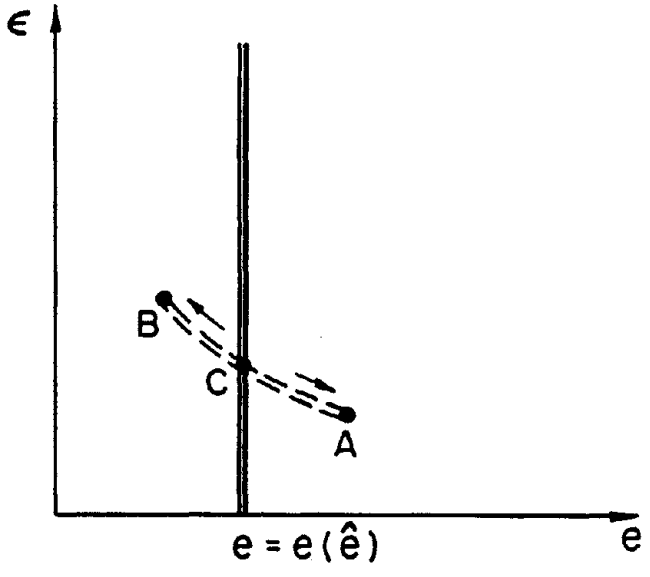

(b) STRAIN-SPACE

FIGURE 2.5 CRITICAL STATE

The critical state is identified in stress-space, as the state in which the value of q/p, denoted by η, reaches the value of the critical state constant M. However, it is possible to identify or define the critical state based upon the value of the void ratio. Indeed, in the original paper in which the critical state concept is introduced (Roscoe, et al., 1958), the emphasis is on the critical void ratio. In strain-space, therefore, the critical state could well be defined by a critical void ratio, denoted by e_c.

It is evident from the critical state concept that e_c will be either a constant or may depend upon the memory variable $\hat{e}$. From the projection of the critical state line on the p-e plane it is clear that e_c is not a constant. Hence e_c must be taken to be a function of $\hat{e}$. This implies that the void ratio at which critical state is reached changes if and only if there are plastic deformations.

It was noted in section 2.2.4 that for the elliptic yield surface model the ratio $\hat{p}/p_c$ is 2. Due to the logarithmic relationship between p and e for elastic swelling and due to the fact that elastic loadings do not change e_c, it is clearly seen that

$$e_c = \hat{e} + K \log_e 2 \quad . \tag{2.37}$$

The projection of the critical state line on the $\log_e p$-e plane along with the normal consolidation line and elastic swelling line are shown in Figure (2.6).

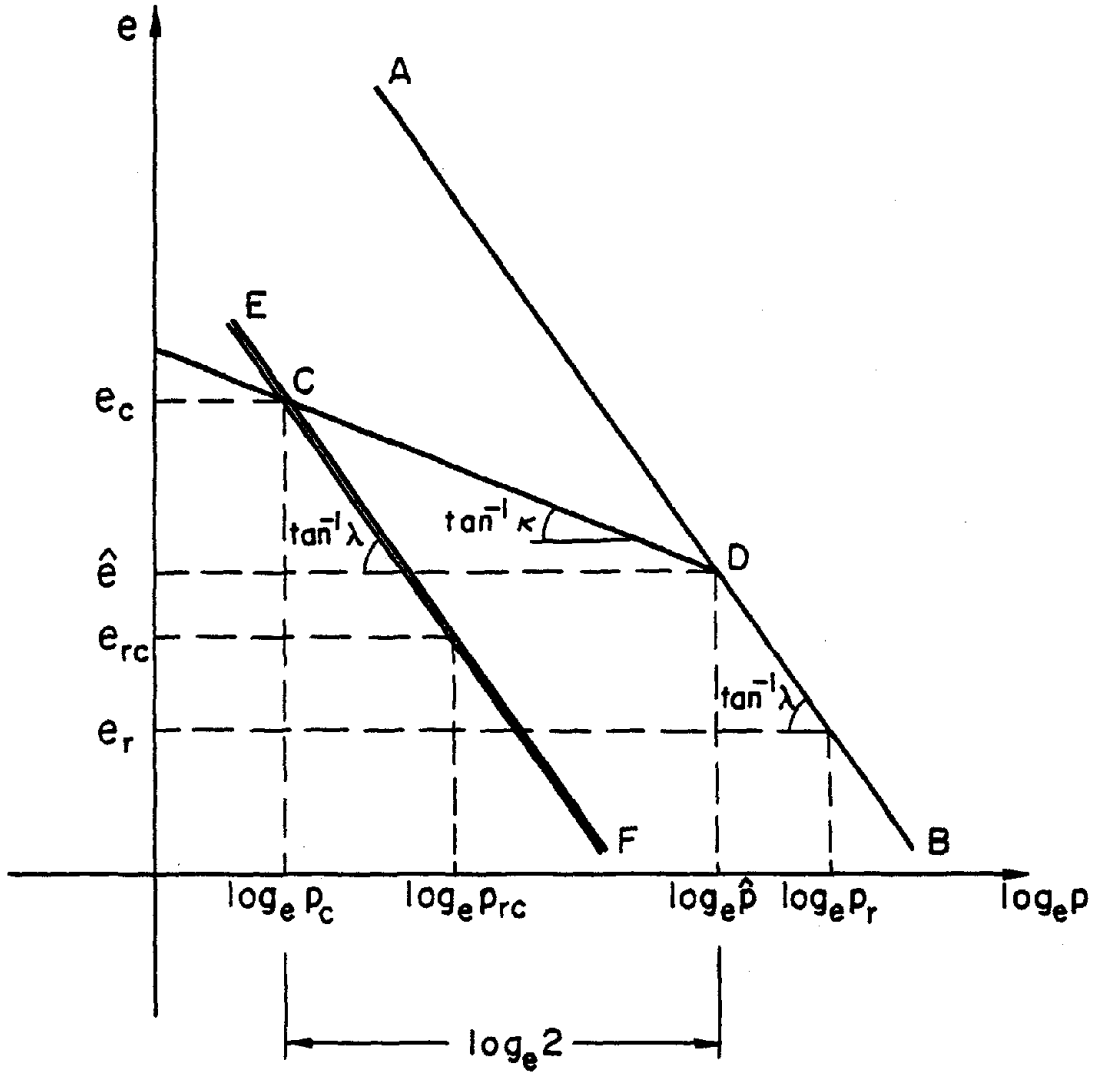

FIGURE 2.6 PROJECTIONS OF THE NORMAL CONSOLIDATION, SWELLING, AND CRITICAL STATE LINES

Having established the basic framework, it is now possible to express the stress variables at critical state in terms of the strain variable. The pressure at critical state can be expressed simply by restating equation (2.16) as

$$p_c = p_{rc} \exp \frac{e_{rc} - e_c}{\lambda} \quad . \tag{2.38}$$

Once the pressure is determined, the shear follows trivially from the second critical state condition that $\eta = M$. This results in

$$q_c = M p_c \quad . \tag{2.39}$$

It should be noted here that any strain-space formulation should satisfy this condition by reaching $q = M p$ without a jump as e reaches e_c.

2.3.3 General Behavior

Having explored the implications of the critical state model in strain-space for some special cases, it is now appropriate to generalize these implications for a more general loading. In the stress-space model, after defining the isotropic relation given by equation (2.14), the behavior is generalized by assuming that, for loadings with non-zero shear stress increment, the relationship between p and e would still be independent of both the instantaneous and incremental shear stresses. This concept is referred to as the 'elastic wall concept.'

Figure (2.7) illustrates this concept. The elastic wall concept implies that all elastic states lie on a surface whose projection on the p-e plane is given by CD. These surfaces are termed elastic walls.

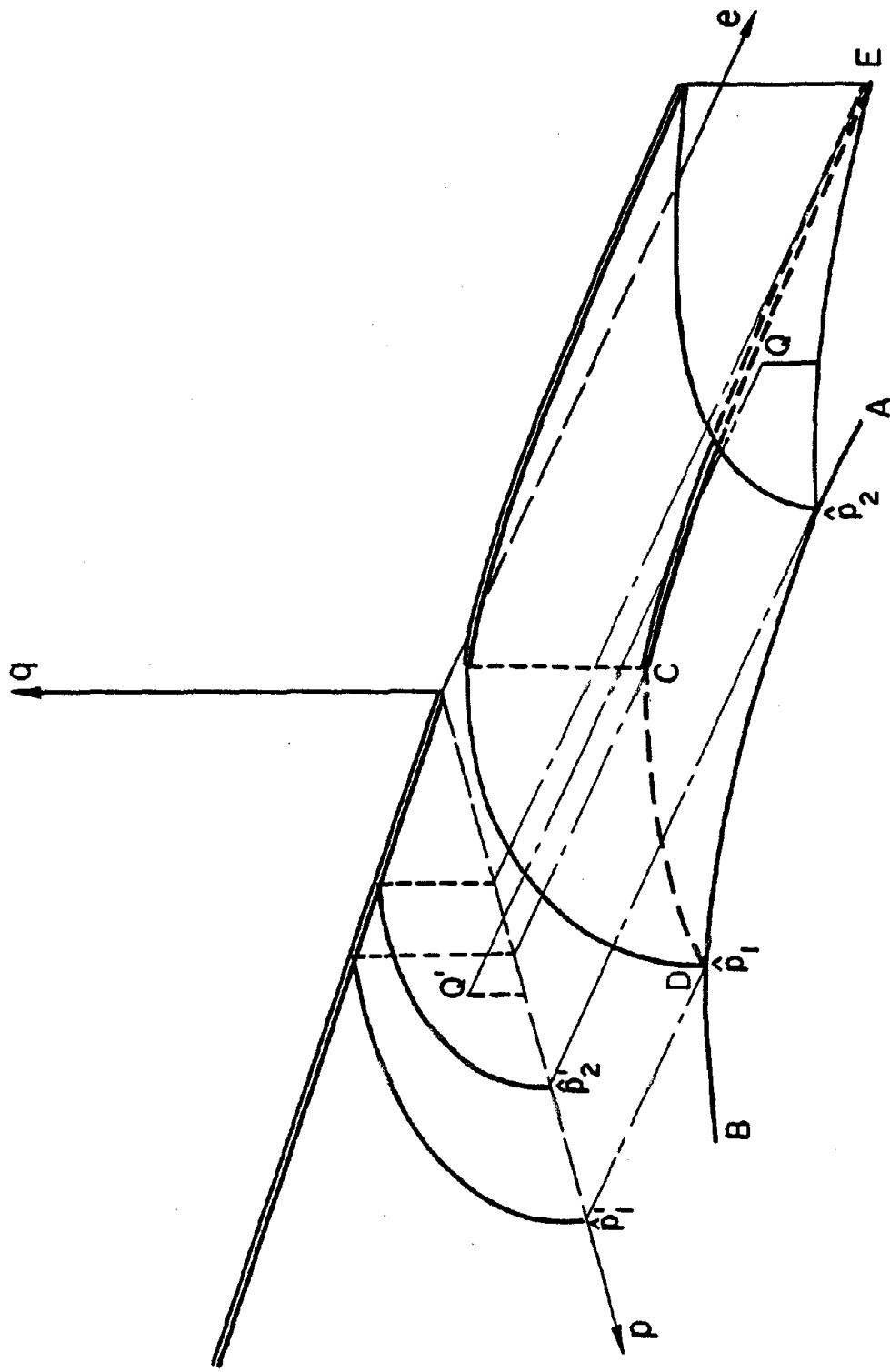

FIGURE 2.7 ELASTIC WALL

Any plastic loading changes the value of $\hat{e}$. Hence, there is a family of elastic walls, each corresponding to a particular value of $\hat{e}$. It can thus be deduced that

$$p = p(e,\hat{e}) \quad . \tag{2.40}$$

Equation (2.36) can therefore be used to determine the values of p due to any general loading. The role of $\hat{e}$, the minimum void ratio reached by the sample during the particular loading, is to account for memory.

2.3.4 Loading Surface in Strain-Space

Two implications of the stress-space models enable a very simple loading surface to be established in strain-space. The first implication is that the ratio of $\hat{p}$ and p_c is a constant. This implies that $(\hat{e}-e_c)$ is a constant and is given in equation (2.37). Hence, in strain-space, for every given elastic wall which implies a given value of $\hat{e}$, the critical state lies a distance $K \log_e 2$ to the right of $\hat{e}$. For wet clays this value of e_c imposes a limiting state in strain-space corresponding to each $\hat{e}$.

The second implication arises from the assumption of zero elastic shear strains. Experiments on soil (Thurairajah 1961, Ko 1966, Roscoe and Burland 1968) tend to validate this assumption. In strain-space this assumption implies a singular loading surface. The loading surface will be a slit parallel to the void ratio axis. The loading surface arising from these two implications is shown in Figure (2.8).

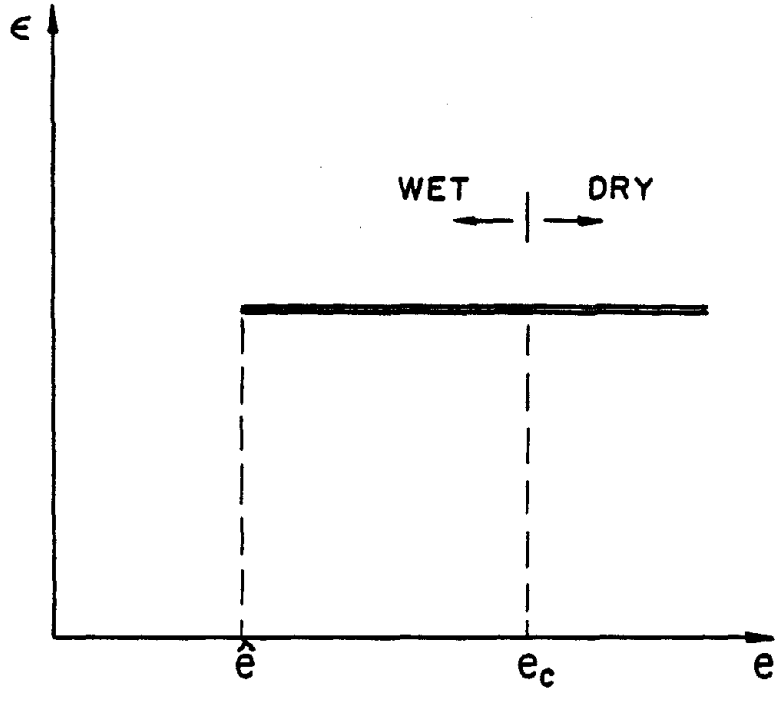

FIGURE 2.8 STRAIN–SPACE LOADING SURFACE

During plastic loading the variable $\hat{e}$ changes and hence the loading surface translates in the e-ε plane without any rotation. It is hence necessary to define a hardening law that will describe the relationship between $\hat{e}$ and the strain-space variables e and ε for plastic loading.

2.4 SUMMARY

From a study of the basic concepts used in the most popular critical state models, it is clear that a model based on those concepts might be formulated with strain as the independent variable. The basic concepts have been used to deduce equations that would predict stresses from strains. Having developed such a basic framework, it is possible to develop a strain-space model.

When viewed from the standpoint of strain-space, the critical state turns out to be a state which is completely defined. The strain-space loading surface, though singular, is much simpler than the corresponding stress-space yield surface. The fundamental assumption on critical state implies that the critical state line is parallel to the normal consolidation line in the $\log_e p$-e plane. This resulted in a loading surface of constant size in strain-space. The observations made in this chapter will be used to formulate a specific strain-space model for soils. This is described in the next chapter.

CHAPTER III

DEVELOPMENT OF THE MODEL

3.1 INTRODUCTION

The purpose of this chapter is to demonstrate the feasibility of the development of a simple strain-space model for wet clays. It is not specifically desired to improve on the accuracy of existing stress-space models. However, in the event of any basic physical behavior not being captured by the stress-space model, an attempt is made to build such behavior into the strain-space model.

The model developed herein differs from the classical plasticity models. These differences are explained and justified in section 3.2.1. This strain-space model is based on a variable new to soil modeling, namely the over compression ratio. This variable is defined and its physical significance is described in section 3.2.2.

Based on the above-mentioned basic concepts, a model is developed in section 3.3. The development starts off with the simple case of undrained triaxial loading which results in only one independent variable. Having developed the model for this simple case it is then generalized to triaxial monotonic loading and finally to general triaxial loadings allowing load reversals.

Section 3.4 lists the model equations in a concise form.

3.2 BASIC CONCEPTS

3.2.1 A New Approach to Constitutive Modeling of Soils

The work presented herein differs from conventional plasticity in three fundamental aspects.

i) No decomposition is performed on stress or strain to distinguish elastic and plastic components.

ii) The flow is non-associative between the hydrostatic and deviatoric components.

iii) The loading surface is singular.

i) In strain-space plastic models applied to metals, the stresses may be decomposed using the concept of relaxation. When a material is subjected to a certain value of strain, it will develop only elastic stresses if the strain remains below the limit at which plastic behavior begins. However, when the strains go beyond the elastic limit, the material stresses relax to some value lower than the elastic value. This reduction of stress from the extrapolated elastic value has been termed the relaxation stress. Such a decomposition is illustrated along with the equivalent stress-space decomposition in Figure (3.1). For a general stress state, the decomposition into elastic and relaxation stresses may be expressed as

$$\underline{\sigma} = \underline{\sigma}^{E} - \underline{\sigma}^{R} \quad , \tag{3.1}$$

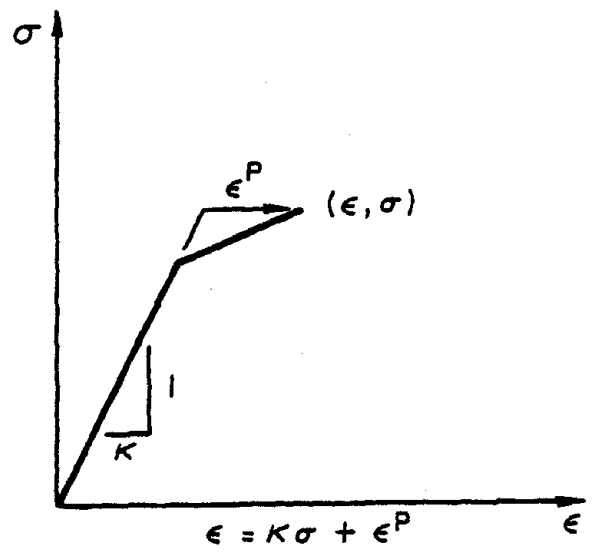

STRAIN–SPACE

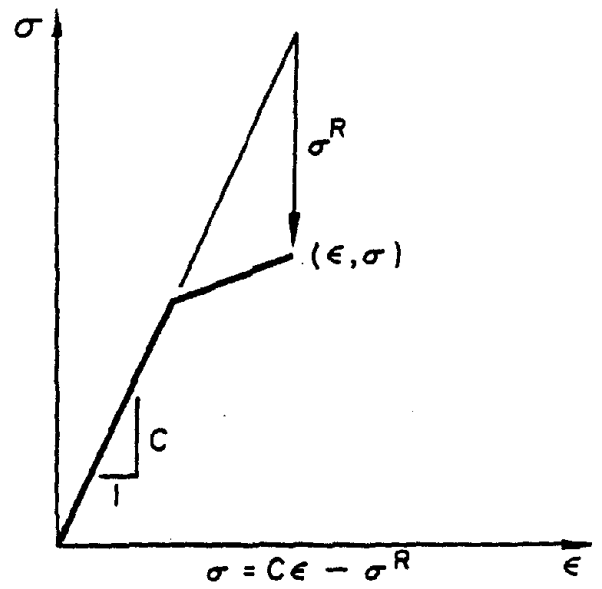

STRESS–SPACE

FIGURE 3.1 STRESS, STRAIN DECOMPOSITIONS

where the superscripts E and R indicate the elastic and relaxation stresses, respectively. The equivalent general stress-space decomposition is

$$\underline{\varepsilon} = \underline{\varepsilon}^{E} + \underline{\varepsilon}^{P} \quad . \tag{3.2}$$

In the case of soils, the decomposition shown in equation (3.1) does not apply for either isotropic behavior or shear behavior. First, consider isotropic behavior. Although there is no finite undeformed state, assume a state with a value of $p = p_r$ which is sufficiently low that all subsequent values of p are larger than p_r. Further, assume p_r to be on the swelling line. All the above assumptions are made so that the isotropic soil behavior will resemble the standard uniaxial stress strain behavior on which the usual decomposition is based. This is shown in Figure (3.2).

Let the soil be loaded from p_r so that p increases and e decreases. The state point, initially moving along the swelling line, will switch to the normal consolidation line at the intersection of the two lines. If the decomposition of stress holds, then,

$$p(e) = p^{E}(e) - p^{R}(e) \tag{3.3}$$

for state points lying on the normal consolidation line shown in Figure (3.2) as AB. Consider a situation in which the loading is reversed at point B. If the decomposition holds for this case, the stress strain curve will follow BC' on unloading since

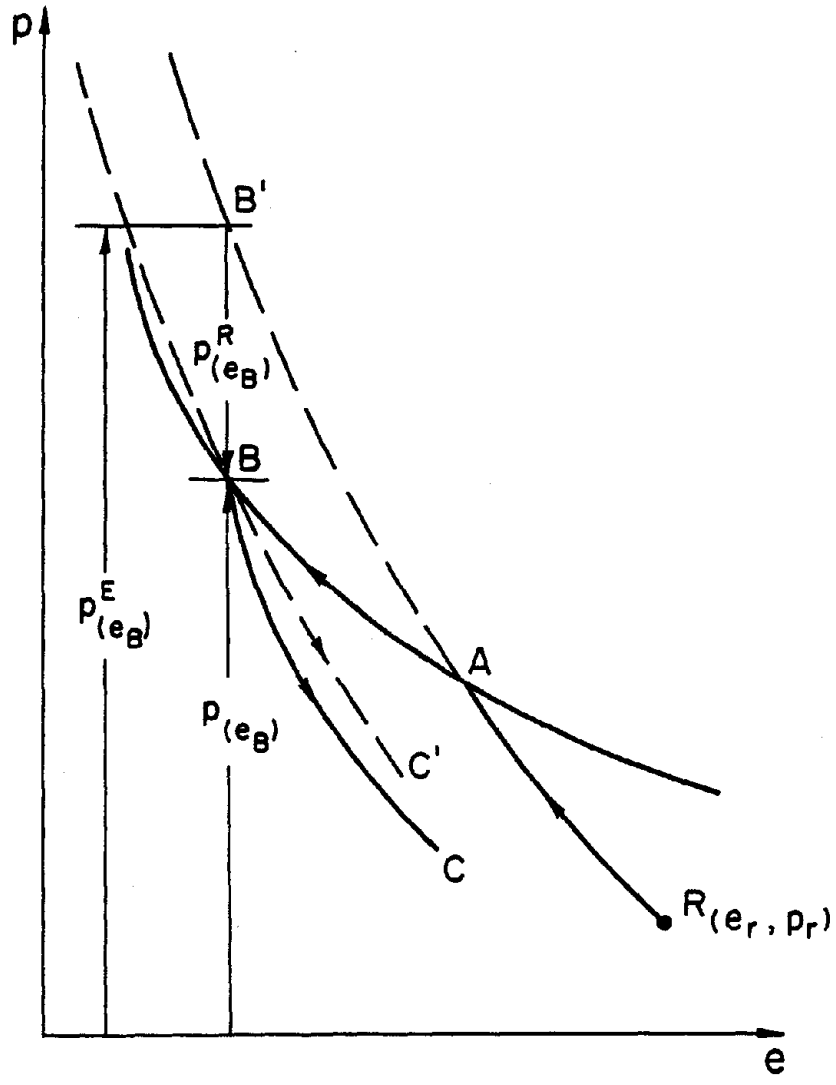

FIGURE 3.2 DECOMPOSITION PROBLEMS FOR SOILS

$$p(e) = p^E(e) - p^R(e_B). \tag{3.4}$$

But experimental observations clearly indicate that this is not the case and that the stress-strain curve follows BC. It is thus clear that the linear decomposition fails to describe the isotropic behavior of soils for isotropic loading. The reason for this lies in the fact that the p-e relationship is non linear. Since the relationship is linear in a $\log_e p - e$ plane, a logarithmic decomposition is required to define the pressure.

Secondly, consider the shear behavior of soil. It has been observed from soil experiments (Ko 1966, Thurairajah 1961) that soil exhibits plastic behavior from the onset of loading. Hence, for shear loading, an elastic shear stress cannot be determined experimentally. It is therefore necessary to artificially introduce a function q^E from which the shear stress relaxes to produce the resulting shear stress. For this reason the shear stress is not decomposed. Instead, a total incremental stress is defined.

ii) The second difference from the classical theory arises in the flow rule. The model developed hereafter assumes that the shear and the hydrostatic stress increments may be obtained by defining two independent hardening rules rather than by the combination of a hardening rule and a flow rule. In the strain-space theory, developed along the lines of the conventional stress-space plasticity theory, the incremental stress relaxation is defined by

$$d\sigma_{ij}^{R} = dk \frac{\partial G}{\partial \varepsilon_{ij}} \tag{3.5}$$

where,

$d\sigma_{ij}^{R}$ Components of the relaxation stress tensor

dk Scalar corresponding to a characteristic incremental stress

G Complementary potential function

ε_{ij} Components of the strain tensor.

The method proposed herein defines each total stress increment independently. For the simple triaxial case this leads to

$$\begin{aligned} dp &= dk_1 \\ d\eta &= dk_2 \quad . \end{aligned} \tag{3.6}$$

Equations (3.6) along with the incremental relationship given below can be used to find dq.

$$\frac{dq}{q} = \frac{d\eta}{\eta} + \frac{dp}{p} \tag{3.7}$$

iii) Finally, it is found that the loading surface used herein is singular in the e–ε plane. However, since the incremental pressure and the incremental shear are defined independently, the discontinuity of the slope at the tips poses no problem. Instead of the normal to the loading surface, two independent hardening rules are proposed as in equation (3.6). Loading is defined along the lines of conventional plasticity. Any time the incremental load vector tries to take the

strain state outside the loading surface, plastic behavior occurs. Thus, the loading condition can be stated as

$$\begin{aligned} &\text{i)} \quad d\varepsilon \neq 0 \qquad \underline{\text{or}} \\ &\text{ii)} \quad e = \hat{e} \quad \text{and} \quad de < 0 \quad . \end{aligned} \tag{3.8}$$

3.2.2 Over Compression Ratio

For wet clays the normal consolidation state and the critical state define two limits for elastic states as shown in Figure (3.3). Hence, it would seem natural to assume that the relative position of a state between the two limiting states would have a great influence on the material behavior. Having this in mind, a dimensionless variable ξ termed the over compression ratio is defined as follows:

$$\xi = \frac{e-\hat{e}}{e_c-\hat{e}} \quad . \tag{3.9}$$

For wet clays, $0 \leq \xi \leq 1$. $\xi = 0$ corresponds to a normally consolidated state whereas $\xi = 1$ corresponds to the critical state.

The stress-space over consolidation ratio (OCR), defined as the ratio of the normal consolidation pressure divided by the current pressure, is related to the over compression ratio as

$$\frac{\hat{p}}{p} = \exp\left[\xi \frac{(e_c-\hat{e})}{K}\right] \quad . \tag{3.10}$$

It has been shown in equation (2.37) that the difference between e_c and $\hat{e}$ is a constant and is given by $K \log_e 2$. This makes the

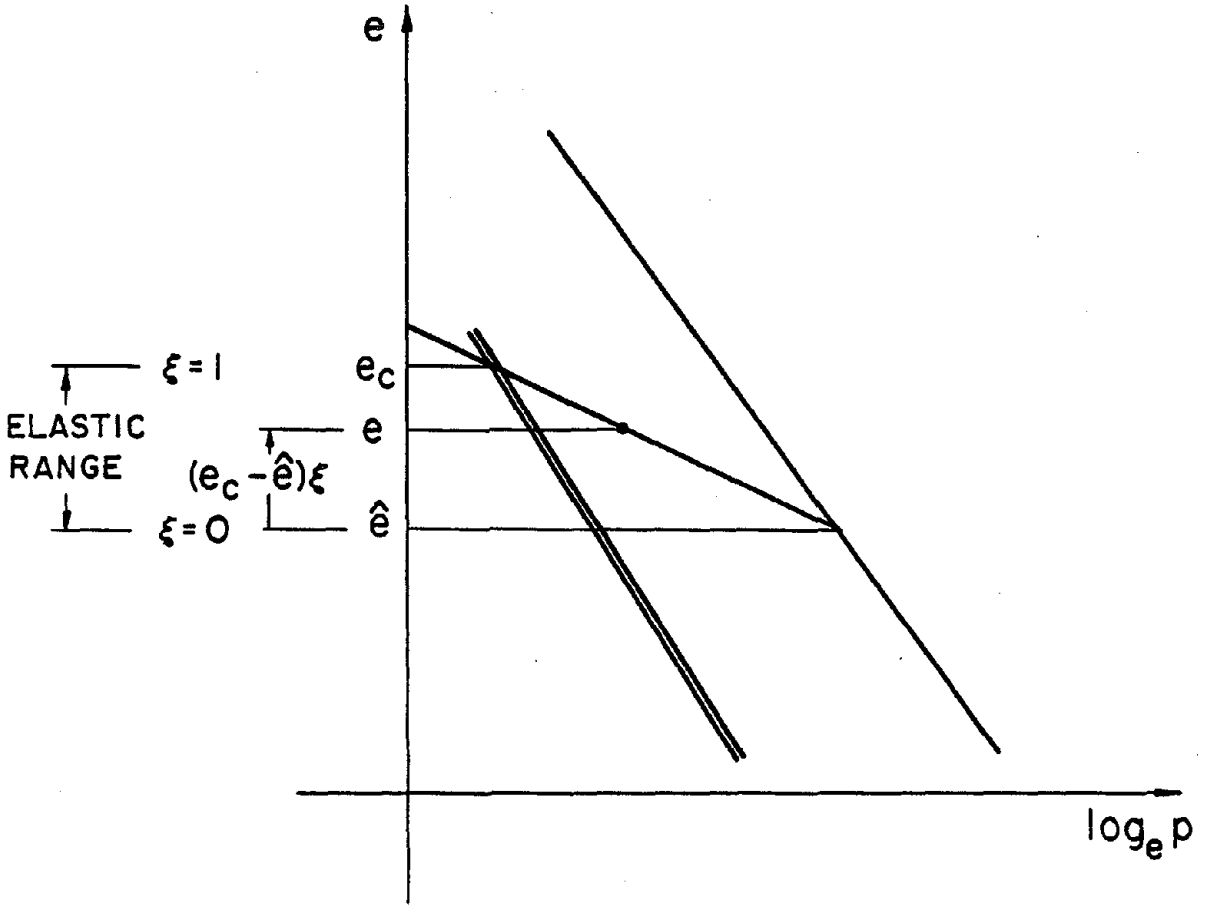

FIGURE3.3 OVER COMPRESSION RATIO

variable ξ linear in e and $\hat{e}$ and reduces equation (3.10) to the very simple form

$$\frac{\hat{p}}{p} = 2^{\xi} \quad . \tag{3.11}$$

3.3 DEVELOPMENT OF THE MODEL

3.3.1 Undrained Behavior

Undrained deformation of soils is one of the simple cases of analysis in strain-space. In the axisymmetric theory, there are two strain-space variables e and ε. For undrained deformation, e remains a constant and hence the only variable in the problem is ε. Due to this simplification, the strain-space soil model is developed first for the special case of undrained deformation and is then extended to general axisymmetric deformations and finally to the most general three-dimensional deformation. The fundamental assumption made in the development of the simple strain-space model is that the incremental behavior of wet clay can be expressed explicitly in terms of the over compression ratio and the incremental and total strain variables.

First, the relationship for incremental pressure is developed. From equations (2.36) it is clear that p is defined if $\hat{e}$ and e are known. For a general strain-controlled deformation, e is given as one of the independent variables. For the undrained case, the value of e is a constant. To define p for undrained deformation it is therefore necessary and sufficient to define $\hat{e}$. Further, the irreversible

behavior of the material is represented by the presence of $\hat{e}$ in p. The variable $\hat{e}$ will be defined here in the incremental form.

Let it be assumed that $d\hat{e}$ can be related to $d\varepsilon$ by the relation

$$d\hat{e} = f_1(e,\xi) \cdot d\varepsilon \quad . \tag{3.12}$$

From the physical characteristics of soils it is known that

$$f_1(e,1) = 0 \quad . \tag{3.13}$$

Equation (3.13) is obtained from the fact that at critical state ε can change indefinitely without affecting any other variable. Assuming that f_1 is sufficiently smooth, this function may be expressed as a Taylor series expansion in terms of ξ about the critical state. This leads to

$$f_1(e,\xi) = \sum_{k=0}^{\infty} a_k(e) \cdot (1-\xi)^k \quad . \tag{3.14}$$

Equation (3.13) implies that

$$a_o(e) = 0 \quad .$$

In order to simplify the model further it will be assumed that f_1 is well approximated by the first non-zero term of the expansion in equation (3.14). This results in

$$f_1(e,\xi) = a_1(e) \cdot (1-\xi) \tag{3.15}$$

From the development of the stress-space model reviewed in Chapter II it is seen that dp and $d\eta$ are related to $(1+e)d\varepsilon$. Hence, using this

observation in strain-space $a_1(e)$ could be written as

$$a_1(e) = -b_1(1+e) \quad . \tag{3.16}$$

The negative sign is included so that b_1 will be positive. Combining equations (3.12), (3.15) and (3.16) $\hat{de}$ can be defined as

$$\hat{de} = -b_1(1+e)(1-\xi) \, . \, d\varepsilon \quad . \tag{3.17}$$

For the undrained loading case, e is a constant. Therefore, equations (3.9) and (3.17) can be solved in closed form for ξ and $\hat{e}$ yielding,

$$\begin{aligned} \xi &= 1 - (1-\xi_o) \exp\left[\frac{-b_1(1+e_o)(\varepsilon-\varepsilon_o)}{\lambda}\right] \\ \hat{e} &= \hat{e}_o - \lambda(1-\xi_o)\left[1 - \exp\frac{-b_1(1+e_o)(\varepsilon-\varepsilon_o)}{\lambda}\right] \end{aligned} \quad , \tag{3.18}$$

where the suffix 0 denotes the value of the corresponding variable at the beginning of undrained loading, and $\lambda = K \log_e 2$. Equation (3.18) can be combined with equation (2.36) to give

$$p = p_o \exp\left[-\left(\frac{1}{K} - \frac{1}{\lambda}\right)\lambda(1-\xi_o)\left(1 - \exp\frac{-b_1(1+e_o)(\varepsilon-\varepsilon_o)}{\lambda}\right)\right] \tag{3.19}$$

Only the first non-zero term of the expansion for f_1 is considered in developing equations (3.17), (3.18), and (3.19). However, if the need arises for any specific clay, it would be possible to include one or more higher order terms. Whether or not such additional complexity is warranted will depend upon the accuracy of the available data along with

confidence limits for the experiment, and the accuracy desired from the model.

Next, consider modeling the shear stress for undrained loading. It has been observed from stress-space calculations that the variable η is more simply related to e and ε than is q. For this reason, it is attempted herein to define a relationship for η as a function of e and ε. Having thus defined p and η, q can be calculated from equation (2.11).

The independent variables in strain-space are e, ε and $\hat{e}$. For undrained loading e remains a constant. Using these observations $d\eta$ can be defined as

$$d\eta = g_1(e,\varepsilon,\hat{e})d\varepsilon + g_2(e,\varepsilon,\hat{e})d\hat{e} \quad . \tag{3.20}$$

Set $g_1 = 0$ and

$$g_2(e,\varepsilon,\hat{e}) = g_3(\frac{\hat{e}-e}{\lambda}) = g_3(\xi) \quad . \tag{3.21}$$

These assumptions reduce equation (3.20) to the simple form

$$d\eta = g_3(\xi) \cdot d\hat{e} \quad . \tag{3.22}$$

Both the incremental variables $d\hat{e}$ and $d\eta$ are zero at the critical state where $\xi = 1$. This implies that $g_3(\xi)$ should be bounded at $\xi = 1$.

It is observed from experiments that the q-ε relationship has a very large slope at the origin. This can be used to deduce the behavior of η around $\xi = 0$. From equation (2.11) it can be shown that

$$dq = \eta dp + p d\eta \quad . \tag{3.23}$$

The value of pressure never becomes zero; that is $p \neq 0$. However, for the state of isotropic consolidation, $q = 0$ and $\xi = 0$. If this state is considered as the initial state, then at that initial state

$$dq = p d\eta \quad . \tag{3.24}$$

Thus, a very large initial slope for q with respect to ε also implies a very large initial slope for η with respect to ξ.

For the undrained loading

$$d\xi = -d\hat{e}/\ell$$

which implies that

$$\frac{\partial \eta}{\partial \hat{e}} \rightarrow \infty \qquad \text{as} \qquad \xi \rightarrow 0 \quad .$$

The implications in the case of load reversals will be treated in section 3.3.3.

The observation of the infinite or very large initial slope under the simplifying assumptions results in

$$\lim_{\xi \rightarrow 0} \; g_3(\xi) = \infty \quad , \tag{3.25}$$

for the undrained loading. From the above observations, it is necessary to construct a function $g_3(\xi)$ which is bounded at $\xi = 1$ and unbounded at the origin. To maintain consistency of accuracy, a single term of the expansion of $g_3(\xi)$ about the critical state is considered. The

singularity at the origin is introduced by $\xi^{-\alpha}$, $\alpha > 0$. This results in

$$g_3(\xi) = C_o \cdot \xi^{-\alpha} \tag{3.26}$$

which leads to

$$d\eta = C_o \, \xi^{-\alpha} \, \hat{de} \quad . \tag{3.27}$$

For the undrained case under consideration, equation (3.27) can be integrated in closed form. The integration produces the result

$$\eta = - \frac{C_o \ell}{(1-\alpha)} \, \xi^{(1-\alpha)} \quad , \quad 0 < \alpha < 1 \quad . \tag{3.28}$$

From experiments, it is evident that $\eta(0) = 0$. This implies that $\alpha < 1$ for a non-trivial solution.

The critical state model implies that if the material is loaded monotonically from $\xi = 0$ to $\xi = 1$, η should reach M at $\xi = 1$. Since the material has no way of knowing any load changes that are likely to take place in the future, it is reasonable to assume that η will behave in a manner such that it will reach M if ξ reaches 1. This fact can be used to evaluate the constant C_o and leads to

$$\eta = M \, \xi^{1-\alpha} \quad , \quad 0 < \alpha < 1 \quad . \tag{3.29}$$

3.3.2 General Monotonic Loading

For undrained loading, it was shown that $\hat{de}$ can be given by equation (3.17). It is assumed that, for general monotonic loading, the effect of changing the void ratio as well as the shear strain is to replace $(1+e)d\varepsilon$ by $d[(1+e)\varepsilon]$. This assumption gives the relationship

between the incremental variables $\hat{de}$, de and dε as

$$\hat{de} = -b_1(1-\xi)\left[(1+e)d\varepsilon + \varepsilon de\right] \quad . \tag{3.30}$$

Equation (3.30) can also be solved in closed form. The solution is given by,

$$(1-\xi) = (1-\xi_o)\exp\left[-\frac{b_1}{\ell}\{(1+e)\varepsilon - (1+e_o)\varepsilon_o\}\right]$$

$$- \int_{t_o}^{t} \frac{e'(\varphi)}{\ell} \cdot \exp\left[\frac{b_1}{\ell}\{(1+e(\varphi))\varepsilon(\varphi) - (1+e(t))\varepsilon(t)\}\right]d\varphi \tag{3.31}$$

where, e = e(t) and ε = ε(t) are parametric representations for the loading path. Equation (3.31) can be used to compute p and q yielding

$$p = p_o \exp\left[-\frac{(e-e_o)}{\lambda}\right] \cdot$$

$$\exp\left[-\gamma \log_e 2 \cdot \left[(1-\xi_o)\left[1 - \exp\left[-\frac{b_1}{\ell}\{(1+e)\varepsilon - (1+e_o)\varepsilon_o\}\right]\right]\right.\right.$$

$$\left.\left. + \int_{t_o}^{t} \frac{e'(\varphi)}{\ell} \exp\left[\frac{b_1}{\ell}\{(1+e(\varphi))\varepsilon(\varphi) - (1+e(t))\varepsilon(t)\}\right] d\varphi\right]\right] \tag{3.32}$$

and

$$q = M p\left[1 - (1-\xi_o)\exp\left[-\frac{b_1}{\ell}\{(1+e)\varepsilon - (1+e_o)\varepsilon_o\}\right] + \int_{t_o}^{t} \frac{e'(\varphi)}{\ell}\exp\left[\frac{b_1}{\ell}\{(1+e(\varphi))\varepsilon(\varphi) - (1+e(t))\,\varepsilon(t)\}\right] d\varphi\right]^{1-\alpha} \quad (3.33)$$

3.3.3 Load Reversals

The model has thus far been developed assuming the loading to be monotonic. In this section the model is modified to take into account the effects of load reversals. First, the term 'load reversal' is defined within the framework of triaxial strain-space plasticity. Then, the effects of load reversals on pressure are modeled. Finally, the effects of load reversals are modeled for the shear stress.

The loading is defined to be "reversed" in strain-space if

1) $d\varepsilon$ changes sign and $0 < \xi < 1$, or

2) de changes sign from negative to positive and $\xi = 0$. The first of the two conditions implies a reversal of the motion of the loading surface in the ε co-ordinate. The second condition relates to the state moving from the normal consolidation curve to the swelling curve in the p-e plane.

The effect of load reversal on the pressure can be modeled by modifying Terzaghi's relationship given by equation (2.36). The modification is simple and merely involves changing the reference or initial values of the variables to their values at the most recent load reversal

state. This results in

$$p = p_o \exp\left[-\frac{(e-e_o)}{K} + \frac{\gamma}{K}(\hat{e} - e_o)\right]$$

$$(\hat{e}-\hat{e}_o) = (e-e_o) - \ell(\xi-\xi_o) \qquad (3.34)$$

where ξ is given by equation (3.31) with $\xi_o, e_o, \varepsilon_o$ corresponding to the most recent point of reversal.

The effects of load reversal on η can be grouped into the effect of reversal on the value of ξ and the effect of reversal on the functional relationship between η and ξ. The former is already dealt with during the modeling of the effects of reversal on p. The latter needs to be defined.

In defining the functional form of η for monotonic loading, the asymptotic value of η as ξ reaches 1 was used. Following the same line of argument it will be assumed that a reversal would cause the function for η to asymptotic to -M. Further, it is seen from experimental results that, just after a load reversal, q changes with an infinite or very large slope. These give rise to

$$d\eta = h(\xi,\xi_o)d\xi$$

with

$$h(\xi,0) = (1-\alpha)\, M\, \xi^{-\alpha}$$

and

$$\lim_{\xi \to \xi_o} h(\xi,\xi_o) = \infty \quad . \tag{3.35}$$

In order to deduce the function h, consider the implications of the Bauschinger effect. The Bauschinger effect for a simple uniaxial case is shown graphically in Figures (3.4a) and (3.4b). Analytically, the effect can be described as follows;

$$\begin{aligned} d\sigma &= h_1(\varepsilon) \cdot d\varepsilon \quad \text{when} \quad \varepsilon_{-1} = \varepsilon_o = 0 \qquad (\Gamma^{(0)}) \\ d\sigma &= h_1\left(\frac{\varepsilon_o - \varepsilon}{2}\right) d\varepsilon \quad \text{for} \quad -\varepsilon_o^{(1)} \leq \varepsilon \leq \varepsilon_o^{(1)} \qquad (\Gamma^{(1)}) \quad , \end{aligned} \tag{3.36}$$

where ε_o denotes the value of ε at the last point of load reversal in the strain trajectory. The symbol ε_{-1} denotes the value of the variable ε corresponding to the next to last load reversal point. Considering Figure (3.4b), let the current state be on curve $\Gamma^{(n)}$. Then, ε_o will be the value of ε at the intersection of $\Gamma^{(n)}$ and $\Gamma^{(n-1)}$, and ε_{-1} will be the value of ε at the intersection of $\Gamma^{(n-1)}$ and $\Gamma^{(n-2)}$.

Equation (3.36) describes the stress strain behavior for a single reversal case including the Bauschinger effect. However, equation (3.36) can be generalized to include a general load trajectory with several reversals by requiring that

$$\begin{aligned} d\sigma &= h_1(|\varepsilon - \varepsilon_o|) \cdot d\varepsilon \quad \text{whenever} \quad |\varepsilon| > \max\{|\varepsilon_{-1}|, |\varepsilon_o|\} \\ d\sigma &= h_1\left(\left|\frac{\varepsilon - \varepsilon_o}{2}\right|\right) \cdot d\varepsilon \quad \text{otherwise} \quad . \end{aligned} \tag{3.37}$$

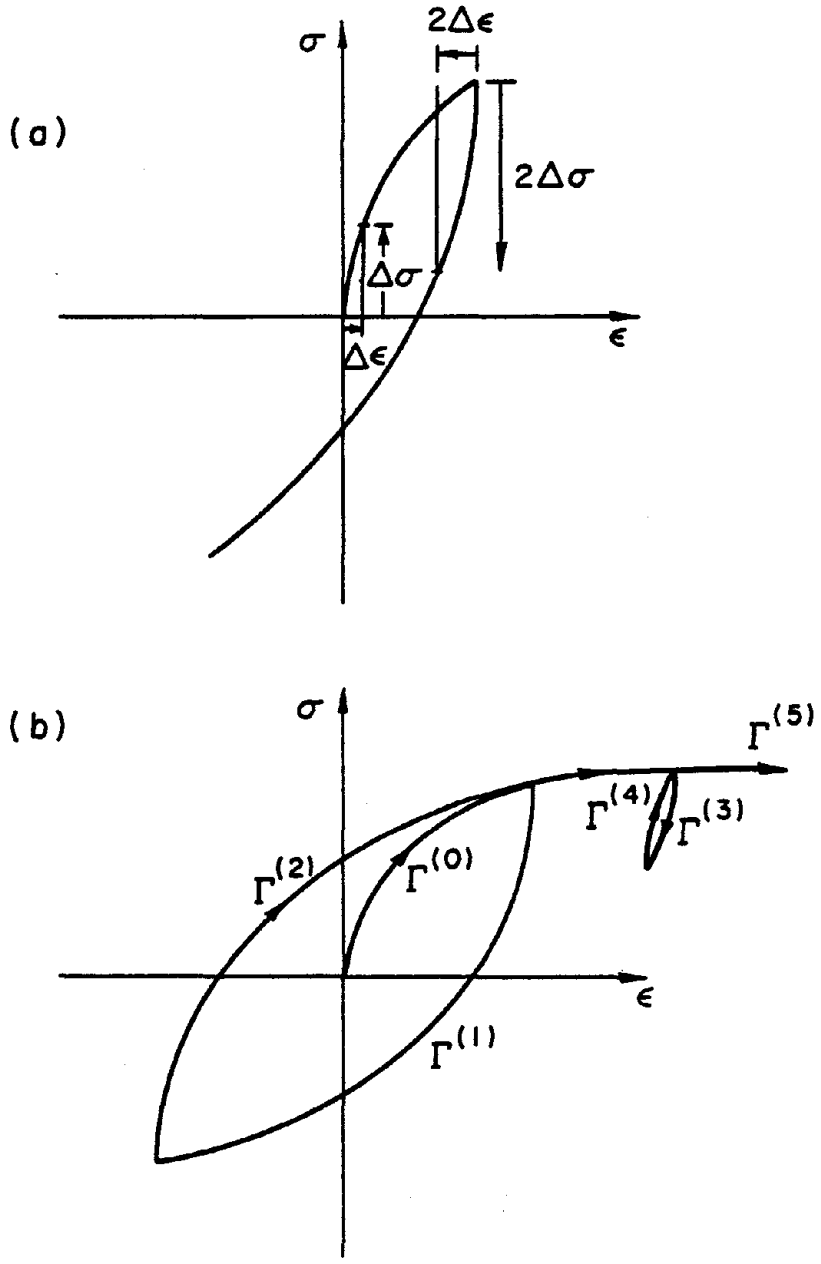

FIGURE3.4 BAUSCHINGER EFFECT

In the strain-space model the easiest way to introduce effects of load reversal on q would be through the η-ξ relationship. Clearly, this is not equivalent to implementing the reversal condition on q-ε. However, as will be explained in the next chapter, it will be seen that such an implementation results in characteristics very much like those observed experimentally. Such an implementation can be summarized as follows:

$$d\eta = (1-\alpha)\, M\, |\xi-\xi_o|^{-\alpha} \cdot \mathrm{sgn}(d\varepsilon) \cdot d\xi \text{ , whenever } |\varepsilon| > \max\{|\varepsilon_{-1}| \text{ , } |\varepsilon_o|\}$$

$$d\eta = (1-\alpha)\, M\, \left|\frac{\xi-\xi_o}{2}\right|^{-\alpha} \cdot \mathrm{sgn}(d\varepsilon) \cdot d\xi \text{ , otherwise}$$

where

$$\begin{aligned} \mathrm{sgn}(d\varepsilon) &= 1 && \text{if } d\varepsilon > 0 \\ &= 0 && \text{if } d\varepsilon = 0 \\ &= -1 && \text{if } d\varepsilon < 0 \end{aligned} \quad . \qquad (3.38)$$

It should be noted that the model for load reversals presented herein is only developed and tested for the undrained axisymmetric load case. The extension of reversal behavior for more complex loading situations is beyond the scope of this work.

3.4 MODEL EQUATIONS

The model can be summarized as follows:

$$\begin{aligned} dv &= d\varepsilon_I + 2d\varepsilon_{II} \\ d\varepsilon &= 2/3(d\varepsilon_I - d\varepsilon_{II}) \\ d\varepsilon_{III} &= d\varepsilon_{II} \\ de &= -(1+e)dv \end{aligned} \quad . \tag{3.39}$$

a) If $d\varepsilon = 0$ and $0 < \xi < 1$, then the behavior is elastic and

$$\begin{aligned} dq &= 0 \\ p &= p_o \exp\left[-\frac{1}{K}(e-e_o)\right] \end{aligned} \quad . \tag{3.40a}$$

b) If $d\varepsilon = 0$ and $de < 0$ and $\xi = 0$, then the behavior is plastic incrementally isotropic, and

$$\begin{aligned} dq &= 0 \\ p &= p_o \exp\left[\frac{1}{\lambda}(e-e_o)\right] \end{aligned} \quad . \tag{3.40b}$$

c) If $d\varepsilon \neq 0$, then the behavior is plastic anisotropic and

$$\begin{aligned} \hat{de} &= -b_1(1-\xi)[(1+e)d\varepsilon + \varepsilon de] \\ d\eta &= (1-\alpha)\, M\, |\xi-\xi_o|^{-\alpha} \operatorname{sgn}(d\varepsilon)d\xi \quad \text{whenever} \quad |\varepsilon| > \max\{|\varepsilon_{-1}|\,,\,|\varepsilon_o|\} \\ &= (1-\alpha)\, M\, \left|\frac{\xi-\xi_o}{2}\right|^{1-\alpha} \operatorname{sgn}(d\varepsilon)d\xi \quad \text{otherwise} \\ p &= p_o \exp\left[-\frac{(e-e_o)}{K} + \frac{\gamma}{K}(\hat{e}-\hat{e}_o)\right] \\ q &= \eta p \end{aligned} \tag{3.40c}$$

The principal stress variables can be found from p and q by the relations

$$\sigma_I' = p + \frac{2}{3}q$$
$$\sigma_{II}' = p - \frac{1}{3}q \qquad (3.41)$$
$$\sigma_{III}' = \sigma_{II}'$$

where

$$\xi = \frac{\hat{e}-e}{f}$$
$$f = K \log_e 2$$
$$\gamma = \frac{\lambda-K}{\lambda}$$
$$\alpha \text{ real and } 0 < \alpha < 1$$
$$b_1 \text{ real and } > 0 \ .$$

Wherever possible, the constitutive relations are stated in integrated form rather than incremental form. For the case of monotonic plastic loading, p and q can be determined in closed form and will produce the results stated previously in equations (3.32) and (3.33).

3.5 SUMMARY AND CONCLUSIONS

A simple strain-space model has been developed in this chapter based on observations made from the development of some stress-space models. It has been established in this chapter that a constitutive model capable of predicting soil behavior can be developed in strain-space.

The model developed herein does not follow the lines of conventional modeling of plasticity. The use of a singular loading surface poses no problems as hardening is defined independently, rather than by a flow rule.

The model is extended to include load reversals. This extension is achieved very simply by incorporating an effect similar to the Bauschinger effect commonly used in metals. This is accomplished in the η-ξ space rather than the q-ε space. The aim of such an approach is two-fold. First, it correctly models the strain softening effect on q. This strain softening effect is achieved in the following manner. During load reversal, the Bauschinger-like effect produces a reversal response similar to the initial η-ξ response. But the shear stress q is the product of η and p, and p decreases during this loading. This reduction in p results in the response of q becoming softer. Next, the modifications performed on η-ξ do not increase the complexity of the model. This is because η and ξ are related by a simple function given by equation (3.38).

As seen in the formulation for the simple case of axisymmetry, the strain-space formulation renders closed form analytic solutions for all strain-controlled monotonic loading cases. This is not the case even for the simplest loading condition for the stress-space model. The extension of the constitutive relations to include load reversals is also carried out in a straightforward manner and does not increase the complexity significantly.

The strain-space model has the further advantage that it uses only three constants, namely, λ, K, and M. These three constants can be evaluated by simple tests. The constants λ and K can be evaluated by one-dimensional tests and M can be evaluated from any of the standard triaxial tests such as the undrained or constant pressure test.

There are two other constants that appear in the model, namely α and b_1. These constants are assumed to be independent of material behavior and they will be verified to be so in Chapter IV. These two constants will hereafter be referred to as the model constants. The constants λ, K and M which are assumed to depend on the material will be referred to as material constants.

CHAPTER IV

MODEL CALIBRATION AND PREDICTIONS

4.1 INTRODUCTION

In this chapter the simple strain-space model is examined against two independent sets of data, one based on the experiments performed at Cambridge University (Roscoe and Burland 1968) and the other based on experiments performed for the International Workshop on Constitutive Behavior of Soil held at Grenoble in 1982. In section 4.2, the material constants are determined from the two data sets.

In section 4.3 the model constants α and b_1 are obtained by calibrating the model based on the undrained Cambridge test data, and then the results are compared with the undrained Grenoble test data. By this exercise, the model constants are obtained and the assumption that they are independent of the material is verified.

In the following sections, the model prediction is compared to the two sets of data under constant pressure and cyclic loading conditions. Wherever applicable the stress-space model prediction is also given for comparison.

4.2 EXPERIMENTAL DATA

4.2.1 Cambridge Test Data

The data used to test the elliptic yield surface model prediction is used here to compare with the strain-space prediction. These data

were obtained on Kaolin. Two sets of experimental data are used herein.

The first set of data was obtained by Thurairajah (1961). Thurairajah performed strain-controlled tests on normally consolidated samples of Kaolin. These data were obtained under undrained conditions. Thurairajah's tests were further confirmed by Loudon (1967). Loudon carried out the strain-controlled tests at half the strain rates of Thurairajah's experiments. The agreement of the results of these two tests cleared up any controversy that existed on the former's results.

The second set of data used herein is from tests performed by Walker (1965). These were stress- controlled triaxial tests. The specific data used herein are for the constant pressure triaxial test.

From both the tests it has been established that for Kaolin,

$$\lambda = 0.27 \qquad \text{(a)}$$

$$\kappa/\lambda = 0.15 \quad \text{and} \qquad \text{(b)}$$

$$M = 0.9 \qquad \text{(c)} \ . \qquad (4.1)$$

The accuracies of these experiments are not given; neither can they be ascertained without the raw data.

4.2.2 Grenoble Test Data

The test data analyzed below were prepared for the International Workshop on Constitutive Behavior of Soils held at Grenoble in 1982. These tests were performed under controlled conditions on a synthetic clay. Unlike the Cambridge test data, the material constants are not

given. For this reason, it is necessary to determine the material constants based on the test data.

Figure (4.1) shows the test results for a one-dimensional consolidation test. These results are plotted on a set of a semi-log axes. The lines of best fit are calculated for the loading and loading-unloading paths. From the slopes of these lines the material constants λ and K are estimated to be as follows;

$$\lambda = 0.21 \quad \pm 15\% \quad \text{(a)}$$

$$K = 0.032 \quad \pm 38\% \quad \text{(b)} \quad . \qquad (4.2)$$

The value of λ was obtained using the method of least squares. The possible error in λ is estimated from the accuracy of the given data. A larger number of data points and/or more accurate measurements would greatly improve the results. The value of K is taken to be the arithmetic average of the slopes of the lines AB, AC, DE and DF shown in Figure (4.1). These slopes show a variation of ±38 about the mean.

An error estimate on the determination of λ and K is essential so that any deviations between the experimental and model prediction can be compared in the light of the accuracy of the model constants as determined from experiment. In the case of Cambridge data, such an estimation is not possible without the raw data for λ and K.

From the test data it can be seen that the critical state ratio, M, should be such that

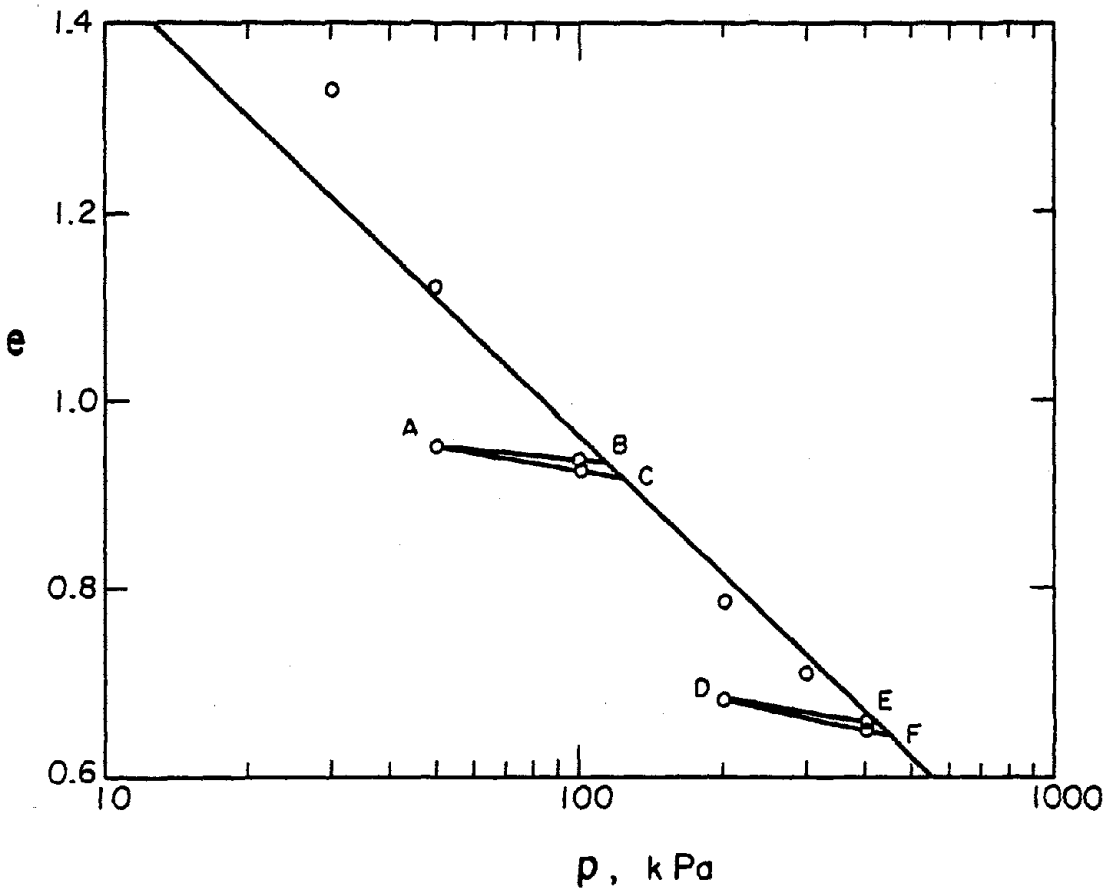

FIGURE 4.1 DETERMINATION OF MATERIAL CONSTANTS

$$M \geq 0.78 \quad . \tag{4.3}$$

The model computations are made for

$$M = 0.78 \quad . \tag{4.4}$$

It is necessary to note at this point that the void ratios for the same effective pressure varies from experiment to experiment. A sensitivity test for the model prediction was conducted based on these variations in the void ratio e.

4.3 UNDRAINED TRIAXIAL TESTS

4.3.1 Model Equations

In this section the incremental constitutive equations of the stress-space and the strain-space models are solved to obtain material response. The variables under consideration are e, ε, p, q and η, where η depends directly on p and q. The models are used to determine the following relations;

$$\begin{aligned} q &= q(\varepsilon) \qquad (a) \\ p &= p(\varepsilon) \quad . \quad (b) \end{aligned} \tag{4.5}$$

From equations (4.5a) and (4.5b) the stress trajectory $f(p,q) = 0$ and the relationship of η with ε can be deduced. Since the load case under consideration is undrained, the variable e remains constant at its initial value and is hence not shown in the relations explicitly.

The strain-space model results in

$$q = M p_o \exp\left[-\frac{\gamma\lambda}{K}(1-\xi_o)\left(1-\exp\left(-b_1\frac{(1+e_o)(\varepsilon-\varepsilon_o)}{\lambda}\right)\right)\right]$$

$$\cdot\left[1-(1-\xi_o)\left(\exp\left(-b_1\frac{(1+e_o)(\varepsilon-\varepsilon_o)}{\lambda}\right)\right)\right]^{(1-\alpha)} \qquad (a)$$

$$p = p_o \cdot \exp\left[-\frac{\gamma\lambda}{K}(1-\xi_o)\left(1-\exp-\frac{b_1(1+e_o)(\varepsilon-\varepsilon_o)}{\lambda}\right)\right] \qquad (b) \qquad (4.6)$$

where,

$$\gamma = (\lambda-K)/\lambda$$

$$\lambda = K\log_e 2$$

$$\xi = \frac{e-\hat{e}}{\lambda}$$

and the suffix o denotes initial values.

From equations (4.6a) and (4.6b) it follows that the stress trajectory is given by,

$$\log_e\left(\frac{p}{p_o}\right) + \gamma\left[\frac{\frac{q}{p}-\frac{q_o}{p_o}}{M}\right]^2 \log_e 2 = 0 \quad . \qquad (4.7)$$

And the relationship of η with ε is given by

$$\eta = M\left[(1-\xi_o)\left(1-\exp-\frac{b_1(1+e_o)(\varepsilon_o-\varepsilon)}{\lambda}\right)\right]^{(1-\alpha)} \quad . \qquad (4.8)$$

The stress-space model does not give a simple explicit closed form solution. However, it could be solved in parametric form. The equations which must be solved are

$$q = p_o \eta \left(\frac{M^2+\eta_o^2}{M^2+\eta^2} \right)^{\gamma} \qquad (a)$$

$$p = p_o \left(\frac{M^2+\eta_o^2}{M^2+\eta^2} \right)^{\gamma} \qquad (b) \qquad (4.9)$$

where η is related to ε by

$$\varepsilon = \varepsilon_o + \frac{\gamma/K}{M(1+e_o)} \left[\log_e \frac{1+\eta/M}{1-\eta/M} - 2\tan^{-1}(\eta/M) \right.$$

$$\left. - \log_e \frac{1+\eta_o/M}{1-\eta_o/M} + 2 \tan^{-1} (\eta_o/M) \right] \quad . \qquad (4.10)$$

However, the stress trajectory can be solved in closed form and yields

$$\frac{p}{p_o} - \left(\frac{M^2+q_o^2/p_o^2}{M^2+q^2/p^2} \right)^{\gamma} = 0 \quad . \qquad (4.11)$$

4.3.2 Model Calibration Using Cambridge Test Data

In this section, the prediction of the strain-space model and the stress-space model given by equations (4.6) through (4.11) are compared with experimental observations. The purpose of this comparison is to determine the best choice of α and b_1 for the strain-space model.

The constant α is a measure of the change in q for changes in ε around ε_o. From equation (4.6a), it is seen that as $(\varepsilon-\varepsilon_o)$ becomes large the influence of α diminishes. For this reason α is determined by considering the experimental behavior around the point (ε_o, q_o) in the $(\varepsilon-q)$ plane. Both model predictions of $\frac{q(\varepsilon)}{p_o}$ along with the data are shown in Figure (4.2).

The constant b_1 is a measure of the rate at which q/p reaches its asymptotic value M. Since the exponential of b_1 gives the exponential rate of convergence to the asymptote, the rate of convergence is quite sensitive to changes in the constant b_1.

When equations (4.6a) and (4.9a), (4.10) are expanded around (ε_o, q_o), it can be found that for the strain-space model

$$(q-q_o) \sim (\varepsilon-\varepsilon_o)^{1-\alpha} \tag{4.12}$$

and for the stress-space model

$$(q-q_o) \sim (\varepsilon-\varepsilon_o)^{0.2} \quad . \tag{4.13}$$

From Figure (4.2) it is seen clearly that the stress-space prediction for q which is substantially higher than the experimental values. This indicates that the exponent in equation (4.12) should be larger than that of equation (4.13), implying that

$$\alpha < 0.8 \quad .$$

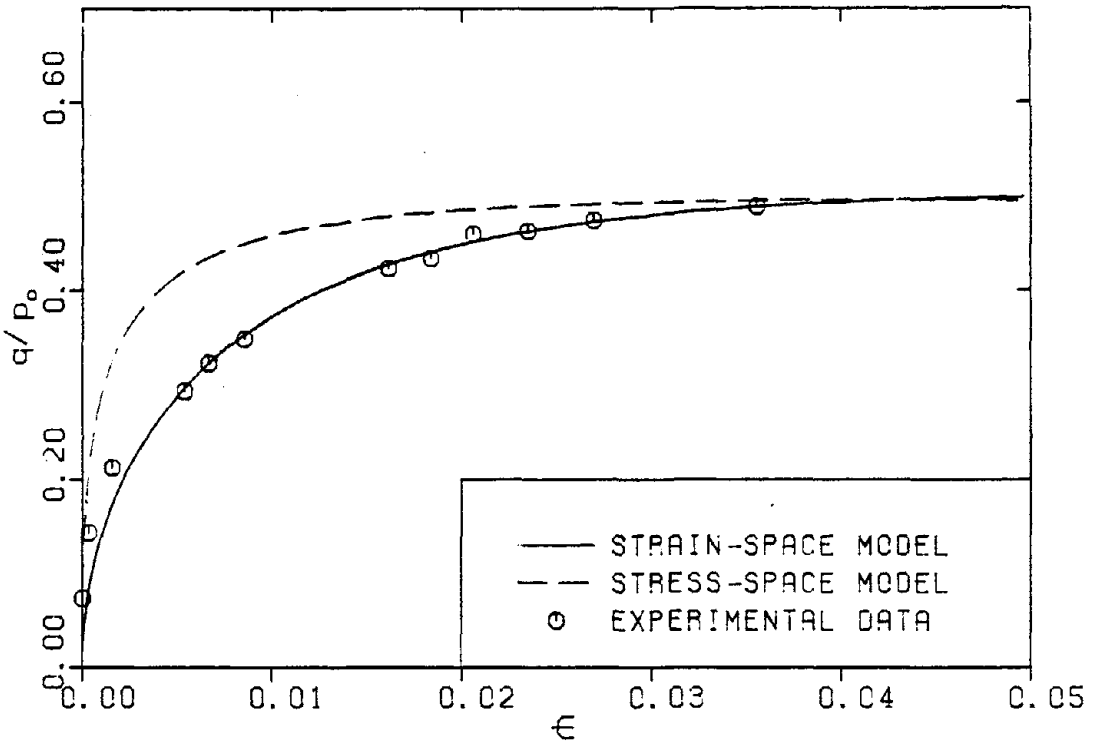

FIGURE 4.2 UNDRAINED TRIAXIAL TEST (KAOLIN)

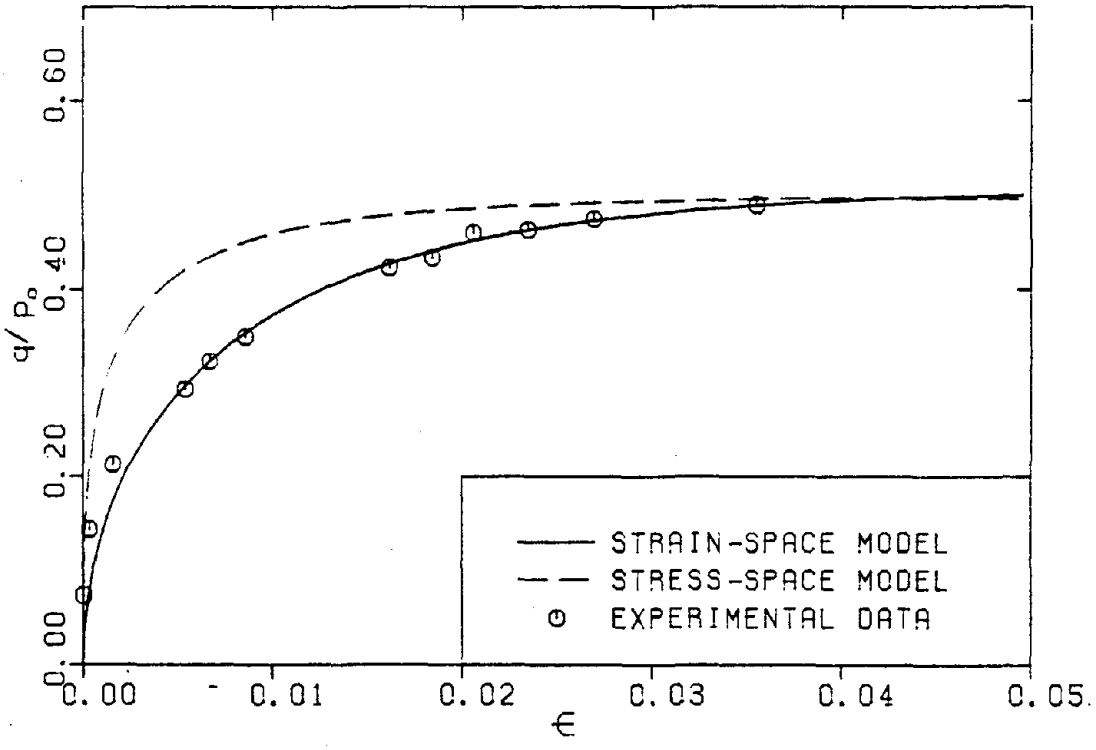

FIGURE 4.3 CALIBRATION FOR MODEL CONSTANT b_1

The value $\alpha = 0.5$ is found to give a good fit to the experimental observation in the neighborhood of (ε_o, q_o). An involved method of curve-fitting leading to a more accurate determination of α is not used at this stage because any higher accuracy of curve fitting would be inconsistent with the experimental accuracies.

Having determined α, the strain-space model prediction for q/p_o as a function of ε is compared with the experimental data for different values of b_1. Figure (4.3) shows the results for several choices of b_1. The value $b_1 = 0.3$ is found to give the best fit to the experimental observations.

For large values of $(\varepsilon-\varepsilon_o)$ the solutions of both the stress-space and strain-space models asymptote to

$$q/p_o = \frac{M}{2\gamma} \quad . \tag{4.14}$$

For Kaolin this value is 0.49.

Equations (4.6b) and (4.9b) with (4.10) give the relationship between p/p_o and ε as predicted by the strain-space and stress-space models, respectively. Pressure data are not available from the Cambridge test. Therefore, only the model predictions are compared. These predictions are shown in Figure (4.4).

Both the stress-space and strain-space model predictions for p asymptote to $\frac{p}{p_o} = \frac{1}{2\gamma}$ for large values of $(\varepsilon-\varepsilon_o)$. For Kaolin, the value of $\frac{1}{2\gamma}$ is 0.56. Since the decay rate of the strain-space model is lower than that of the stress-space model, the strain-space prediction of the pressure is seen to be higher than for the stress-space model. However,

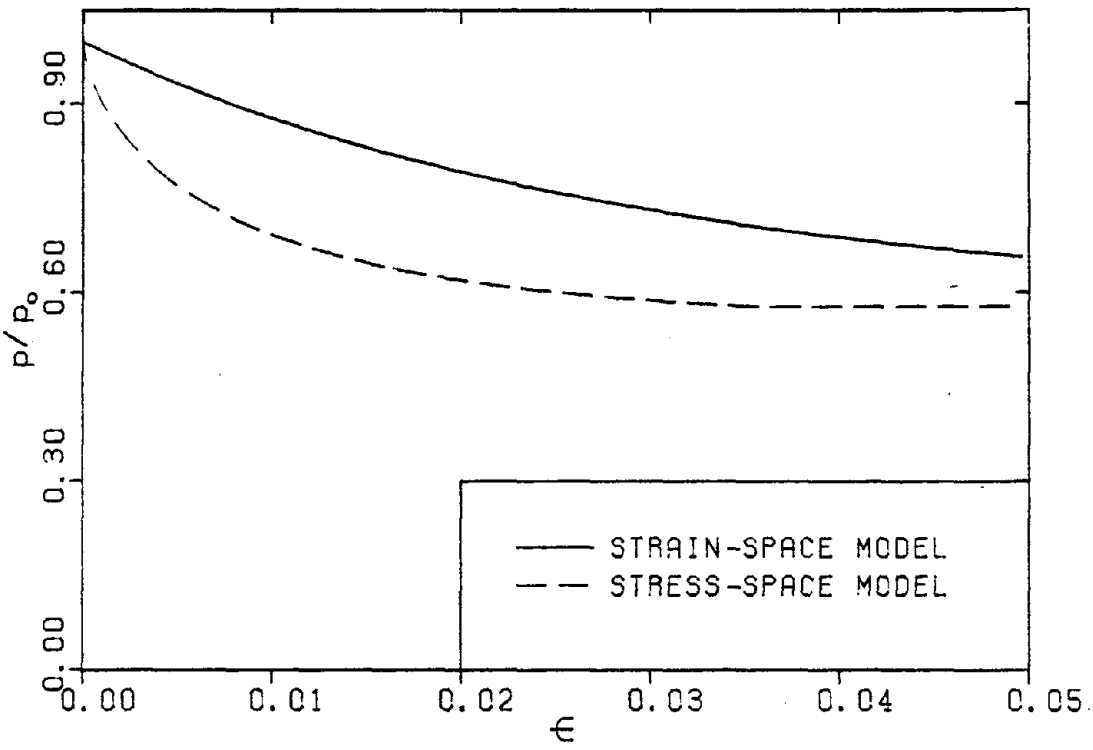

FIGURE 4.4 UNDRAINED TRIAXIAL TEST (KAOLIN)

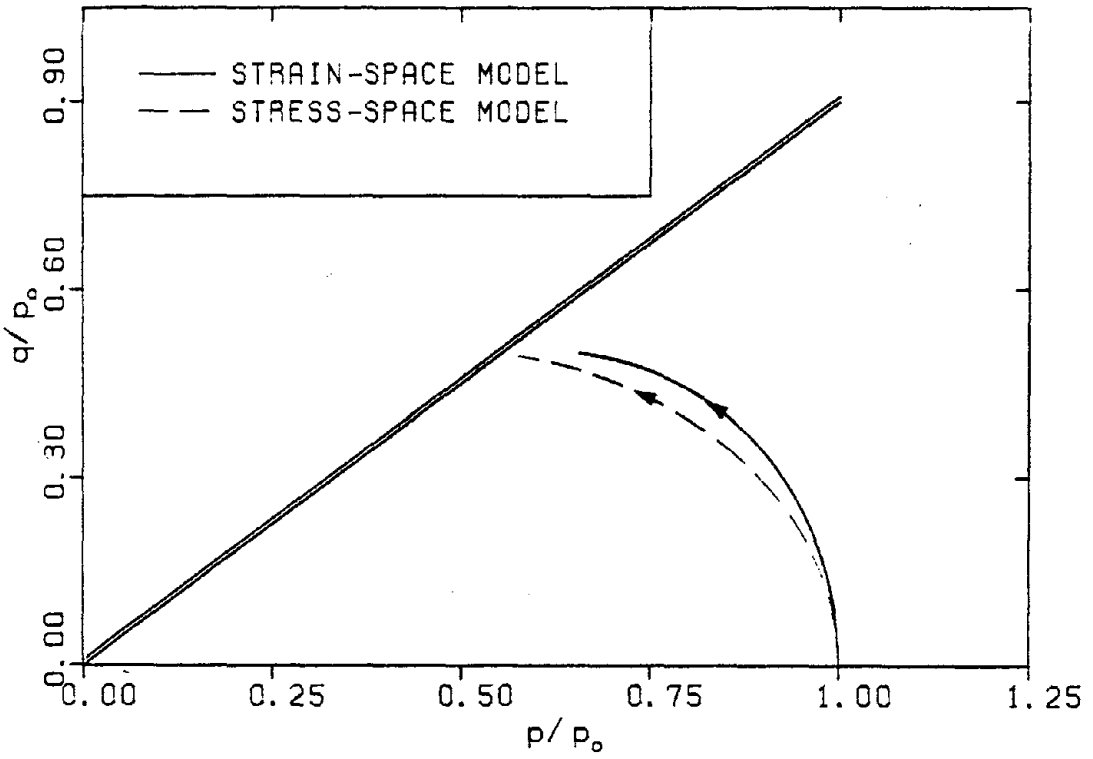

FIGURE 4.5 UNDRAINED TRIAXIAL TEST (KAOLIN)

the lower decay rate appears more consistent with the experimental observations presented in Figure (4.2).

The strain-space model yields a stress trajectory for undrained loading given by equation (4.7) and the stress-space prediction is given by equation (4.11). Both trajectories are shown in Figure (4.5). They each start with infinite slope in the $p/p_o - q/p_o$ plane, and they both intersect the critical state line at

$$p = \frac{p_o}{2\gamma} \qquad \text{(a)}$$

$$q = M\frac{p_o}{2\gamma} \qquad \text{(b)} \quad . \qquad (4.15)$$

However, at the point of intersection of the critical state, the two trajectories have different slopes. The slope of the trajectory implied by the stress-space model is given by

$$\frac{dq}{dp} = -\frac{1}{\gamma} \quad , \qquad (4.16)$$

whereas that of the strain-space model is given by

$$\frac{dq}{dp} = -\frac{M}{2\gamma \log_e 2} \quad . \qquad (4.17)$$

The slope predicted by the strain-space model is smaller than that predicted by the stress-space model by a factor of 0.721 M. For Kaolin this factor would be 0.649. This implies that for the strain-space model to have no change in void ratio close to critical state, there must be greater reduction in pressure to shear stress compared to the stress-space model. However, during the initial stages of loading, the

strain-space model requires more change in shear stress than the stress-space model to maintain undrained conditions.

From the results obtained thus far, it is evident that the simple strain-space model captures all of the qualitative behavior of the data and the stress-space model. Having established this, the Grenoble test data will be used to further demonstrate the accuracy of the strain-space model.

4.3.3 Comparison with Grenoble Test Data

This section uses the values for the model constants α and b_1 determined from section 4.3.2. These values are

$$\alpha = 0.5$$
$$b_1 = 0.3 \quad .$$

The strain-space results with these model constants are plotted with the stress-space prediction and the test data. The material constants used are as follows:

$$\lambda = 0.21$$
$$\kappa = 0.032$$
$$M = 0.78 \quad .$$

Figures (4.6) and (4.7) show the strain-space and stress-space model predictions of the variation of pressure along with the experimental data.

The strain-space model clearly shows much better agreement with the test data compared to the stress-space model. One aspect in which the

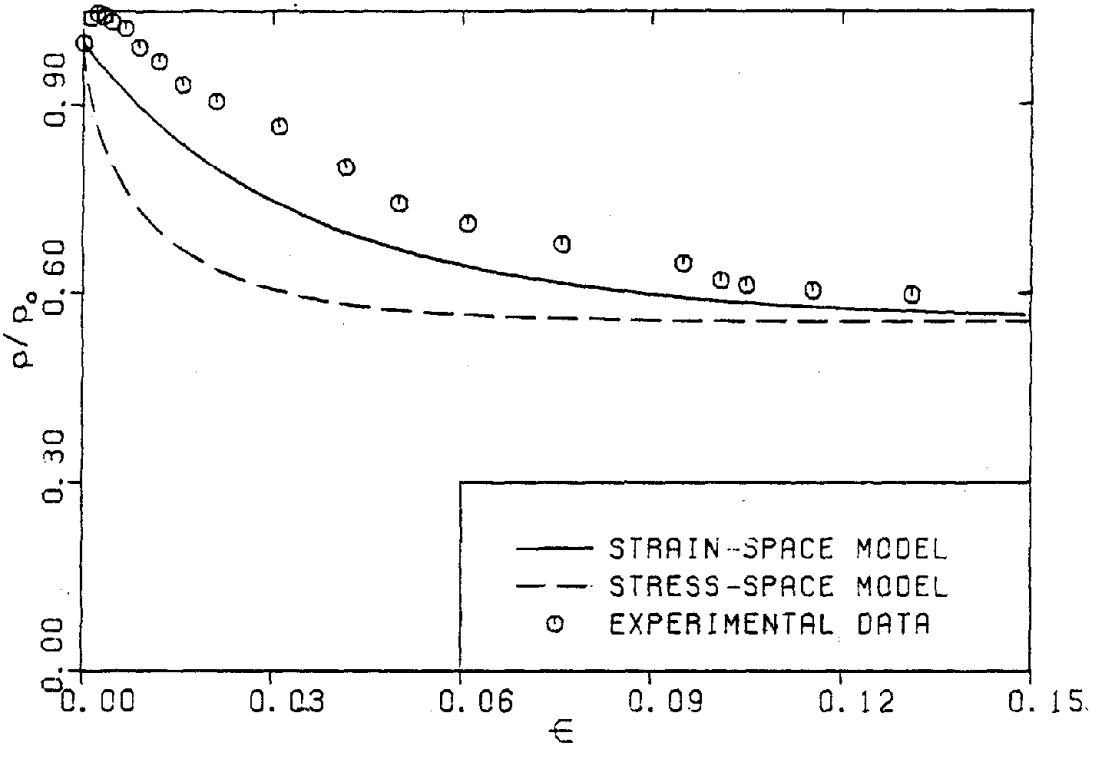

FIGURE 4.6 UNDRAINED TRIAXIAL TEST (GRENOBLE, 1982)

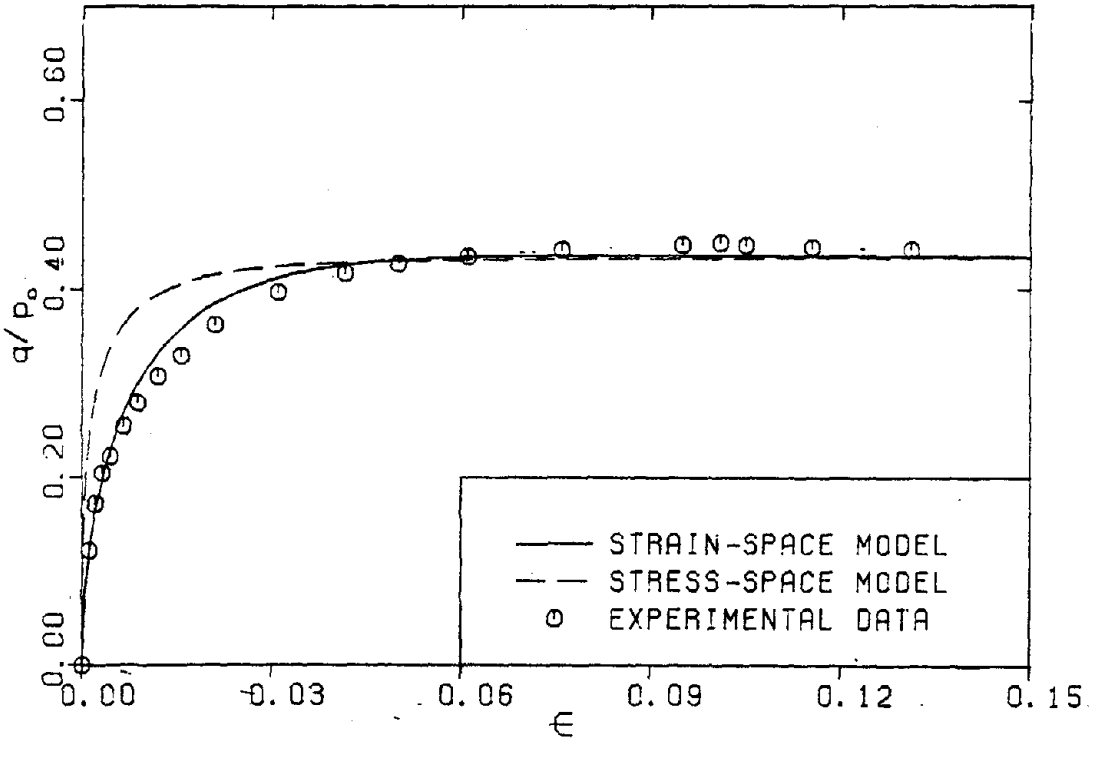

FIGURE 4.7 UNDRAINED TRIAXIAL TEST (GRENOBLE, 1982)

experimental results differ from both model predictions is the initial increase in pressure with shear strain. It is believed that this difference is not due to inaccurate model prediction but rather to inaccuracies in the experimental data. If the clay was actually saturated, it would not be possible to have such a pressure increase. However, if the model was not completely saturated, an increase could occur. The rest of the behavior observed experimentally is predicted very well by the model.

Figure (4.7) shows for both model predictions the variation of the shear stress with the shear strain. Once again the strain-space model predicts results which are much closer to the data as compared to the stress-space prediction. It can also be seen that the stress-space model reaches critical state much faster than the strain-space model and the test data.

Figure (4.8) shows the stress trajectories. Again, the strain-space model prediction is better as expected from the individual p/p_o and q/p_o predictions. The discrepancy with the data around the beginning of the trajectory is believed to be due to experimental errors as discussed above. One further effect observed in the experimental trajectory is the slight decrease of q around critical state line. The basic physics used in the model does not predict such behavior. If it is found that this behavior is important, the model will have to include some additional basic physical behavior. However, at this point it is not clear whether this behavior is real or is due to experimental inaccuracies.

Figure (4.9) shows the variation of η with the shear strain.

4.3.4 Model Constants

In section 4.3.2 the strain-space model was calibrated using the Cambridge test data. From this comparison it was determined that

$$\alpha = 0.5$$
$$b_1 = 0.3 \quad .$$

These constants were postulated to be independent of the material. This postulate has been verified by using the results of the Grenoble experiments. Therefore, these constants will be assigned the numerical values stated above and treated as an integral part of the model. This results in there being only three constants to be evaluated for any material and they may be obtained from well-established experiments.

4.4 CONSTANT PRESSURE TRIAXIAL TEST

4.4.1 Model Equations

For constant pressure tests,

$$dp = 0 \quad .$$

This condition is easily incorporated into the stress-space model as p is one of the independent variables. For the strain-space model the condition that the incremental pressure is zero has to be imposed

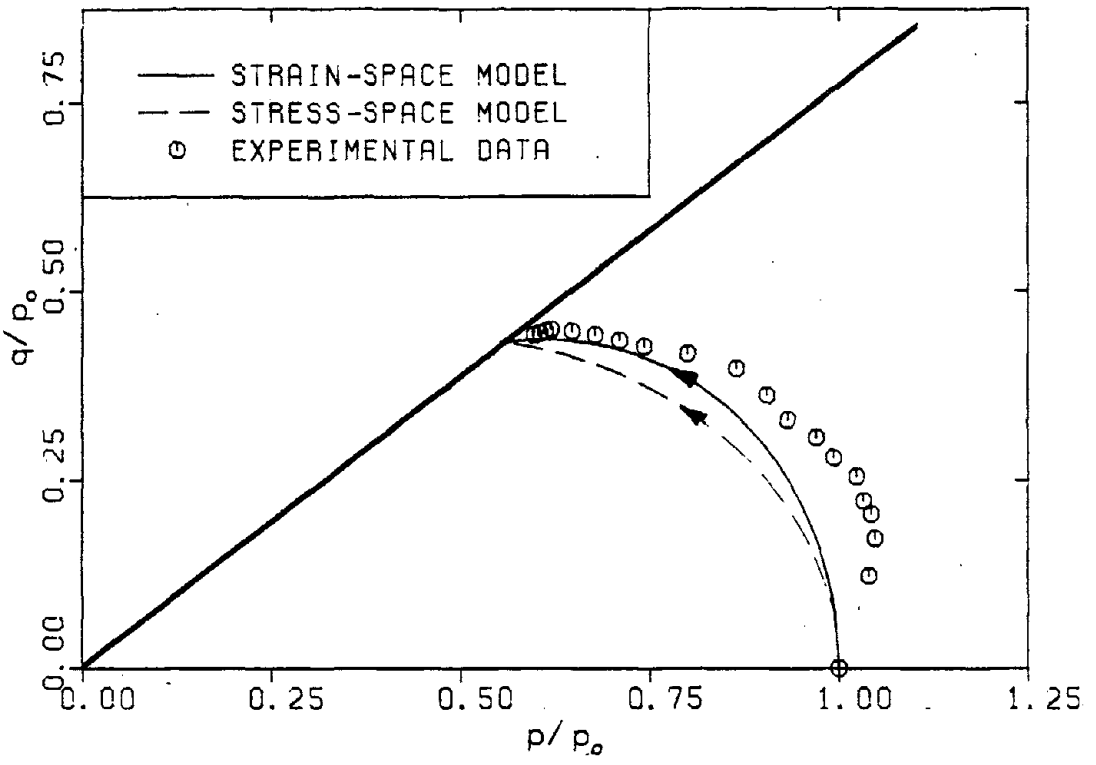

FIGURE 4.8 UNDRAINED TRIAXIAL TEST (GRENOBLE, 1982)

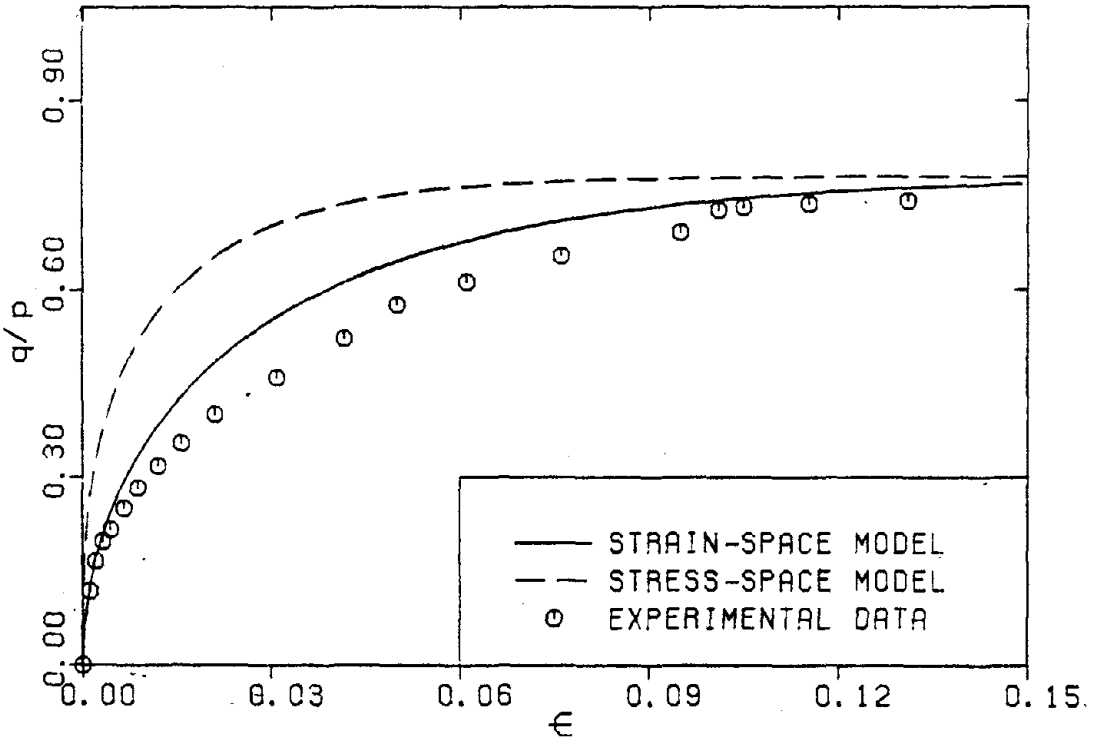

FIGURE 4.9 UNDRAINED TRIAXIAL TEST (GRENOBLE, 1982)

implicitly. However, this results in the simple incremental condition that

$$\hat{de} = \frac{1}{\gamma} de \quad .$$

This condition gives way to a closed form solution for η, given by

$$\eta = \eta_o + (M-\eta_o)\left[\frac{e_o-e}{(\lambda-\kappa)\log_e 2}\right]^{0.5} \quad . \qquad (4.18)$$

The stress-space model produces the result that

$$\eta = \eta_o + (M-\eta_o)\left[\exp\frac{e_o-e}{\lambda-\kappa} - 1\right]^{0.5} \quad . \qquad (4.19)$$

For values of e close to e_o which implies state points close to the initial state, equation (4.19) can be approximated as

$$\eta = \eta_o + (M-\eta_o)\left[\frac{e_o-e}{\lambda-\kappa}\right]^{0.5} \quad . \qquad (4.20)$$

From equations (4.18) and (4.20) it is clear that the two models behave very similarly close to the initial loading state and differ only by a scaling constant of

$$\left(\frac{1}{\log_e 2}\right)^{0.5} = 1.2 \quad .$$

Once again, the strain-space model provides an explicit closed form solution for the relationship between η and ε given by

$$\eta = \eta_o + (M-\eta_o)\left[1-\exp \frac{-0.3[(1+e)\varepsilon-(1+e_o)\varepsilon_o]}{\lambda \log_e 2}\right]^{0.5} (1-\xi_o)^{0.5} \quad . \qquad (4.21)$$

However, the stress-space model yields only an incremental solution which cannot be integrated in closed form. This stress-space result is given by

$$\varepsilon-\varepsilon_o = \int_{\eta_o}^{\eta} \frac{\lambda-K}{1+e} \frac{4\eta^2}{M^4-\eta^4} \cdot d\eta \quad , \qquad (4.22)$$

where $e = e(\eta)$ and is given by equation (4.19).

For the strain-space model, the strain trajectory necessary to produce constant pressure is found to be given by

$$e_o - e = (\lambda-K)(\log_e 2) \cdot (1-\xi_o)\left[1-\exp \frac{-0.3[(1+e)\varepsilon-(1+e_o)\varepsilon_o]}{\lambda \log_e 2}\right] \qquad (4.23)$$

For the stress-space model, the constant pressure condition results in e and ε related by

$$\varepsilon-\varepsilon_o = -\int_{e_o}^{e} \frac{2(M-\eta_o)^3\left[\exp \frac{e_o-e}{\lambda-K}-1\right]^{0.5} / (1+e)}{(\lambda-K)\left[M^4-(M-\eta_o)^4\left[\exp \frac{e_o-e}{\lambda-K}-1\right]^2\right]} \cdot de \qquad (4.24)$$

4.4.2 Comparison with Cambridge Test Data

The results of the calculations for $\eta(e)$ made with the stress-space model and the strain-space model along with the test data of Walker (1965) are shown in Figure (4.10). It can be seen from this

figure that both models predict results in agreement with the experimental data, the stress-space model predicting the experimental observations more closely around the inception of loading and the strain-space model predicting better elsewhere.

From equations (4.18) and (4.19) it is seen that both predictions of η reach the critical state value, M, when

$$(e_o - e) = (\lambda - K) \log_e 2 \quad .$$

For Kaolin this value is 0.155, and M is 0.90. The experimental data, though not available for values of $(e_o - e)$ close to 0.155, indicate that this could be an accurate prediction for $(e_o - e)$ at critical state.

Figure (4.11) shows both model predictions along with the test data for the function $\eta(\varepsilon)$. The stress-space prediction of η for any given value of ε under constant pressure loading is somewhat higher than the experimental values while that of the strain-space model is somewhat lower. The closeness of prediction of both models to the experimental observations is comparable. It is seen that the strain-space model prediction of η with e lies above the stress-space model prediction in the (η, e) plane, whereas in the (η, ε) plane the strain-space model prediction lies below the stress-space model prediction. The reason for such a change is clearly seen by observing the strain trajectories for constant pressure conditions implied by the two models.

The trajectories given by equations (4.23) and (4.24) are plotted in Figure (4.12). From equation (4.23) it is seen that

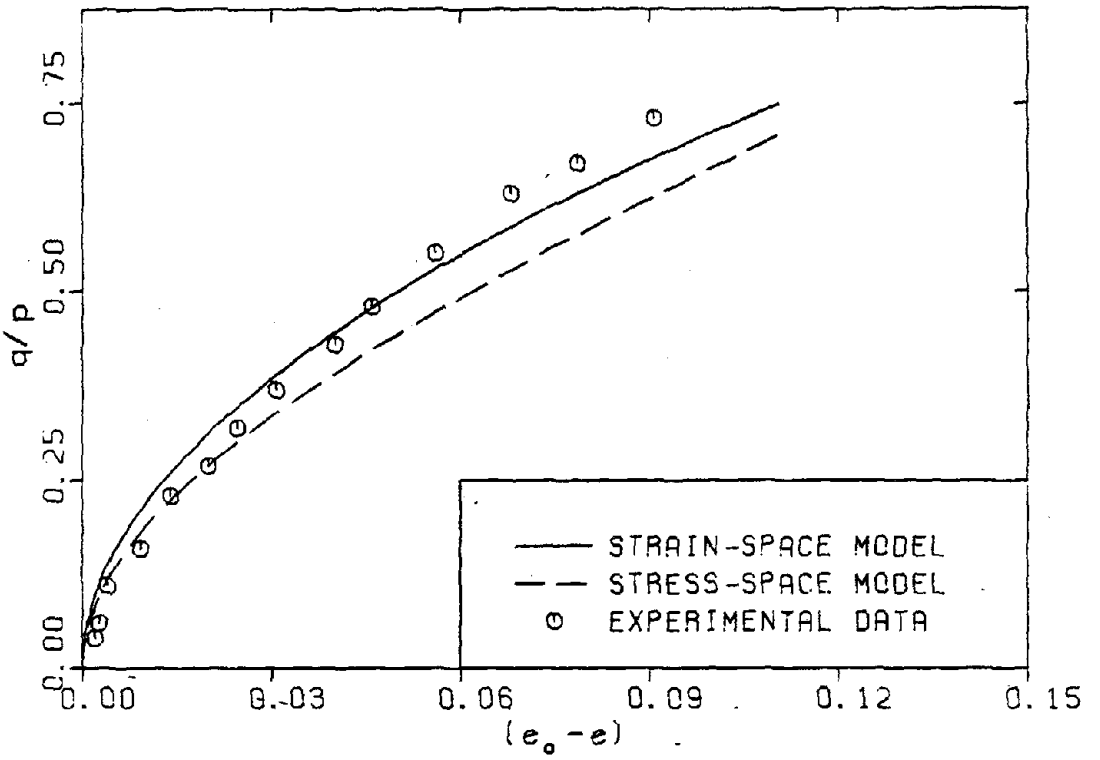

FIGURE 4.10 CONSTANT PRESSURE TRIAXIAL TEST (KAOLIN)

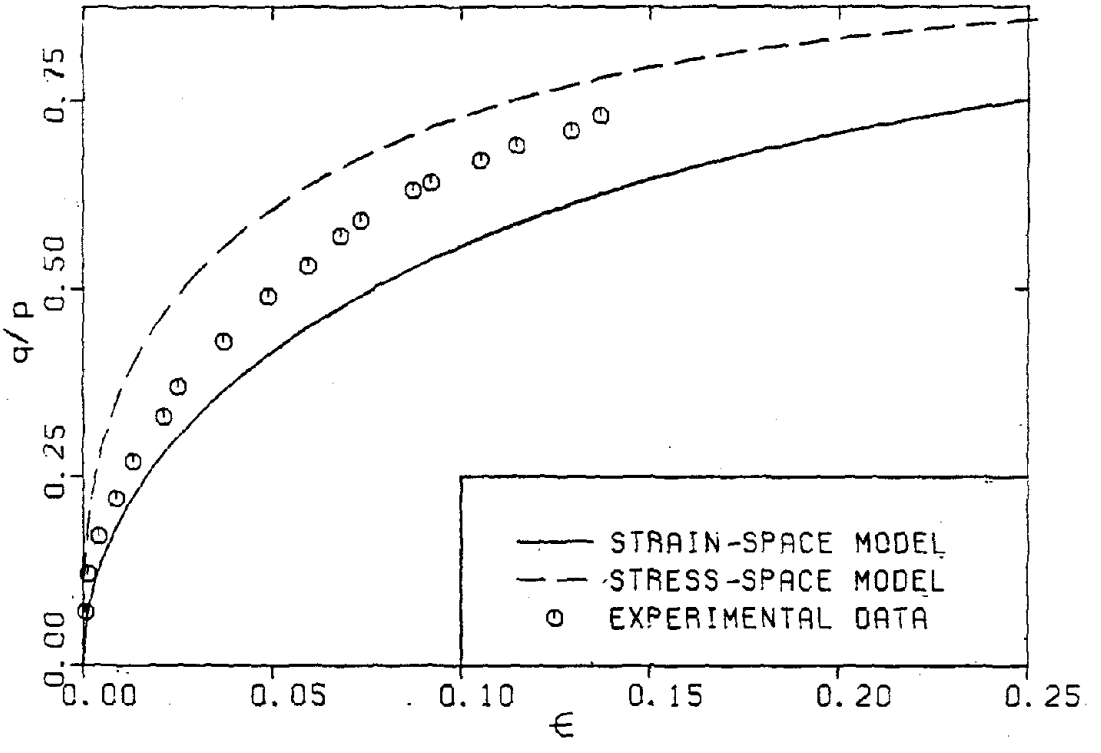

FIGURE 4.11 CONSTANT PRESSURE TRIAXIAL TEST (KAOLIN)

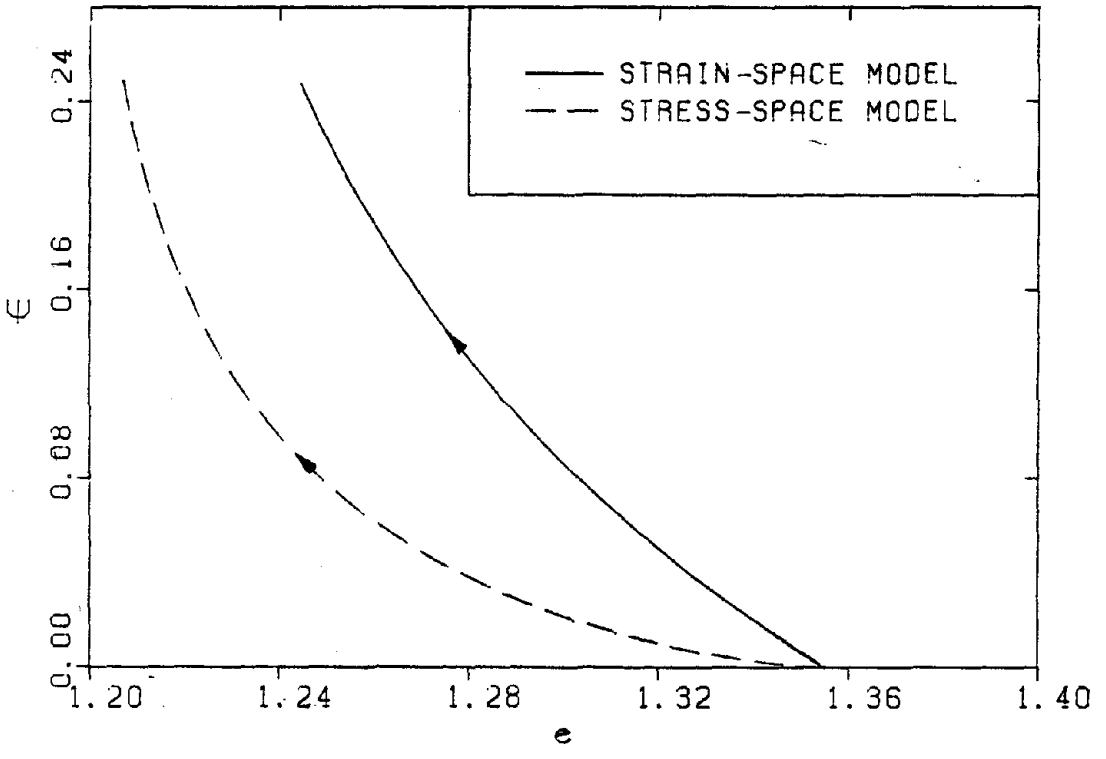

FIGURE 4.12 STRAIN TRAJECTORY FOR THE CONSTANT PRESSURE TRIAXIAL TEST (KAOLIN)

$$\varepsilon \rightarrow \infty \quad \text{as} \quad (e_o - e) \rightarrow (\lambda - \kappa) \log_e 2 \quad .$$

For the case shown in Figure (4.12) this occurs when

$$e = 1.20 \quad .$$

The numerical evaluation of equation (3.56) shows that the asymptotic value of e for the strain-space model is also 1.20. However, the stress-space model, due to its faster rate of reaching critical state, reaches the asymptote faster than the strain-space model.

The reason for the stress-space prediction being below the strain-space prediction in the $(e_o-e)-\eta$ plane but above the strain-space prediction in $(\varepsilon-\eta)$ plane is found in the strain trajectories predicted by the two models. For a given value of (e_o-e), the corresponding value of ε for the strain-space model is much larger than that of the stress-space model. This effect results in the stress-space prediction of the (η,ε) relation being pushed towards larger ε compared to the stress-space prediction. Since the two curves are close together in the $(e_o-e)-\eta$ plane, the effect of the strain trajectory is larger in magnitude and hence pushes the strain-space curve in the $(\varepsilon-\eta)$ plane below the corresponding stress-space curve.

4.5 CYCLIC LOADING TESTS

The soil models commonly in use fail to predict cyclic test results very well. The stress-space model considered herein fails to predict any hysteretic loops. For this reason the experimental observations are

compared only to the strain-space model. Load reversals considered herein are only for undrained conditions. Such an analysis has a wide scope of application for most reversals encountered commonly in practice. For example, earthquake loads have periods much smaller than that of the drainage time for most clays. When the material is subject to one cycle of such high frequency load it would not have drained by any significant amount. Therefore, the assumption that the response is undrained is well justified.

4.5.1 Model Equations

For load reversal under undrained conditions,

$$\xi = 1 - (1-\xi_o) \exp \frac{-b_1(1+e_o)(\varepsilon-\varepsilon_o)}{\ell} \qquad (a)$$

$$\hat{e} = e_o - \ell\xi \qquad (b)$$

$$p = p_o \exp\left[\frac{-\gamma\ell}{K}(1-\xi_o)\left(1-\exp\frac{-b_1(1+e_o)(\varepsilon-\varepsilon_o)}{\ell}\right)\right] \qquad (c)$$

$$d\eta = (1-\alpha)\, M \left|\frac{\xi-\xi_o}{1+c}\right|^{-\alpha} \operatorname{sgn}(d\varepsilon) \cdot d\xi \qquad (d) \quad (4.25)$$

where,

$$\gamma = (\lambda-K) / \lambda$$

$$\ell = K \log_e 2$$

$c = 0$ if $|\varepsilon| > \max [|\varepsilon_{-1}| , |\varepsilon_o|]$

$= 1$ otherwise

ε_o = value of ε at the last lineup of load reversal

ε_{-1} = of ε at the point of load reversal before the last one.

4.5.2 Comparison with Cambridge Test Data

Monotonic undrained test results of Roscoe and Burland (1968) were used to calibrate the strain-space model in section 4.3.2. In this section small load reversals are imposed on the previously monotonic loading. The strain-space prediction along with the experimental observations for the loading with reversals are shown in Figure (4.13). The model prediction is remarkably close to the experimental observations. It is not surprising that the monotonic parts of the curve are well predicted as the model has been calibrated for monotonic loading.

Several salient aspects observed experimentally during load reversals are well captured by the strain-space model. These are:

1. As the loading progresses, the hysteresis loops become larger. This is achieved by the model because of the proximity of the latter points of reversal to the critical state. As the material gets closer to the critical state, the pressure reduces. Since the shear stiffness predicted by the model is proportional to the pressure, the reduction in pressure results in softening. This gives rise to larger hysteresis loops.

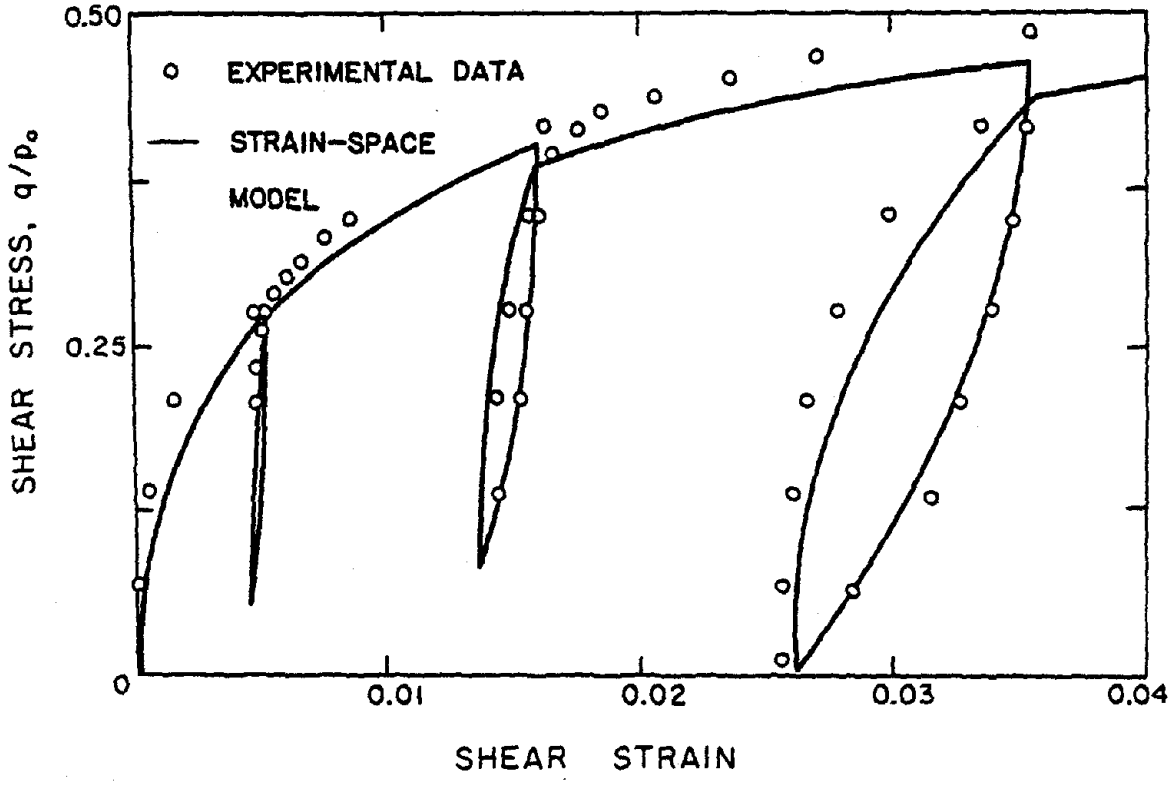

FIGURE 4.13 UNDRAINED TRIAXIAL TEST WITH LOAD REVERSAL (KAOLIN)

2. On load reversal, when the shear strain returns to the value at which the loading was reversed, the shear stress reaches a value lower than the value at the inception of load reversal. This is seen in both the experimental observations and the model prediction. The Bauschinger effect by itself implies that on return to the initial strain, the stress would be the same. But the strain-space model applies the Bauschinger effect to the (η,ξ) relationship. Since

$$q = \eta \cdot p \quad ,$$

and during a complete loop the pressure would have decreased, the value of q would be less on return although the value of η is the same on return.

On continued loading after a reversal, the strain-space model exhibits a discontinuity in the slope, whereas the experimental observations imply a smooth curve. The discontinuity arises because of the switching condition described in equation (4.25). However, as the hysteresis loops get larger, the discontinuity on the slope reduces significantly.

4.5.3 Comparison with Grenoble Test Data

Next, the strain-space model is used to predict cyclic behavior between fixed strains. This prediction is compared with the test data prepared for the International Workshop on Constitutive Behavior of Soils held in Grenoble in 1982. The tests were performed under controlled conditions on a synthetic clay. Figures (4.14a) and (4.14b)

show the test data and model prediction, respectively, for the variation of the octahedral shear stress with axial strain.

The model predicts shakedown and a limit cycle. But the shakedown predicted by the model is very rapid at the beginning and hence reaches the limit state more quickly than the test data. The rate of shakedown depends greatly on the pressure behavior.

The limit cycle is reached between 45kPa and -36kPa for the test data and between ±35kPa for the model. The maximum stress reached is 60kPa on for the test data and -59kPa for the model prediction. These values are within allowable errors. More importantly, the basic characteristics seen in the test data are all captured by the model except for one.

From the test data it is seen that, on reversal, the material reaches an octahedral stress of 60kPa which is higher than the stress at reversal, 55kPa. This implies a kinematic hardening of a negative sense combined with isotropic hardening. That is, the center of the loading surface moves in a direction opposite to that of loading. This is very uncommon in conventional plasticity. Unless such a hardening is built into the strain-space model it will not predict such higher stresses on reversal. However, the experimental observations made by Walker shown in Figure (4.13) do not show the effect observed in the Grenoble test data. As such, more experimental data are necessary to make any conclusions regarding this negative "kinematic" hardening.

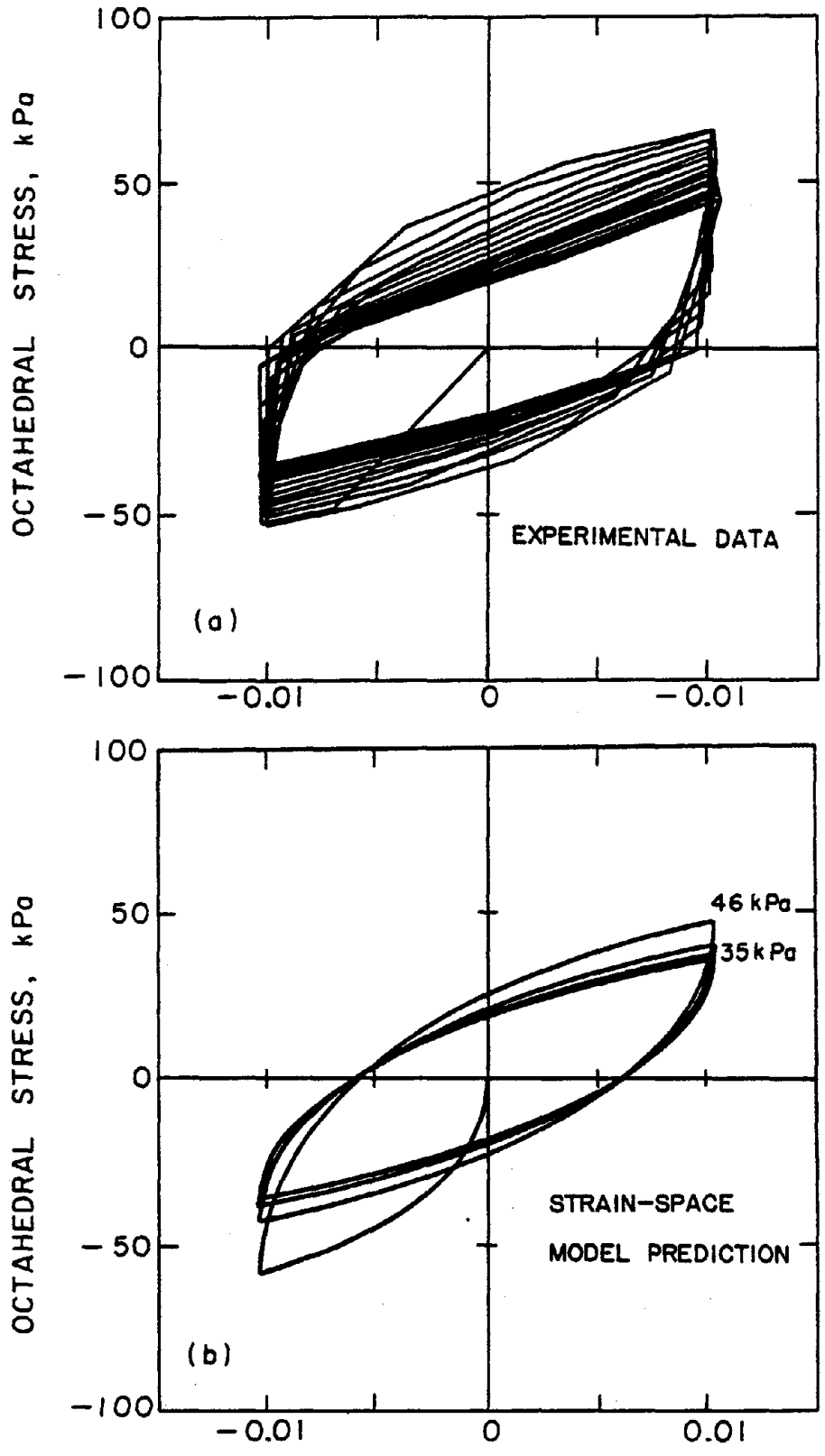

FIGURE 4.14 UNDRAINED CYCLIC TRIAXIAL TEST (GRENOBLE, 1982)

One other possibility is that the material behaves differently in compression and in tension. The material may have different values of M in tension and in compression. From the experimental data if it is seen that indeed this is the reason, then the value of M would be larger in tension than in compression. This can be very simply included in the model by replacing M by either M_e or M_c, depending on whether it is tension or compression, respectively.

In Figures (4.15a) and (4.15b) the Grenoble test data and the strain-space model predictions are shown for the variation of pressure with strain. It is seen that the strain-space model predicts shakedown but at a rate faster than that of the test data. This can, however, be improved by making the model calibration constant b_1 depend on strain.

A second and more important difference arises from the loops described by the test data. The strain-space model does not predict these loops because the plastic variable $\hat{e}$ is modelled to vary monotonically with cyclic variations of ε. According to Terzaghi's equation, p depends only on e and $\hat{e}$. For undrained loading the relationship further simplifies to

$$p = p(\hat{e}) \quad .$$

From the modeling of plastic hardening, $\hat{e}$ is expressed as a function of ε. The relationship given by Terzaghi for p as a function of $\hat{e}$ is monotonic. Hence, it follows that for there to be loops in the $p-\varepsilon$ plane, $d\hat{e}$ should change sign depending on the change of sign of $d\varepsilon$. More data

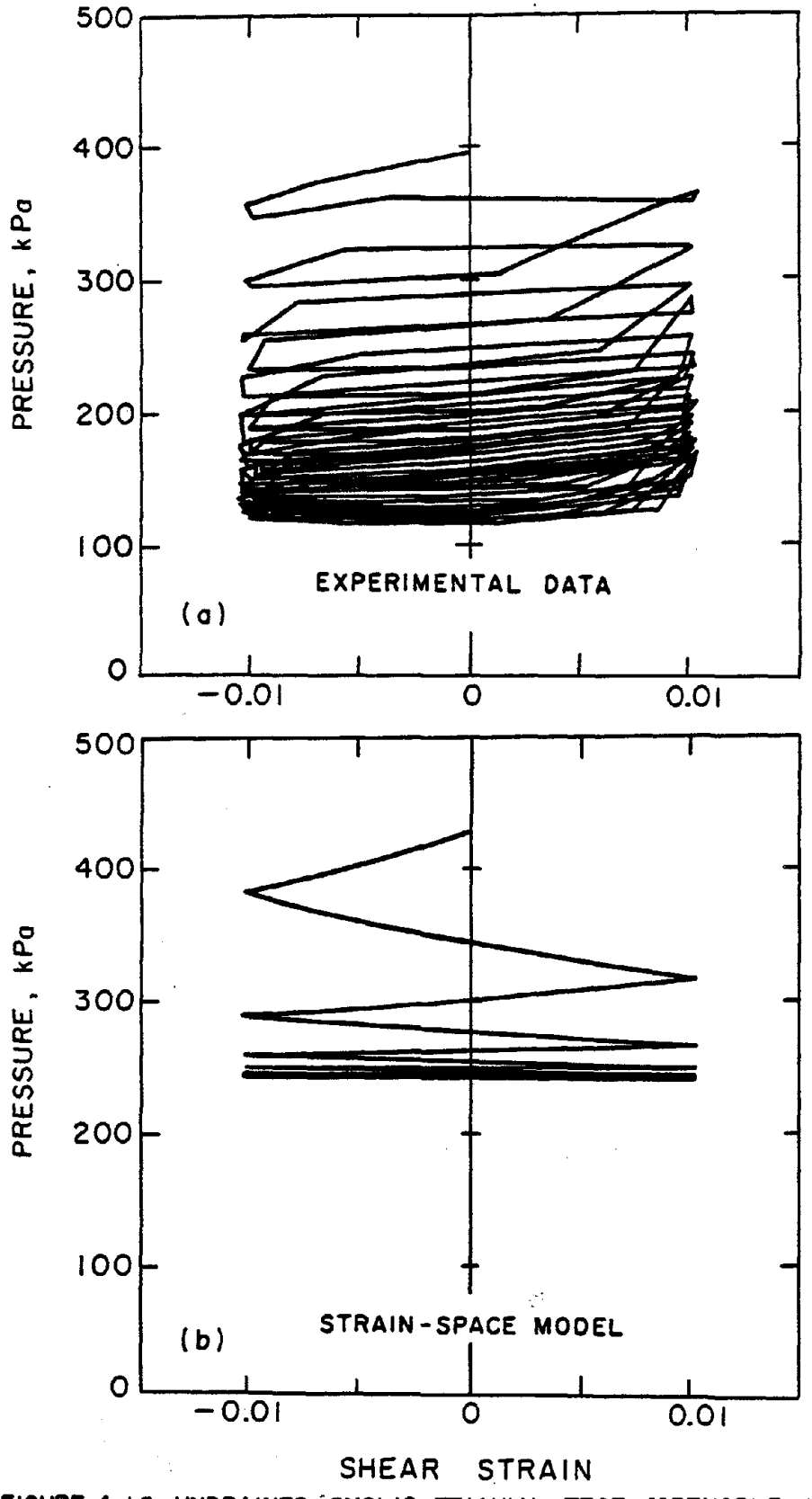

FIGURE 4.15 UNDRAINED CYCLIC TRIAXIAL TEST (GRENOBLE, 1982).

substantiating such pressure loops would be necessary to build such an effect into the strain-space model.

4.5.4 Comparison with Other Models

In this section, the strain-space model is compared with two stress-space models for the case of cyclic loading between constant strain limits described in the previous section. The models used in this comparison are,

i) The Dafalias-Herrmann model (Dafalias, 1979; Dafalias, et al., 1980, 1982). This model is based on the bounding surface theory developed by Dafalias. It has nine material constants.

ii) A critical state model by Houlsby, Wroth and Wood (1982). Houlsby, et al., developed a model based on the modified Cam-Clay model, incorporating Hvorslev's failure criterion. This model is named by the authors as the Roscoe-Hvorslev model. This has six material constants.

The material constants used in the Dafalias-Herrmann model are:

1. Slope of the normal consolidation line in the $\log_e p$-e plane, λ.
2. Slope of the elastic swelling line in the $\log_e p$-e plane, K.
3,4. Critical state constants, M_e, M_c.
5. Shear modulus, G.
6,7. Characteristic lengths of the bounding surface, R_e, R_c.
8,9. Another set of characteristic lengths of the bounding surface, A_e, A_c.

The Dafalias-Herrmann model predictions shown here are from the paper presented by Dafalias, et al., at the Grenoble workshop (1982). The values used for the material constants are given in Table (4.1).

TABLE 4.1

λ	K	M_e	M_c	R_e	R_c	A_e	A_c	G
0.20	0.1	0.8	0.78	2.0	2.5	0.02	0.02	15 MPa

The material constants used in the Roscoe-Hvorslev model are:

1. Critical state constant, M.
2. Slope of the normal consolidation line in the $\log_e p - \log_e v$ plane, λ^*.
3. Slope of the elastic swelling line in the $\log_e p - \log_e v$ plane, K^*.
4. Shear modulus, G.
5. Critical specific volume at unit pressure Γ.
6. Hvorslev surface intercept α.

The Roscoe-Hvorslev model predictions shown herein are taken from the proceedings of the International Workshop on the Constitutive Behavior of Soils, held at Grenoble in 1982. These predictions are made by the proponents of the model, namely, Houlsby, Wroth, and Wood. The values used for the material constants are given in Table (4.2).

TABLE 4.2

M	λ^*	κ^*	G	Γ	α
0.74	0.1225	0.0165	7MPa	undetermined	0.141

The strain-space model, as described herein, uses solely three material constants. They are:

1. Slope of the normal consolidation line in the $\log_e p$ - e plane, λ.
2. Slope of the elastic swelling line in the $\log_e$ - e plane, κ.
3. Critical state constant, M.

The values of these three constants are shown in Table (4.3).

TABLE 4.3

λ	κ	M
0.21	0.032	0.78

Figure (4.16) shows the variation of the shear stress with axial strain. The loading is between constant strain limits of ±0.010. The figure contains four curves. These curves are predicted by,

i) The Grenoble experimental data,

ii) The Dafalias-Herrmann model,

iii) The Roscoe-Hvorslev model, and

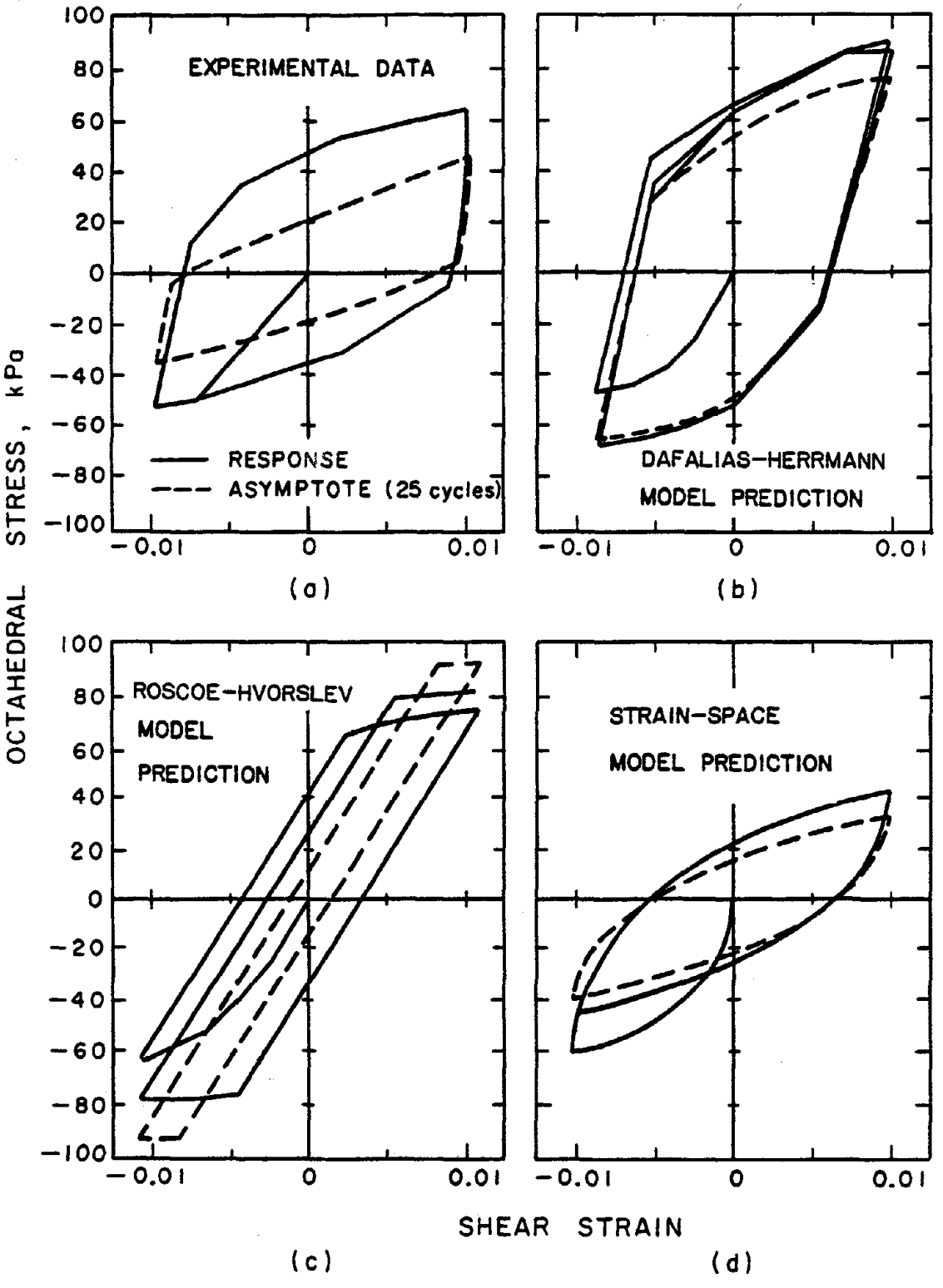

FIGURE 4.16 COMPARISON WITH OTHER MODEL PREDICTIONS

iv) The strain-space model.

The bounding surface model predicts octahedral stresses much higher than those observed experimentally. Although the experimental results clearly show that the maximum stresses decrease as the loading progresses, the bounding surface prediction shows a large increase in the maximum compressive stress during the initial cycles.

The Roscoe-Hvorslev model predicts cycles that get smaller in the strain direction and larger in the stress direction. This produces the result that, as the material is loaded between constant strain limits, the octahedral stress limits keep increasing. This is again contrary to the experimental observations.

By comparison with the bounding surface model prediction and the Roscoe-Hvorslev model prediction, it is seen that the strain-space model prediction is much closer to the experimental observations.

A main feature observed in several experiments is missing in the predictions of both the Dafalias-Herrmann model and the Roscoe-Hvorslev model. This feature is the infinite slope in the e-q plane just after reversal. Both models fail to predict this because of the usage of an elastic shear modulus. This problem does not arise in the strain-space model because it does not use an elastic shear modulus.

Figure (4.17) shows the variation of pressure with axial strain during cyclic loading between constant strain limits. The predictions of the three models are shown along with the experimental data.

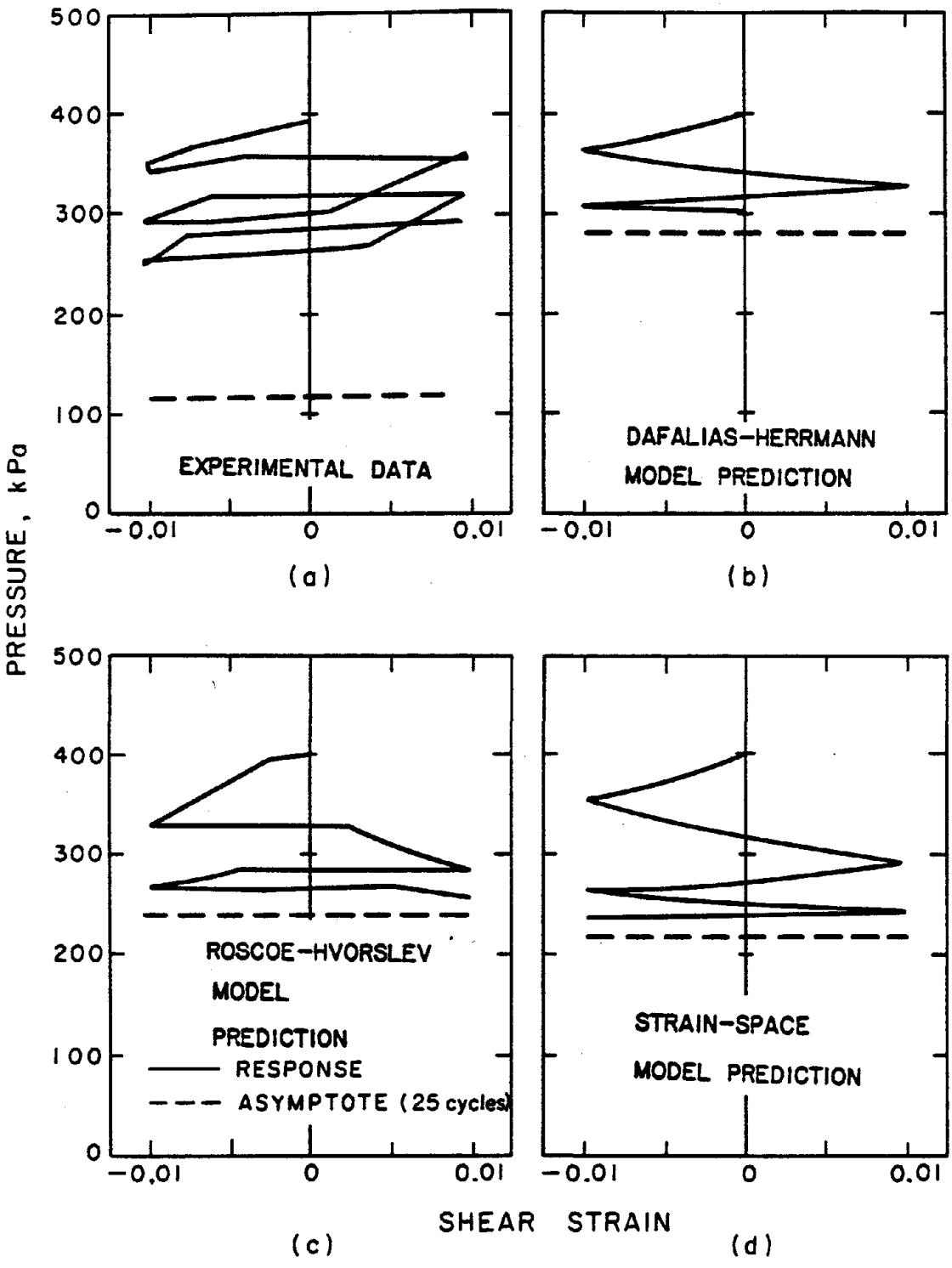

FIGURE 4.17 COMPARISON WITH OTHER MODEL PREDICTIONS

The bounding surface model shakes down monotonically in pressure. The limit cycle is reached at a pressure value of 281kPa. This is much higher than the value of about 120kPa observed from the experimental results. The pressure reduces by large steps during the initial cycles. As the loading progresses, the reduction in pressure becomes smaller. The initial pressure reductions are about the same as those observed experimentally.

The Roscoe-Hvorslev model predicts a shakedown in pressure which is also monotonically decreasing. The final value reached is 236kPa compared to the mean value of about 120kPa observed from the experimental results. This model also predicts a large reduction in pressure initially but the amount of reduction decreases rapidly as the number of cycles increases.

Again, the strain-space model yields better predictions than the other two models. All of the models predict a monotonic decrease in pressure which contradicts the looping seen in the experimental data. The predictions of the values of the pressure at limit cycles are given below for the three models, as a percentage of the mean limit cycle pressure observed experimentally.

Bounding surface model	234%
Roscoe-Hvorslev model	197%
Strain-space model	158%

4.5.5 Comparison for Cyclic Loading Between Constant Stress Limits

The comparison made herein is based on test data for cyclic loading between constant stress limits. These tests were also performed for the International Workshop on Constitutive Behavior of Soils. There are three load cases in this test as listed in Table (4.4). The variables τ_1 and τ_2 denote the stress limits in terms of octahedral stresses.

TABLE 4.4

Load Case	Consolidation Pressure kPa	Cell Pressure kPa	τ_1 kPa	τ_2 kPa	Void Ratio After Consolidation
1	400	400	-27.8	30.6	0.720
2	400	400	-37.7	42.4	0.713
3	400	400	-47.1	52.8	0.745

The values of the void ratio after consolidation for those load cases shown in Table (4.4) differ significantly from those given in the previous cases. The void ratio values given in the monotonic loading cases under the same consolidation pressure of 400kPa were 0.665 and 0.670. The maximum discrepancy in void ratio for a consolidation pressure of 400kPa is 0.080, which is 11.4% of the mean value. When making comparisons, these experimental inconsistencies must be taken into consideration.

Figures (4.18) a, b and c show the extremum axial strain values reached during each cycle as a function of the logarithm of the number of cycles, N. Figures (4.18) a, b and c represent load cases 1, 2 and 3

respectively. Denote the extremum axial strain values reached in compression and in extension during the N^{th} cycle by $\varepsilon_c(N)$ and $\varepsilon_e(N)$, respectively. The following observations can be made from Figures (4.18) a, b and c.

It can be seen that the model predictions for all three load cases show that;

a) $\varepsilon_e(N)$ increases monotonically with N.

b) $\varepsilon_c(N)$ decreases initially with N and then increases with N.

c) $\varepsilon_c(N)$ becomes positive beyond a certain value of N.

The experimental data, on the other hand, indicate that $\varepsilon_e(N)$ increases with N, while $\varepsilon_c(N)$ decreases with N. Load case 1 shows very low values of $\varepsilon_e(N)$ and $\varepsilon_c(N)$ for all the values of N considered. But in load cases 2 and 3 this effect is seen very prominently. This discrepancy is to be expected because of an assumption made during the development of the model.

The reason for the discrepancy between the model prediction and the experimental observation is better explained with the aid of some figures. Figure (4.19) shows the model prediction for the load case 1 in the ε–τ plane. Let the term 'forward path' denote that part of the cycle corresponding to increasing strain and stress and let the term 'reverse path' denote the rest of the cycle corresponding to decreasing strain and stress.

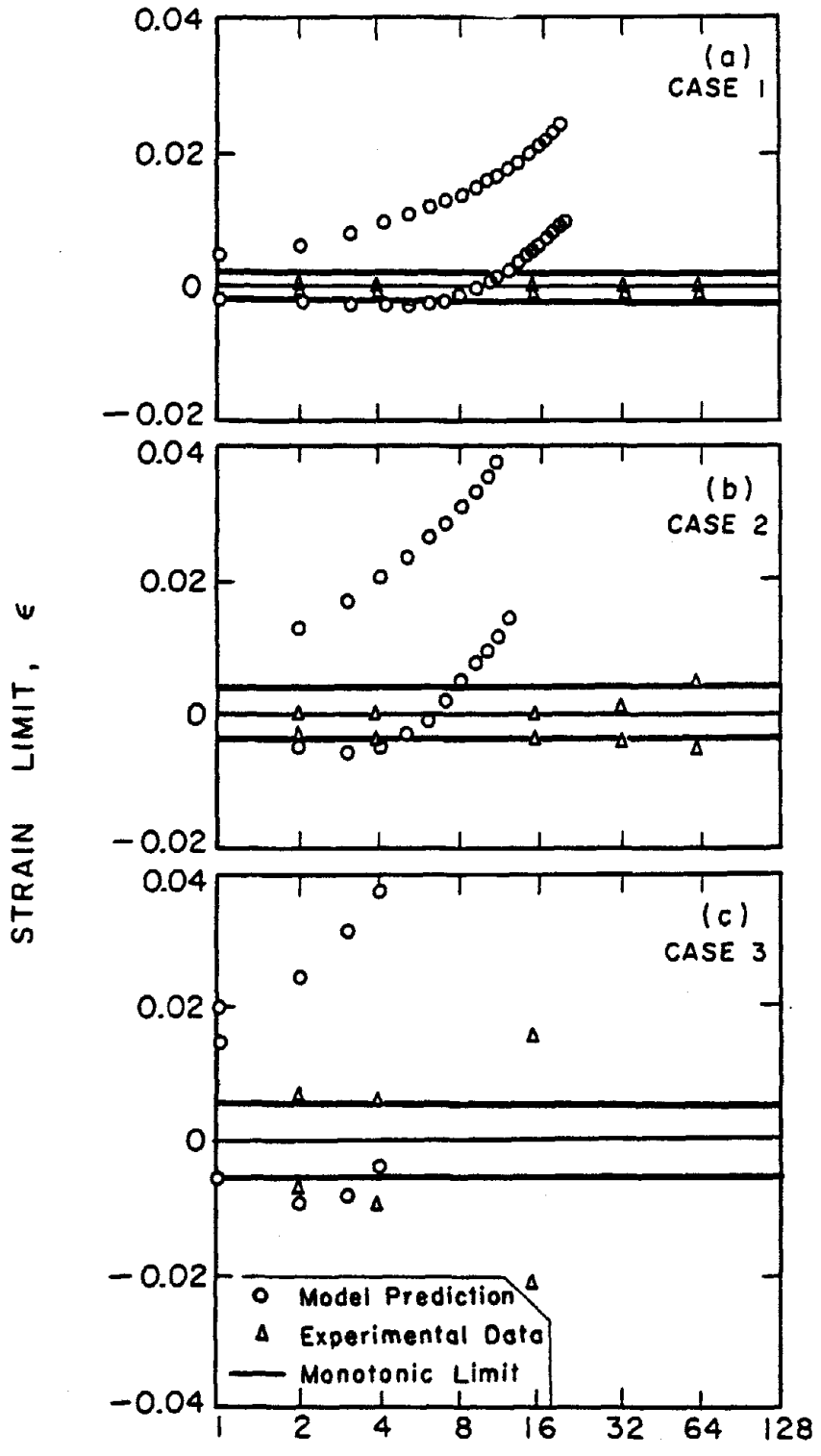

FIGURE 4.18 STRAIN EXTREMA FOR CYCLIC LOADING WITH CONSTANT STRESS LIMITS

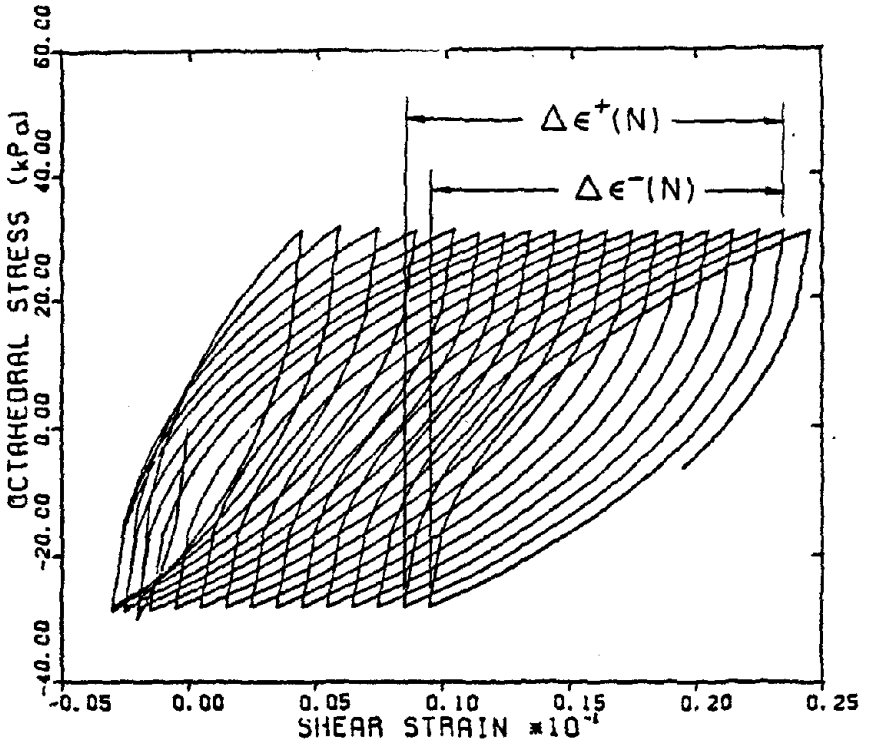

FIGURE 4.19 CYCLIC LOADING UNDER CONSTANT STRESS LIMITS

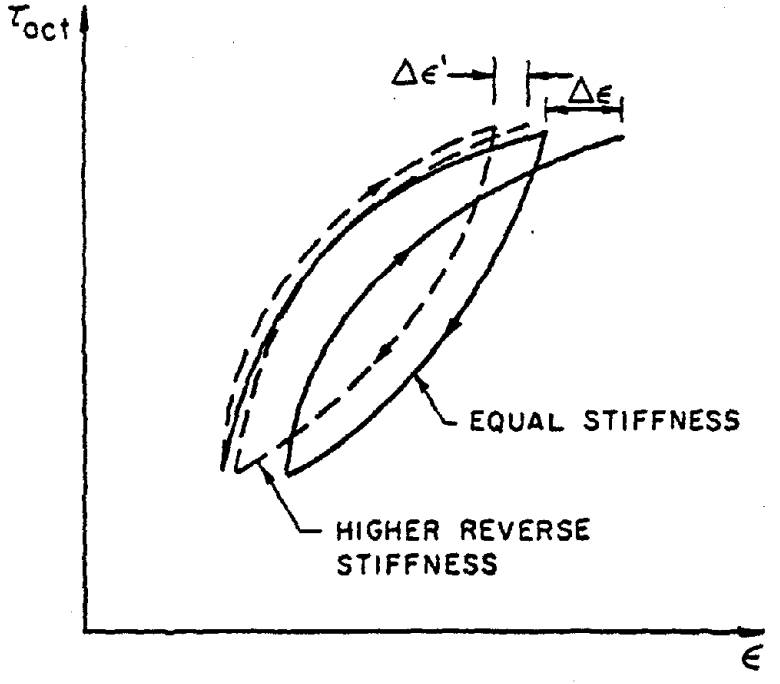

FIGURE 4.20 EFFECT OF UNEQUAL STIFFNESSES

From Figure (4.19) it is seen that the model predicts limit cycles after about 5 cycles. Further, it can be noted that the strain increment $\Delta\varepsilon^{+}(N)$ in the forward path is larger than the strain decrement $\Delta\varepsilon^{-}(N)$ in the reverse path of the limit cycle. This difference clearly results in a linear increase in the values of $\varepsilon_e(N)$ and $\varepsilon_c(N)$ with N, for values of N larger than the limit cycle value.

It is also seen from Figure (4.19) that the prediction softens. This would result in the difference $(\varepsilon_e(N) - \varepsilon_c(N))$ increasing with N up to a value corresponding to the limit cycle. Such a softening tends to increase $\varepsilon_e(N)$ and decrease $\varepsilon_c(N)$. During the first few cycles the softening effect dominates over the shifting effect arising from the difference between $\Delta\varepsilon^{+}$ and $\Delta\varepsilon^{-}$. Hence, $\varepsilon_e(N)$ increases and $\varepsilon_c(N)$ decreases for low values of N depending on the loading case. But as loading progresses, softening reaches its maximum limit and the shift effect dominates, thereby increasing both $\varepsilon_e(N)$ and $\varepsilon_c(N)$.

This shift is reduced if the forward stiffness increases while the reverse stiffness remains unchanged. This type of behavior is shown in Figure (4.20). This can be achieved in the model by simply increasing the value of M for the forward path. In that case the model would predict strain extrema such that $\varepsilon_e(N)$ increases with N while $\varepsilon_c(N)$ decreases with N.

A second observation relates to $\varepsilon_c(1)$. The value of $\varepsilon_c(1)$ should coincide with the value of strain obtained from a monotonic loading test corresponding to the same stress. This must be the case because the material has no way of knowing the difference between a loading which

will be continued monotonically and one which will be reversed. Therefore, it is possible to compare those values of $\varepsilon_c(1)$ for the different loading cases with those obtained from the monotonic loading case shown in Figure (4.7). The strain values corresponding to the monotonic loading case are shown in Table (4.5).

TABLE 4.5

Load case	Stress value (q) at first reversal (kPa)	q/p_0	Strain from monotonic data
1	- 59	-0.15	0.0019
2	- 80	-0.20	0.0038
3	-100	-0.25	0.0060

The values of ε tabulated in Table (4.5) are shown by horizontal lines in Figures (4.18) a, b and c. It is also known that during cyclic loading in shear, soil samples soften. This fact is further substantiated by the experimental data shown in the previous section. Therefore, the initial strain limit $\varepsilon_c(1)$ should lie on the line corresponding to the monotonic loading value of ε, and at least one of the two strain limits $\varepsilon_c(N)$, $\varepsilon_e(N)$ of the subsequent cycle should lie outside one of those lines. This is not the case for the experimental data except for load case 3. This is clearly a contradiction. For this reason the experimental data in this case are suspect.

Finally, it is interesting to compare the strain amplitudes (peak-to-peak) at limit cycle. The limit cycle amplitudes of the strain-space

model predictions are compared with the maximum amplitude available from the experimental data. These values are presented in Table (4.6).

TABLE 4.6

Load Case	Maximum Strain Amplitude	
	Experimental Data	Model Prediction
1	Negligible	0.014
2	0.010	0.026
3	0.036	0.040

From the values of Table (4.6) it can be seen that load case 3 has only a 10% difference between the experimental data and model prediction. This is to be expected because this is the only load case that is consistent with the monotonic loading results as far as the experimental data are concerned. Load cases 1 and 2 start with very low strain amplitudes, in the case of the experimental data. Hence, the two load cases 1 and 2 cannot really be used in the comparison.

4.1 SUMMARY AND CONCLUSIONS

The model developed in Chapter III is first calibrated in this chapter by comparing its undrained predictions with the Cambridge model predictions. From this calibration, the model constants α and b_1 are evaluated. These constants are then verified by checking with Grenoble data. In all the undrained cases, the strain-space model outperforms the comparable stress-space model. The strain-space model does better

despite its simplicity which leads to simple closed form solutions for many cases of loading.

Secondly, the model is tested for constant pressure loading. Although this is a loading condition in stress-space, the strain-space model still gives easier and simpler solutions than its stress-space counterpart. Its quantitative predictions are at least as good as those of the stress-space model. Finally, the strain-space model is used to predict cyclic behavior. Most models are incapable of reproducing this behavior. Once more, the simple strain-space model predicts cyclic behavior very well. All the qualitative behaviors explainable by basic physical concepts and observed experimentally are captured by the strain-space model.

When compared to some well-accepted stress-space models, the simple strain-space model predicts the cyclic behavior significantly better. Further, the strain-space model requires only three material constants as opposed to six or nine for the other two models considered. These three material constants can be determined from some very simple tests.

In conclusion, the tests performed show very clearly the usefulness of the strain-space model. The model is based on highly simplified assumptions. If desired, it would be possible to make this model more complex, thus achieving higher accuracy of prediction. But within the experimental accuracies available, such complexity does not appear

justified. Further, the purpose of this work is to develop a simple model.

CHAPTER V

GENERALIZATION OF THE INFINITESIMAL STRAIN AXISYMMETRIC MODEL

5.1 INTRODUCTION

The strain-space constitutive model developed for wet-clay thus far holds for axisymmetric load deformation systems with infinitesimal deformations. In this chapter the infinitesimal deformation model will be generalized, assuming that the same type of basic material behavior holds during finite deformations. The stresses and the strains could be defined along the lines of finite deformation, nonlinear elasticity theory. However, as could be shown, when taking the limit of infinitesimal deformation, the finite theory will approach the infinitesimal theory, thereby ensuring consistency with the results obtained previously.

Most soil engineering problems do not have a simple geometry or loading. Nevertheless, the study of simple cases such as axisymmetry and plane strain provide a deeper understanding of the material behavior. Having conducted one such study, it is desirable to extend the understanding thus obtained to more general situations. With this in mind, the model is generalized to relate a general state of strain to a general state of stress.

Section 5.2 sets up the basic notions of motion, strain and stress. This is followed by a discussion of the existence and coincidence of the principal axes of the stress and the strain tensors chosen. The concept

of effective stress is motivated mathematically. Finally, some variables are defined from the stress and strain tensors.

In section 5.3 the axisymmetric constitutive model is generalized to the general 3-dimensional case based on a pair of assumptions.

5.2 DEFINITION OF THE BASIC VARIABLES

5.2.1 Deformation and Strain During a General Admissible Motion

Consider a solid body which, in its reference state, occupies a region R_o in the three-dimensional Euclidean space $\mathbb{R}^3$. Without loss of generality, the time corresponding to this reference state may be taken as zero. Edges, corners, and connectivity are permitted to exist in the region R_o. During subsequent deformation in time t, the body occupies a sequence of regions R_t, in $\mathbb{R}^3$.

Let an infinitesimal region in R_o be defined as a 'particle.' Pick an origin 0 in $\mathbb{R}^3$ and let $\underset{\sim}{x}$ be the position vector of such a particle in R_o. Let $\underset{\sim}{y}$ be the position vector from 0 to the point in R_t, which is occupied at time t by the same particle.

The motion of such a solid body can now be described by

$$\underset{\sim}{y}(\underset{\sim}{x},t) = \underset{\sim}{x} + \underset{\sim}{u}(\underset{\sim}{x},t) \qquad \forall(\underset{\sim}{x},t) \in \mathbb{R}^3 \times \tau \quad , \quad \tau = [0,T] \quad . \tag{5.1}$$

The vectors $\underset{\sim}{x}, \underset{\sim}{u}$ and $\underset{\sim}{y}$ along with the regions R_o and R_t are shown in Figure (5.1). Equation (5.1) describes a general motion. In order to be able to carry out analysis, certain conditions are imposed on this motion. These conditions are motivated by the following physical ideas:

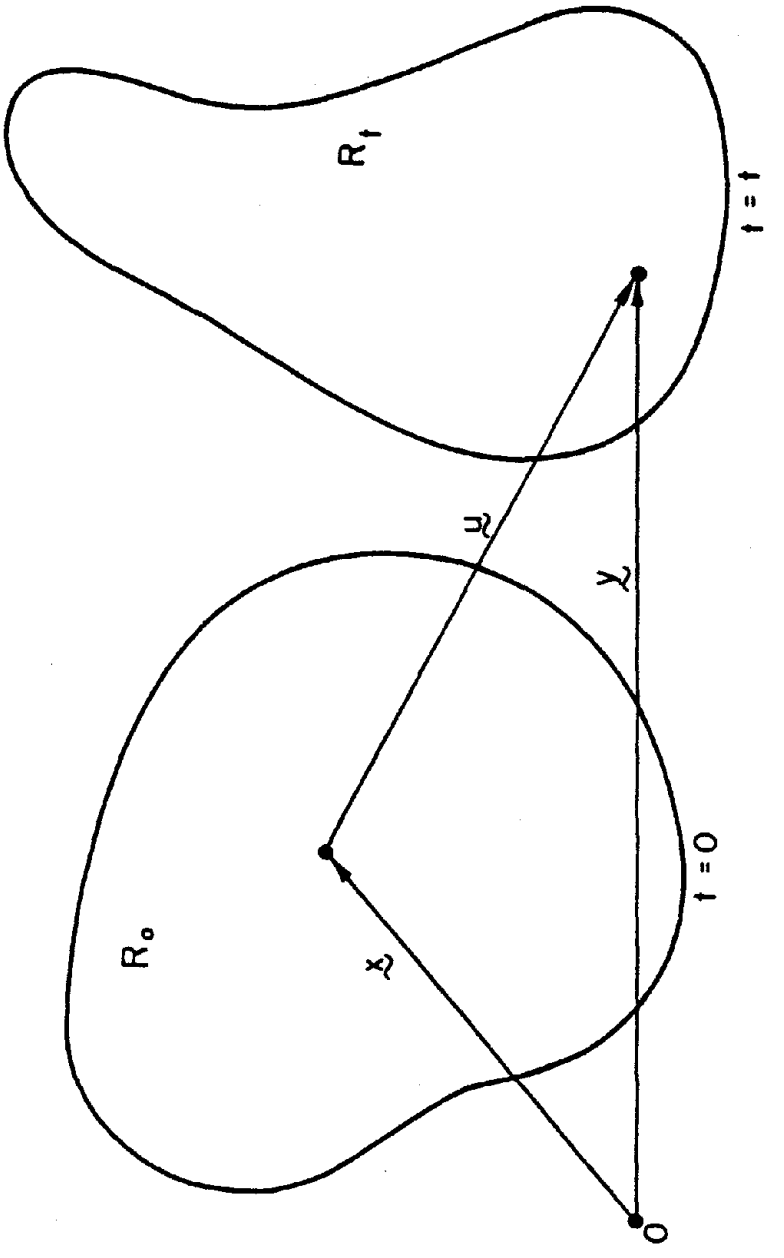

FIGURE 5.1 DEFORMATION OF A CONTINUUM

i) Motion takes place without rupture or tearing.

ii) No two particles occupy the same position at any one given point in time.

iii) Lines through any point $\underset{\sim}{x}$ in R_o should correspond uniquely with lines through $\underset{\sim}{y}(\underset{\sim}{x},t)$ in R_t and vice versa.

iv) Velocities $\underset{\sim}{v}$, and accelerations, $\underset{\sim}{a}$, should exist such that

$$\underset{\sim}{v}(\underset{\sim}{x},t) = \frac{\partial}{\partial t}\underset{\sim}{y}(\underset{\sim}{x},t) \quad ; \quad \underset{\sim}{a}(\underset{\sim}{x},t) = \frac{\partial^2}{\partial t^2}\underset{\sim}{y}(\underset{\sim}{x},t) \;\forall\; \underset{\sim}{y} \in R_t \quad . \tag{5.2}$$

The above ideas translate into the following mathematical statements, not necessarily in the same order:

i) $$\underset{\sim}{y}(\underset{\sim}{x},0) = \underset{\sim}{x} \qquad \forall\, \underset{\sim}{x} \in R_o \tag{5.3}$$

ii) $$\underset{\sim}{y} \in C^2(\mathbb{R}^3 \times \tau) \tag{5.4}$$

iii) $\underset{\sim}{y}(.,t)$ is (1-1) on R_t $\forall\, t \in \tau$

iv) $\nabla(\underset{\sim}{y})\underset{\sim}{x}(\underset{\sim}{y},t)$, $\frac{\partial}{\partial t}\underset{\sim}{x}(\underset{\sim}{y},t)$ are continuous for $\forall\, \underset{\sim}{y} \in R_t$, $t \in \tau$.

Any motion defined by a $\underset{\sim}{y}$ satisfying the above conditions is hereafter referred to as an admissible motion.

Define the deformation gradient tensor $\underset{\sim}{F}$ as follows,

$$\underset{\sim}{F} = \nabla(\underset{\sim}{x})\underset{\sim}{y}(\underset{\sim}{x},t) \qquad \forall \underset{\sim}{x} \in R_o \qquad \underset{\sim}{y} \in R_t, \qquad t \in \tau \; . \tag{5.5}$$

Using $\underset{\sim}{F}$, the Lagrangian strain tensor can be defined by

$$\underset{\sim}{E} = \frac{1}{2}(\underset{\sim}{F}^T\underset{\sim}{F} - \underset{\sim}{1}) \quad . \tag{5.6}$$

Note that such a definition results in extensive strains being positive.

From its definition, it is clearly evident that the strain tensor $\underset{\sim}{E}$ given by equation (5.6) is symmetric. This property of symmetry will be found to be very useful during the generalization of the simple constitutive model. The Lagrangian strain tensor is chosen here in preference to the Eulerian or the Almansi strain tensor for the reason that a Lagrangian formulation of the equilibrium equations is more commonly used in the mechanics of solids.

5.2.2 Traction and Stress

Consider the particle P given by $\underset{\sim}{x}$ in R_o, and which is mapped to $\underset{\sim}{y}$ in R_t by an admissible motion, $\underset{\sim}{y} = \underset{\sim}{y}(\underset{\sim}{x},t)$. Let D_o be the region containing all particles in a neighborhood of P bounded by the surface S_o. By the definition of the admissible motion these particles will be mapped onto a corresponding neighborhood D_t in R_t bounded by a surface S_t. These surfaces and regions are shown in Figure (5.2).

Postulate the existence of a vector field

$$\underset{\sim}{t} = \underset{\sim}{t}(\underset{\sim}{y},\underset{\sim}{n},t) \quad , \quad \underset{\sim}{y} \in R_t \quad , \quad t \in \tau \tag{5.7}$$

where $\underset{\sim}{n}$ is an arbitrary unit vector.

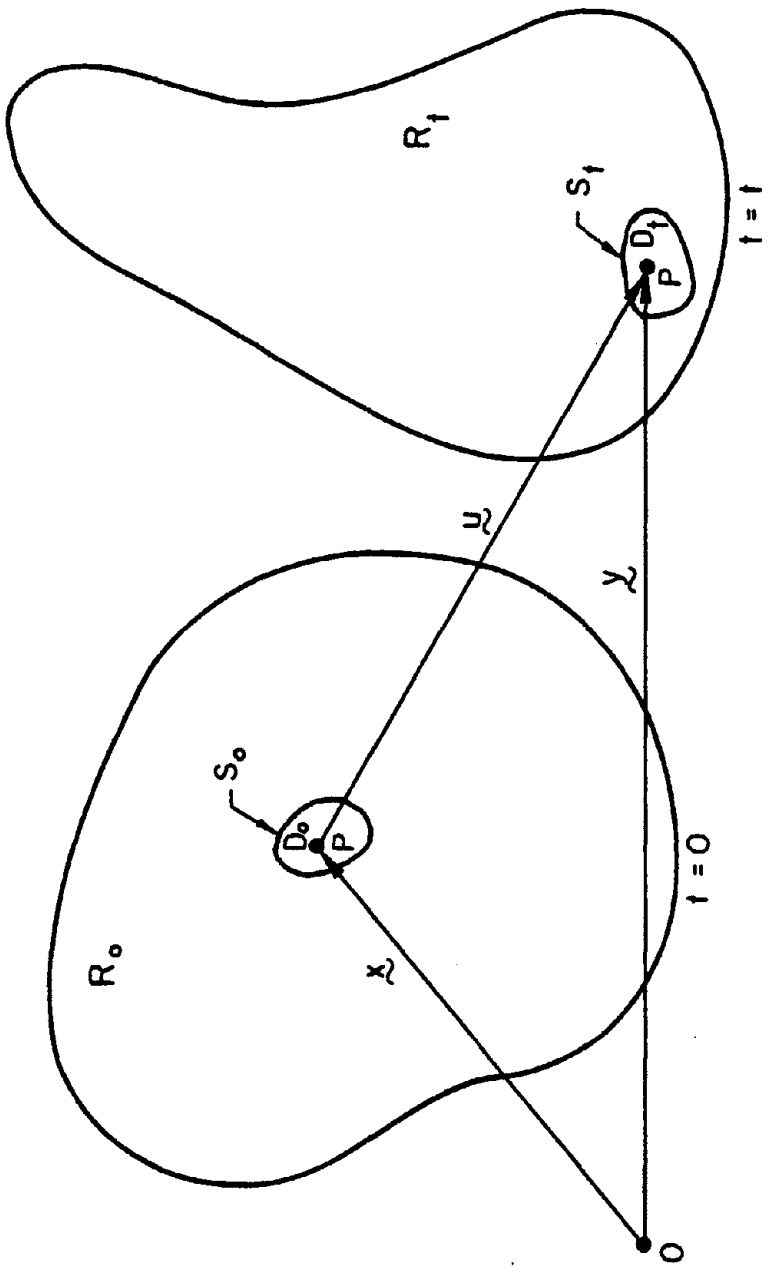

FIGURE 5.2 DEFORMATION OF A LOCAL SURFACE

Further, require that,

i) $\underset{\sim}{t}$ be continuous in $\underset{\sim}{y}$, $\underset{\sim}{n}$ and t.

ii) The total force on D_t due to contact be

$$\int_{S_t} \underset{\sim}{t}(\underset{\sim}{y},\underset{\sim}{n},t) \cdot d\underset{\sim}{A}(\underset{\sim}{y})$$

when $\underset{\sim}{n}$ is the unit normal to S_t at the particle under consideration, and $d\underset{\sim}{A}(\underset{\sim}{y})$ is the infinitesimal area normal to $\underset{\sim}{n}$.

iii) The total moment about 0 on D_t due to contact be

$$\int_{S_t} \underset{\sim}{y} \times \underset{\sim}{t}(\underset{\sim}{y},\underset{\sim}{n},t)dA(\underset{\sim}{y}) \quad . \tag{5.8}$$

The vector field $\underset{\sim}{t}$ satisfying all the above requirements is termed the traction vector field.

Let $\underset{\sim}{\tau}(\underset{\sim}{y},t)$ be a tensor field whose components in a frame e are given by $\{\tau\}^e_{ij} = \tau_{ij}$ and are related to the components $\{\underset{\sim}{t}\}^e_j = t_j$ of the vector field $\underset{\sim}{t}$ in the same frame e by the relationship

$$\tau_{ij}(\underset{\sim}{y},t) = t_j(\underset{\sim}{y},\underset{\sim}{e}_i,t) \quad . \tag{5.9}$$

Such a tensor field $\underset{\sim}{\tau}(\underset{\sim}{y},t)$ is the Cauchy stress tensor (also referred to as the True stress tensor).

Clearly, the Cauchy stress tensor depends on the current configuration R_t rather than on the reference configuration R_o. However, solid mechanics is more amenable to solutions in its Lagrangian form. As such

it would be convenient to define a stress tensor referred to the configuration R_o.

Cauchy's Theorem: For any $\underset{\sim}{y}$ in R_t and any unit vector n the traction vector can be expressed as,

$$\underset{\sim}{t}(\underset{\sim}{y},n,t) = \underset{\sim}{\tau}(\underset{\sim}{y},t)n \quad , \quad \underset{\sim}{y} \in R_t \; , \; t \in \tau \; , \; ||n||_2 = 1 \qquad (5.10)$$

where $\underset{\sim}{\tau}(\underset{\sim}{y},t)$ is the Cauchy stress tensor. Also it can be shown that the relationship between the unit normal N in the reference configuration and the unit normal n in the deformed configuration can be given by,

$$N = \frac{dA(y)}{dA(x)} F^T (\det F)^{-1} n \quad . \qquad (5.11)$$

From (5.10) and (5.11) it can be shown that

$$\underset{\sim}{t}(\underset{\sim}{y},n,t) = \underset{\sim}{\tau}(\underset{\sim}{y},t)n = (\det F) \frac{dA(x)}{dA(\underset{\sim}{y})} \tau F^{-T} N \quad . \qquad (5.12)$$

Define a stress tensor σ by the following relation,

$$\sigma = (\det F) \tau F^{-T} \quad . \qquad (5.13)$$

Then,

$$\underset{\sim}{t}(\underset{\sim}{y}(x,t) \; , \; n,t) = \frac{dA(x)}{dA(\underset{\sim}{y})} \sigma N \quad . \qquad (5.14)$$

The stress tensor defined by equation (5.13) is termed the Nominal stress tensor (also referred to as Piola-Kirchhoff stress tensor, Engineering stress tensor, and Pseudo-stress tensor).

The symmetry of the stress and strain tensors is a property which greatly simplifies analysis. For this reason a second Piola-Kirchhoff stress tensor, $\underline{S}$, is defined as follows,

$$\underline{S} = \underline{F}^{-1}\underline{\tau} \quad . \tag{5.15}$$

The definition of the admissible motion demands that $\underline{F}$ be non-singular. This non-singularity clearly justifies the existence of the tensor $\underline{F}^{-1}$. Combining equations (5.13) and (5.15) it can be seen that

$$\underline{S} = (\det \underline{F})\underline{F}^{-1}\underline{\tau}\underline{F}^{-T} \quad . \tag{5.16}$$

5.2.3 The Existence and Coincidence of the Principal Frames of the Stress and Strain Tensors

In conventional plasticity, it is common to assume that the principal frames of the stress and strain tensors coincide. This coincidence assumption simplifies the constitutive relations. It is sufficient, under this assumption, to relate the incremental principal components of the stress tensor to the incremental and total components of the principal strain tensor. If such a coincidence assumption is not made, then the six incremental components of the stress tensor need to be specified independently. Such a specification would involve some alternate assumptions. For this reason, the coincidence assumption is widely used. It can be shown that coincidence is also implied by some other fundamental assumptions commonly made in plasticity.

Before addressing the issue of coincidence of the principal frames, it is clearly necessary to establish the existence of such principal frames for the tensors under consideration. From linear algebra it is seen that a necessary and sufficient condition for the existence of the principal frame of a tensor is that it be symmetric. For this reason it is necessary to explore the symmetry of the stress and strain tensors.

The Lagrangian strain tensor is symmetric by definition and hence will possess a principal frame. However, the symmetry of the stress tensor is not so obvious.

The conservation of angular momentum of a continuum free of body moments implies that

$$\underset{\sim}{\tau} = \underset{\sim}{\tau}^{T} \quad . \tag{5.17}$$

Equation (5.15) along with equation (5.13) results in

$$\underset{\sim}{\sigma}\underset{\sim}{F}^{T} = \underset{\sim}{F}\underset{\sim}{\sigma}^{T} \quad .$$

For infinitesimal deformations the influence of $\underset{\sim}{F}$ is very small, and therefore the three stress tensors $\underset{\sim}{\tau}, \underset{\sim}{\sigma}$ and $\underset{\sim}{S}$ are almost equal. However, during finite deformations, the components of $\underset{\sim}{F}$ differ significantly from those of $\underset{\sim}{1}$, and hence the three stress tensors have quite different properties.

The first Piola-Kirchhoff stress tensor $\underset{\sim}{\sigma}$ is symmetric only under very special motions. As it is preferable to develop constitutive equations not restricted to some special motions, except for the very essen-

tial restrictions such as admissibility, the second Piola-Kirchhoff stress tensor is used in this work.

From equation (5.16) and equation (5.17) it follows that

$$\underset{\sim}{S} = \underset{\sim}{S}^{T} \quad , \tag{5.18}$$

which implies that for admissible motions under the absence of body moments the second Piola-Kirchhoff stress tensor is symmetric. Which in turn implies that this tensor possesses a principal frame at every state point.

Within the framework of elasticity theory it can be shown that the principal frames of the Lagrangian strain tensor and the principal frame of the second Piola-Kirchhoff stress tensor coincide for isotropic materials.

Under classical plasticity theory using any general flow rule, it can be shown that the principal frames coincide incrementally under restrictive circumstances. The condition sufficient for the coincidence is that the plastic potential function g should depend on the stress tensor, only through its invariants. When this condition is satisfied, it can be shown that the incremental plastic strain tensor will have a principal frame coinciding with that of the stress tensor. By the basic definition of the elasticity tensor, the principal frame of the incremental elastic Lagrangian strain tensor and that of the second Piola-Kirchhoff stress tensor coincide. Therefore, the principal frame of the

second Piola-Kirchhoff stress tensor and that of the incremental total strain tensor coincide.

In this work the constitutive equations are developed without using a restrictive assumption of flow rules. For this reason, the coincidence of the principal frames of the incremental second Piola-Kirchhoff stress tensor and the total Lagrangian strain tensor is taken as an assumption.

It is worth noting at this point that within the framework of conventional plasticity, it can only be shown that isotropy is a sufficient condition for the coincidence of the principal frames. For this reason it cannot be argued that the coincidence assumption demands isotropy. Furthermore, the theory developed herein is free of any flow rule, and even the sufficiency proof depends greatly on the existence of a flow rule.

5.2.4 Effective Stresses

Saturated soil is a two-phase medium consisting of pore fluid which is commonly water and a solid lattice of soil particles. The concepts of stress and strain developed hereto arise from continuum mechanics where there is only a single medium. Hence, to address the state of stress on a mixture such as soils, certain modifications are necessary. In the area of practical soil mechanics it has been observed that it is possible to describe a stress termed 'effective stress' more accurately than the total stress. In the paragraphs that follow an

attempt is made to present this concept of effective stresses within a mathematically rigorous framework.

Figure (5.3) shows a sample region of soil composed of a solid lattice and pore fluid. This region is cut along a plane and an elemental area dA is considered. In this elemental area dA, a part dA_s is occupied by solids whereas another part dA_f is occupied by the pore fluid.

Assume that there exist continuous and twice continuously differentiable tensor and scalar fields $\underline{S}_s(\underline{x},t)$ and $p_f(\underline{x},t)$ respectively so that

$$\begin{aligned} \underline{F}_s &= \int_{A_s} \underline{S}_s(\underline{x},t)\underline{n}dA_s \\ \underline{F}_f &= \int_{A_f} -p_f(\underline{x},t)\underline{n}dA_f \end{aligned} \tag{5.19}$$

where, $\underline{F}_s$ is the force transmitted across A_s by solids and $\underline{F}_f$ is the force transmitted across A_f by fluids.

The total force transmitted by the two-phase medium across the area A would be

$$\underline{F} = \underline{F}_s + \underline{F}_f \quad . \tag{5.20}$$

Further,

$$A = A_s + A_f \quad . \tag{5.21}$$

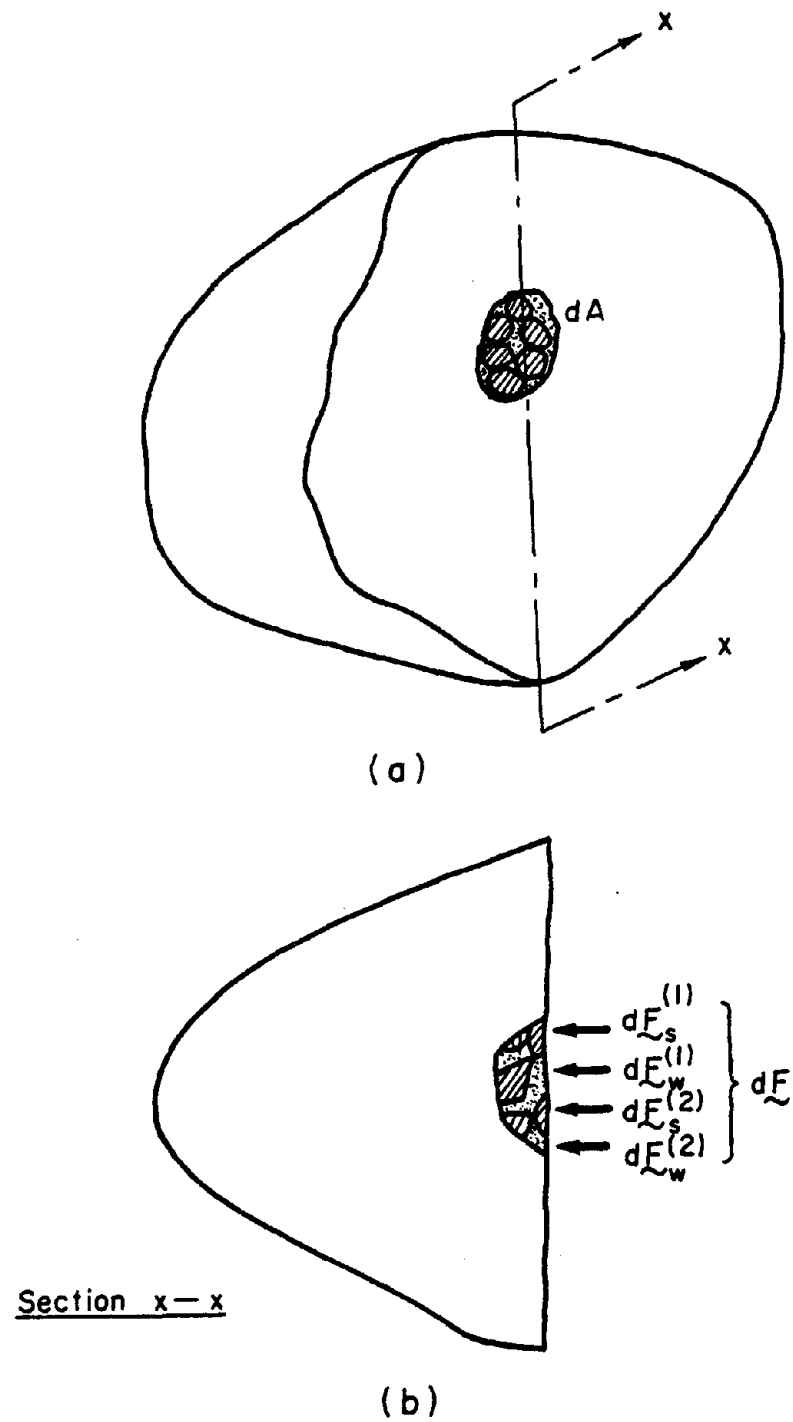

FIGURE 5.3 STRESSES AT AN INFINITESIMAL SOIL AREA

Postulate the existence of another continuous and twice continuously differentiable tensor field $\underline{S}(\underline{x},t)$ so that,

$$\underline{F} = \int_A \underline{S}(\underline{x},t)\underline{n}\, dA \quad . \tag{5.22}$$

This tensor $\underline{S}(\underline{x},t)$ would be the stress tensor if the media were treated as a single phase homogeneous material.

From equations (5.19), (5.20) and (5.22) it follows that,

$$\int_A \underline{S}(\underline{x},t)\underline{n}dA = \int_{A_s} \underline{S}_s(\underline{x},t)\, \underline{n}\, dA_s + \int_{A_f} -p_f(\underline{x},t)\underline{n}dA_f \quad . \tag{5.23}$$

If equation (5.23) is taken to hold for every choice of A, then

$$\underline{S}(\underline{x},t) = \underline{S}_s(\underline{x},t)\, \frac{dA_s}{dA} - p_f(\underline{x},t)\, \underline{1}\, \frac{dA_f}{dA} \quad .$$

Using the decomposition of A from equation (5.21), in the incremental form,

$$\underline{S}(\underline{x},t) = \underline{S}_s(\underline{x},t)\, \frac{dA_s}{dA} - p_f(\underline{x},t)\underline{1}\left(1 - \frac{dA_s}{dA}\right) \quad . \tag{5.24}$$

Let $r(\underline{x})$ be defined by

$$\lim_{dA \to 0} \frac{dA_s(\underline{x})}{dA(\underline{x})} = r(\underline{x}) \quad . \tag{5.25}$$

Then,

$$\underline{\underline{S}}(\underline{x},t) = \underline{\underline{S}}_s(\underline{x},t)r(\underline{x}) - p_f(\underline{x},t)\underline{\underline{1}}(1 - r(\underline{x})) \quad . \tag{5.26}$$

It is argued commonly in soil mechanics that

$$r(\underline{x}) \rightarrow 0 \quad \text{and} \quad \underline{\underline{S}}_s(\underline{x},t) \cdot r(\underline{x}) \rightarrow \underline{\underline{S}}'(\underline{x},t) \quad , \tag{5.27}$$

where $\underline{\underline{S}}'(\underline{x},t)$ is finite. Invoking (5.27) on (5.26) results in

$$\underline{\underline{S}}(\underline{x},t) = \underline{\underline{S}}'(\underline{x},t) - p_f(\underline{x},t) \cdot \underline{\underline{1}} \quad . \tag{5.28}$$

Equation (5.28) is the commonly used stress decomposition equation, where

$\underline{\underline{S}}(\underline{x},t)$	total stress tensor
$\underline{\underline{S}}'(\underline{x},t)$	effective stress tensor
$p_f(\underline{x},t)$	pore fluid pressure .

The sign convention for stress is still maintained as tensile stresses positive. However, pressures are taken as compressive positive.

Although the decomposition given by equation (5.28) is the form commonly used in soils, some investigators (Garg and Nur, 1973; Nur and Byerlee, 1971; Terzaghi, 1923; Robinson, 1959; Handin et al., 1963; Murrell, 1963; Skempton, 1961; Geertsma, 1957; Suklje, 1969; and Biot and Willis, 1957) have looked deeper into the effect of $r(\underline{x})$ on the stresses and suggest different forms of scalar multipliers for the fluid pore pressure. Since no one of these alternative approaches is as widely accepted as the simple decomposition given by equation (5.28), the simple decomposition will be used herein.

5.2.5 Stress and Strain Variables

Since the existence of the principal frames for stress and strain tensors to be used herein has been established and their coincidence assumed, it is sufficient to relate the incremental principal components of stress to the principal components of strain.

In order to remain along the lines of the development of the axisymmetric theory, certain stress and strain variables are defined here to be related by the three-dimensional constitutive relations. These variables are defined in general terms based on the stress and strain invariants. The volumetric dilatation denoted by v is given by

$$v = \det \underline{F} \quad .$$

Since the strain tensor $\underline{E}$ is defined in terms of $\underline{F}$, v can be related to $\underline{E}$ as

$$v = \{1 + 2I_1(\underline{E}) + 4I_2(\underline{E}) + 8I_3(\underline{E})\}^{1/2} - 1 \quad . \qquad (5.29)$$

In soils, the void ratio e is more commonly used than the volumetric strain v and these are related in the Lagrangian sense as

$$dv = \frac{de}{1+e_o} \quad , \qquad (5.30)$$

where e_o is the void ratio at a reference state related to $\underline{x}$. This results in e being related to $\underline{E}$ as

$$e = (1+e_o)\{1 + 2I_1(\underline{E}) + 4I_2(\underline{E}) + 8I_3(\underline{E})\}^{1/2} - 1 \quad . \qquad (5.31)$$

A measure of shear strain is defined by e as follows,

$$\varepsilon = \frac{2}{3} I_1^{1/2} \left[\left(\underline{E} - \frac{1}{3} I_1(\underline{E}) \underline{1} \right)^2 \right] \quad . \qquad (5.32)$$

It is found that the variables e and ε reduce to those defined in Chapter II when $\underline{E}$ reduces to the axisymmetric principal strain. Hence, the definitions are consistent with those made previously.

The stress is the dependent tensor in the formulation developed herein. Since the theory is developed as an incremental theory, it is necessary to define some variable based on the incremental stress tensor. As described earlier, the stress used is the second Piola -Kirchhoff stress.

The incremental pressure is defined by simply taking a third of the first invariant of the incremental stress tensor and reversing the sign.

$$dp = -\frac{1}{3} I_1(d\underline{S}') \qquad (5.33)$$

A measure of the shear stress is defined as

$$dq = \frac{3}{2} I_1^{1/2} \left[(d\underline{S}' + dp\underline{1})^2 \right] \quad . \qquad (5.34)$$

The normalized shear stress variable used extensively in the model is defined in terms of the total stress variables and is given by

$$\eta = q/p \quad . \qquad (5.35)$$

As in the case of the strain variables, the stress variables are also chosen so as to approach the variables defined in Chapter II when the stress tensor is principal and axisymmetric. This ensures the consistency of the general three-dimensional model.

5.3 THREE DIMENSIONAL CONSTITUTIVE MODELING

5.3.1 Basic Assumptions

In the previous section the independent model variables e and ε had been defined for a general state of stress. These were the model variables that were employed in the axisymmetric theory. Therefore, by using these variables directly in the axisymmetric constitutive model, the incremental stress variables dp and dq can be found. The general theory, however, should give all the components of $d\underline{\sigma}'$. At this stage, to achieve the goal of predicting all the components of $\underline{\sigma}'$, some basic assumptions are required.

For the axisymmetric stress-strain situation the state of stress or strain can be completely specified by the magnitudes of the hydrostatic and deviatoric components. This is seen clearly from Figure (5.4). Either the stress or strain tensor at any given point can be completely specified by their principal components. This enables the state to be plotted in a three-dimensional space. For the case of axisymmetry about one of the principal axes ε_I, say, all states would lie on the plane, $\varepsilon_{II} = \varepsilon_{III}$. Hence each such state point is uniquely determined by the magnitude of the projection of the state vector along and normal to the

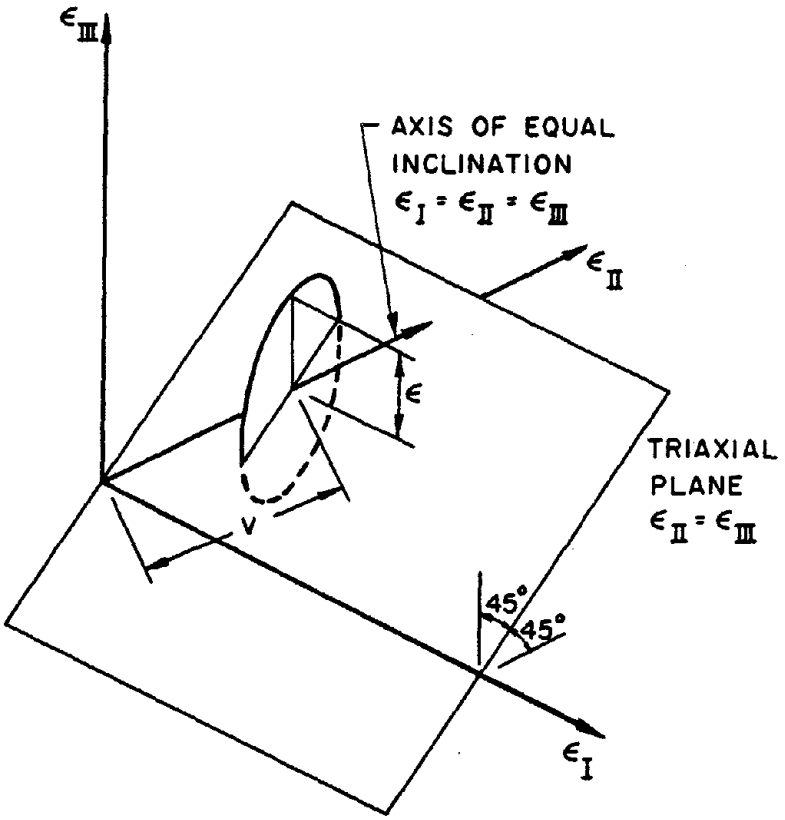

FIGURE 5.4 GEOMETRIC REPRESENTATION OF THE STRAIN VARIABLES

axis of equal inclination. However, when the axisymmetry assumption is relaxed and a general state is considered, such specification will not give a unique state but a set of states lying on a circle on the deviatoric plane with its radius equal to the magnitude of the deviatoric component. Therefore, not only the magnitude but also the direction of the deviatoric component is necessary to specify the state completely.

It is assumed here that during a general state of stress and strain the magnitudes of the components of the stress and strain tensors along and perpendicular to the axis of equal inclination have the same relationship as in the case of axisymmetric stress-strain situations. This justifies the use of the constitutive equation developed in Chapter III to determine dp and dq using e and ε. Furthermore, this assumption will render consistency when the tensors take the special case of axisymmetry.

Having made the first assumption, a rule is to be prescribed now to determine the direction of the incremental deviatoric component. It is assumed here that the incremental deviatoric components of stress and the corresponding deviatoric components of strain are parallel to each other and have the same sense. In the stress-space formulations, a very similar assumption is made.

5.3.2 Implications of the Basic Assumptions

The first assumption mentioned states that all states having the same magnitude of the deviatoric strain have the same dp and dq. This

implies that equations (3.40) hold for the general stress-strain state when de, dε, dp and dq are defined as in equations (5.31) through (5.34).

The second assumption states that the incremental deviatoric stress and the deviatoric strain are parallel. This assumption implies that,

$$\frac{dS'_I - dS'_{II}}{\varepsilon_I - \varepsilon_{II}} = \frac{dS'_{II} - dS'_{III}}{\varepsilon_{II} - \varepsilon_{III}} = \frac{dS'_{III} - dS'_I}{\varepsilon_{III} - \varepsilon_I} \quad . \tag{5.36}$$

Equations (5.33) and (5.34) result in the following equations when expressed in terms of the principal incremental stresses

$$dp = -\frac{1}{3}(dS'_I + dS'_{II} + dS'_{III}) \tag{5.37}$$

$$dq = \frac{1}{\sqrt{2}}[(dS'_I - dS'_{II})^2 + (dS'_{II} - dS'_{III})^2 + (dS'_{III} - dS'_I)^2]^{1/2} \tag{5.38}$$

Equations (5.35), (5.36) and (5.37) result in,

$$dS'_I = dp - \frac{dq}{3\sqrt{2}} \frac{(\varepsilon_{II} + \varepsilon_{III} - 2\varepsilon_I)}{\varepsilon}$$

$$dS'_{II} = dp - \frac{dq}{3\sqrt{2}} \frac{(\varepsilon_{III} + \varepsilon_I - 2\varepsilon_{II})}{\varepsilon}$$

$$dS'_{III} = dp - \frac{dq}{3\sqrt{2}} \frac{(\varepsilon_I + \varepsilon_{II} - 2\varepsilon_{III})}{\varepsilon} \quad . \tag{5.39}$$

5.3.3 The Loading Surface

In order to be consistent with the first of the two assumptions made in the previous section, the loading surface is defined as the pair of surfaces of two concentric cylinders of radii differing by an

infinitesimal quantity. This is shown in Figure (5.5). This loading surface is not the same as the Von Mises surface because of the fact that all the state points lie on or just below the surface.

5.4 SUMMARY

In this chapter the strain-space plastic constitutive model developed for the axisymmetric stress-strain system is generalized to include general stress and strain states.

The strain and stress defined rather loosely previously are defined more rigorously and the limiting assumptions more clearly stated. The idea of effective stress is motivated mathematically. Having defined the stress decomposition in this manner a well-accepted simple decomposition is used and its limitations stated. Based on the strain and stress tensors chosen, some simple strain and incremental stress variables are defined along the lines of those defined in the axisymmetric case.

Finally, two assumptions are made in order to generalize the axisymmetric model to a general state. The first assumption implies that the magnitude of the deviatoric stress and strain are related in the same manner as the shear stress and strain variables in the axisymmetric case. The second assumption is used to derive the direction of the incremental deviatoric stress by setting it parallel to the incremental deviatoric strain.

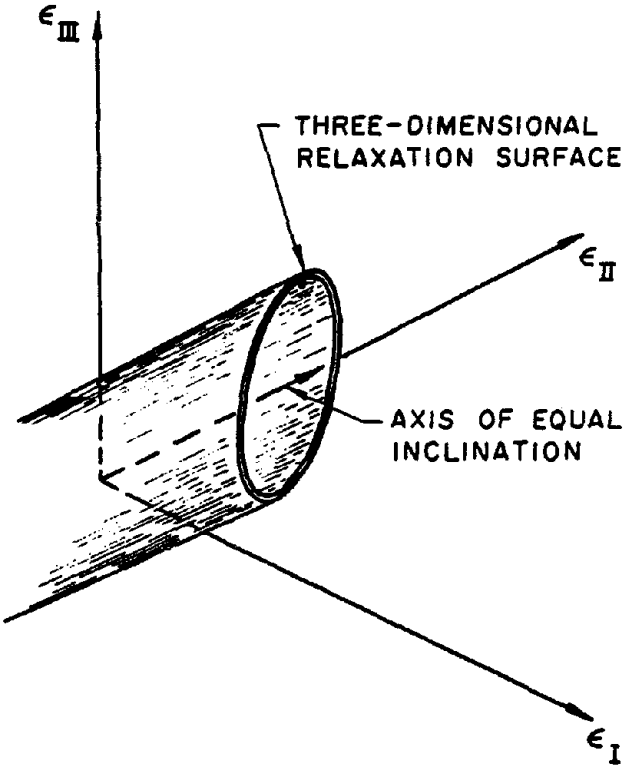

FIGURE5.5 THREE DIMENSIONAL RELAXATION SURFACE

The model thus developed is simple and quite accurate. All the assumptions have been laid down clearly so that the domain of application of the model is well defined. The main aim behind the development of this model was simplicity without loss of rigor and it appears that this has been achieved.

CHAPTER VI

APPLICATION OF THE MODEL TO THE EXPANSION OF A CYLINDRICAL CAVITY

6.1 INTRODUCTION

In this chapter, the simple strain-space model generalized in Chapter V is applied to a general problem. The problem of an expanding cylindrical cavity is considered because it is representative of a pile driving problem. An understanding of the stress fields arising from the expansion of the cylindrical cavity will provide a better insight into the properties of the stress field produced during the driving of a pile.

In section 6.2 the problem of an expanding cylindrical cavity in an infinite medium is modeled as a plane strain axisymmetric problem. The governing equations are deduced. The rapid expansion of the cavity is imposed and the deformation field is hence derived. Based on that deformation field, the stresses and pore pressures are determined.

In section 6.3 the equations are solved numerically and the solutions are presented. These solutions are compared with some experimental results and two other predictions in section 6.4. The predictions used herein are those made by Ladanyi (1963) and Davis and Mullenger, (1984) Interestingly enough, Ladanyi's calculations are indeed a strain-space approach.

Finally, the observations made in this chapter are summarized and presented along with conclusions in section 6.5.

6.2 MATHEMATICAL MODELING

6.2.1. Deformation and Strain

From equation (5.6) it is seen that the Lagrangian strain tensor $\underset{\sim}{E}$ is defined as

$$\underset{\sim}{E} = \tfrac{1}{2}(\underset{\sim}{F}^T\underset{\sim}{F} - \underset{\sim}{1}) \quad ,$$

where

$$\underset{\sim}{F} = \nabla(\underset{\sim}{x})\underset{\sim}{y}(\underset{\sim}{x},t)$$

and

$$\underset{\sim}{y}(\underset{\sim}{x},t) = \underset{\sim}{x} + \underset{\sim}{u}(\underset{\sim}{x},t) \quad .$$

Substituting $\underset{\sim}{u}$ for y results in

$$\underset{\sim}{F} = \underset{\sim}{1} + \nabla(\underset{\sim}{x})\underset{\sim}{u}(\underset{\sim}{x},t) \quad . \tag{6.1}$$

This in turn gives rise to

$$\underset{\sim}{E} = \tfrac{1}{2}((\nabla\underset{\sim}{u})^T + (\nabla\underset{\sim}{u}) + (\nabla\underset{\sim}{u})^T(\nabla\underset{\sim}{u})) \quad . \tag{6.2}$$

In the case of infinitesimal deformations, the term $(\nabla\underset{\sim}{u})^T(\nabla\underset{\sim}{u})$ is dropped as it turns out to be much smaller than $(\nabla\underset{\sim}{u})$ and $(\nabla\underset{\sim}{u})^T$. However, in order to allow for finite deformations, this term is retained herein.

Select a cylindrical polar coordinate system with the z axis coinciding with the axis of symmetry of the cavity. In this system of axes the gradient operator will be

$$\nabla(\underline{x}) = \underline{e}_R \frac{\partial}{\partial R} + \frac{\underline{e}_\theta}{R} \frac{\partial}{\partial \theta} + \underline{e}_z \frac{\partial}{\partial z} \quad , \tag{6.3}$$

where $\underline{e}_R$, $\underline{e}_\theta$ and $\underline{e}_z$ are the unit vectors in the R, θ and z directions, respectively. Let the frame defined by this set of axes be e.

Let u_R, u_θ, u_z be the components of the displacement vector $\underline{u}$ in the R, θ and z directions, respectively. Then,

$$\begin{aligned}
\nabla(\underline{x})\underline{u} = {} & (\underline{e}_R \frac{\partial u_R}{\partial_R}) \otimes \underline{e}_R + (\underline{e}_R \frac{\partial u_\theta}{\partial R}) \otimes \underline{e}_\theta + (\underline{e}_R \frac{\partial u_z}{\partial R}) \otimes \underline{e}_z \\
& + (\frac{\underline{e}_\theta}{R} \frac{\partial u_R}{\partial \theta}) \otimes \underline{e}_R + (\frac{\underline{e}_\theta}{R} u_R) \otimes \frac{\partial \underline{e}_R}{\partial \theta} \\
& + (\frac{\underline{e}_\theta}{R} \frac{\partial u_\theta}{\partial \theta}) \otimes \underline{e}_\theta + (\frac{\underline{e}_\theta}{R} u_\theta) \otimes \frac{\partial \underline{e}_\theta}{\partial \theta} \\
& + (\frac{\underline{e}_\theta}{R} \frac{\partial u_z}{\partial \theta}) \otimes \underline{e}_z \\
& + (\underline{e}_z \frac{\partial u_R}{\partial z}) \otimes \underline{e}_R + (\underline{e}_z \frac{\partial u_\theta}{\partial z}) \otimes \underline{e}_\theta + (\underline{e}_z \frac{\partial u_z}{\partial z}) \otimes \underline{e}_z
\end{aligned} \tag{6.4}$$

where the components of $\underline{a} \otimes \underline{b}$ are defined in terms of the components of $\underline{a}$ and $\underline{b}$ as, $(\underline{a} \otimes \underline{b})_{ij} = a_i b_j$, $i, j \in (1,3)$.

But
$$\frac{\partial \underline{e}_R}{\partial \theta} = \underline{e}_\theta \quad \text{and} \quad \frac{\partial \underline{e}_\theta}{\partial \theta} = -\underline{e}_R \quad . \tag{6.5}$$

Substituting equations (6.5) in (6.4) and writing the components of $\nabla(\underline{x})\underline{u}$ in e, the frame under consideration,

$$\{\nabla(\mathbf{x})\mathbf{u}\}^e = \begin{pmatrix} \frac{\partial u_R}{\partial R} & \frac{\partial u_\theta}{\partial R} & \frac{\partial u_z}{\partial R} \\ \frac{1}{R}\frac{\partial u_R}{\partial \theta} - \frac{u_\theta}{R} & \frac{1}{R}\frac{\partial u_\theta}{\partial \theta} + \frac{u_R}{R} & \frac{1}{R}\frac{\partial u_z}{\partial \theta} \\ \frac{\partial u_R}{\partial z} & \frac{\partial u_\theta}{\partial z} & \frac{\partial u_z}{\partial z} \end{pmatrix} . \quad (6.6)$$

For an axisymmetric problem without twist,

$$u_R = u_R(R, z, t)$$

$$u_\theta = 0$$

$$u_z = u_z(R, z, t) \quad . \quad (6.7)$$

The conditions given by equation (6.7) will result in

$$\{\nabla(\mathbf{x})\mathbf{u}\}^e = \begin{pmatrix} \frac{\partial u_R}{\partial R} & 0 & \frac{\partial u_z}{\partial R} \\ 0 & \frac{u_R}{R} & 0 \\ \frac{\partial u_R}{\partial z} & 0 & \frac{\partial u_z}{\partial z} \end{pmatrix} \quad (6.8)$$

If it is assumed further that the continuum deforms under plane strain conditions then,

$$u_R = u_R(R, t) \quad \text{and} \quad u_z = 0 \quad . \quad (6.9)$$

This assumption simplifies the gradient to

$$[\nabla(\underset{\sim}{x})\underset{\sim}{u}]^e = \begin{pmatrix} u_{R,R} & 0 & 0 \\ 0 & \frac{u_R}{R} & 0 \\ 0 & 0 & 0 \end{pmatrix} \qquad (6.10)$$

where,

$$u_{R,R} = \frac{\partial u_R}{\partial R} \quad .$$

Equation (6.10) and equation (6.2) together define $\underset{\sim}{E}$ as

$$[\underset{\sim}{E}]^e = \begin{pmatrix} u_{R,R} + \frac{1}{2}(u_{R,R})^2 & 0 & 0 \\ 0 & \frac{u_R}{R} + \frac{1}{2}(\frac{u_R}{R})^2 & 0 \\ 0 & 0 & 0 \end{pmatrix} . \qquad (6.11)$$

6.2.2 Stress and Equilibrium

Consider the current configuration of the infinitesimal region of continuum shown in Figure (5.2). For the equilibrium of this region, balance of linear momentum implies that

$$\int_{D_t} \underset{\sim}{f} \cdot dV(\underset{\sim}{y}) + \int_{S_t} \underset{\sim}{t} dA(\underset{\sim}{y}) = \int_{D_t} \rho \cdot \frac{\partial^2 \underset{\sim}{u}}{\partial t^2}(\underset{\sim}{x},t) \cdot dV(\underset{\sim}{y}) \quad . \qquad (6.12)$$

$\underset{\sim}{f}$ body force vector,

$\underset{\sim}{t}$ traction vector in the deformed configuration,

ρ density in the deformed configuration, and

$\underset{\sim}{u}$ displacement vector

In the absence of body forces, and when inertial effects are negligible, equation (6.12) reduces to

$$\int_{S_t} \underset{\sim}{t} \cdot d\underset{\sim}{A}(\underset{\sim}{y}) = \underset{\sim}{0} \quad . \tag{6.13}$$

From Equation (5.14)

$$\underset{\sim}{t} = \frac{d\underset{\sim}{A}(\underset{\sim}{x})}{d\underset{\sim}{A}(\underset{\sim}{y})} \underset{\sim}{\sigma} \underset{\sim}{N} \quad .$$

When this is applied to equation (6.13) it gives rise to,

$$\int_{S_o} \underset{\sim}{\sigma}\, \underset{\sim}{N}\, d\underset{\sim}{A}(\underset{\sim}{x}) = \underset{\sim}{0} \quad . \tag{6.14}$$

From the divergence theorem,

$$\int_{D_o} (\underset{\sim}{\nabla}(\underset{\sim}{x}) \underset{\sim}{\sigma})\, dV(\underset{\sim}{x}) = 0$$

for every choice of D_o. Therefore,

$$\underset{\sim}{\nabla}(\underset{\sim}{x}) \underset{\sim}{\sigma} = \underset{\sim}{0} \quad . \tag{6.15}$$

From equation (5.15)

$$\underset{\sim}{\sigma} = \underset{\sim}{E}\, \underset{\sim}{S}$$

and from equation (5.28)

$$\underline{\underline{S}} = \underline{\underline{S}}' - p_f \underline{\underline{1}} \quad .$$

These relations reduce equation (6.15) to

$$\nabla(\underline{x})^T(\underline{\underline{E}}\underline{\underline{S}}') - \nabla^T(\underline{x})(\underline{\underline{E}}\, p_f) = \underline{0} \quad . \tag{6.16}$$

At this point the assumption regarding the coincidence of principal frames greatly simplifies the problem. The Lagrangian strain tensor, under the assumption of axisymmetry and plane strain, turns out to have a diagonal component matrix in the coordinate frame chosen herein. This, along with the coincidence assumption, implies that the second Piola Kirchhoff stress tensor, $\underline{\underline{S}}$, and hence $\underline{\underline{S}}'$, will also have a diagonal component matrix in this frame, and the components are given by

$$[\underline{\underline{S}}]^e = \begin{pmatrix} S'_R & 0 & 0 \\ 0 & S'_\theta & 0 \\ 0 & 0 & S'_z \end{pmatrix} \tag{6.17}$$

$$[\underline{\underline{E}}]^e = \begin{pmatrix} 1+u_{R,R} & 0 & 0 \\ 0 & 1+\frac{u_R}{R} & 0 \\ 0 & 0 & 1 \end{pmatrix}. \tag{6.18}$$

From equations (6.16), (6.17) and (6.18)

$$\frac{\partial}{\partial R}\left((1+u_{R,R})S'_R\right) + \frac{1}{R}\left((1+u_{R,R})S'_R - (1+\frac{u_R}{R})S'_\theta\right)$$

$$+ \frac{1}{R}\left(u_{R,R}-\frac{u_R}{R}\right)p_f - \frac{\partial}{\partial_R}\left((1+u_{R,R})p_f\right) = 0 \qquad (a)$$

$$\frac{1}{R}\frac{\partial}{\partial\theta}\left((1+\frac{u_R}{R})S'_\theta\right) - \frac{1}{R}\frac{\partial}{\partial\theta}\left((1+\frac{u_R}{R})p_f\right) = 0 \qquad (b)$$

$$\frac{\partial S'_z}{\partial z} - \frac{\partial}{\partial z}p_f = 0 \qquad . \qquad (c) \qquad (6.19)$$

Equations (6.19a, b and c) describe the equilibrium conditions. Since the strains are only functions of R and T, this will also be the case for stresses. For this reason,

$$\frac{\partial p_f}{\partial\theta} = 0 \qquad \text{and}$$

$$\frac{\partial p_f}{\partial z} = 0 \quad .$$

These two conditions imply that

$$p_f = p_f(R,t) \quad . \qquad (6.20)$$

Therefore, the entire problem depends on two independent variables namely, R and t.

6.2.3 Simplifying Assumptions

There are two main assumptions made in analyzing the initial expansion of the cavity. The first assumption is that the cavity

already exists and only its expansion is modeled. This assumption renders the corresponding motion to be admissible. If the inception of the cavity is considered, then a rupture of the continuum is inevitable. A rupture violates assumptions i) and ii) of section 5.2.1, which are required for the motion to be admissible. For this reason, it is assumed here that the cavity already exists.

The second assumption is that the expansion rate of the cavity is much higher than the velocity of pore water through the soil medium under the pressure gradients developed during the expansion. This flow of fluid is given by Darcy's equation

$$v = -\frac{k}{\rho_f g}\frac{\partial p_f}{\partial R} \quad , \tag{6.21}$$

where

v the velocity of the pore fluid relative to the soil lattice

p_f pore fluid pressure

k permeability of soil

ρ_f density of the pore fluid

Under the pressure gradients commonly encountered in clay, v is on the order of 10^{-8} cm/sec. Therefore, the assumption is valid for expansion rates on the order of mm/hr, or faster.

This assumption implies that during initial expansion of the cavity the relative velocity of the pore fluid may be assumed to be negligible. Hence, the soil may be assumed to be deforming under undrained conditions.

6.2.4 Formulation Associated with the Rapid Expansion

From the second assumption made in the previous section it follows that the deformation may be taken as undrained. Since in soil mechanics the deformation of the solid soil particles is neglected and water is taken to be incompressible, an undrained deformation implies that the volume of the sample is conserved. The conservation of volume implies that

$$\det(\underline{F}) = \det(\underline{1} + \underline{\nabla u}) = 1 \quad .$$

This results in

$$(1 + u_{R,R})(1 + \frac{u_R}{R})1 = 1$$

and hence

$$u_{R,R} + \frac{u_R}{R} + \frac{u_R}{R} \cdot u_{R,R} = 0 \quad . \tag{6.22}$$

Equation (6.22) can be solved in closed from resulting in

$$u_R = \sqrt{R^2 + r_o^2(t) - R_o^2} - R \, , \tag{6.23}$$

where

R_o initial radius of the cavity

$r_o(t)$ cavity radius at any given time t

The current radius r can be given by

$$r = R + u_R = \sqrt{R^2 + r_o^2 - R_o^2} \ .$$

Figure (6.1) shows a cross section of the infinite medium perpendicular to the z axis.

A non-dimensional current radius r* can be defined as follows:

$$r^* = \frac{r}{R} = \sqrt{1 + \frac{r_o^2 - R_o^2}{R^2}} \ . \qquad (6.24)$$

Then,

$$u_{R,R} = - \frac{r^*-1}{r^*} \ .$$

The introduction of r* in this manner produces a strain tensor dependent only on r*. This, in turn, produces stresses which are only dependent on r*. Therefore, it is sufficient to derive the response for varying r*.

The strain tensor can be expressed in terms of r* as

$$\underline{E}(r^*) = \begin{pmatrix} -\frac{r^{*2}-1}{2r^{*2}} & 0 & 0 \\ 0 & \frac{r^{*2}-1}{2} & 0 \\ 0 & 0 & 0 \end{pmatrix} . \qquad (6.25)$$

Therefore,

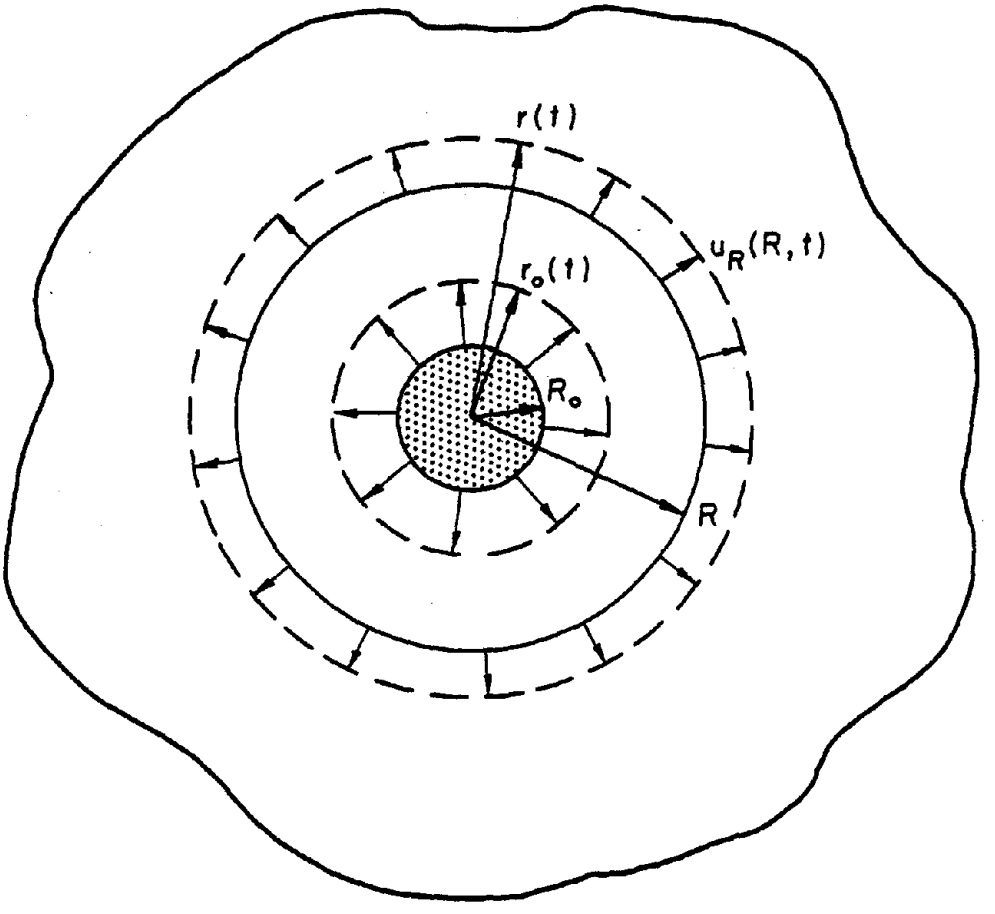

FIGURE 6.1 GEOMETRY OF THE EXPANDING CYLINDRICAL CAVITY

$$\varepsilon_R = -\frac{r^{*2}-1}{2r^{*2}} \qquad (a)$$

$$\varepsilon_\theta = \frac{r^{*2}-1}{2} \qquad (b)$$

$$\varepsilon_z = 0 \qquad (c) \qquad (6.26)$$

which results in

$$e = e_o \qquad (a)$$

$$\varepsilon = \frac{r^{*2}-1}{3r^{*2}} \cdot \sqrt{1 + r^{*2} + r^{*4}} \quad . \qquad (6.27)$$

If the expansion begins from a normally consolidated state, then $\varepsilon_o = 0$. Solving the constitutive equations for this case results in

$$p = p_o \exp\left[-\frac{\gamma f}{K}\left(1-\exp\frac{-0.3(1+e_o)\varepsilon(r^*)}{f}\right)\right] \qquad (a)$$

$$q = Mp\left[1-\exp\frac{-0.3(1+e_o\varepsilon)\varepsilon(r^*)}{f}\right]^{0.5} \quad . \qquad (b) \qquad (6.28)$$

Equation (5.39) defines the principal stress components in terms of p and q. And hence the principal stress components can be given by

$$S'_R = p + \frac{1}{3}\int_{q_o}^{q} \frac{2+r^{*2}}{\sqrt{1+r^{*2}+r^{*4}}}\,dq - p_o + S'_{Ro} \qquad (a)$$

$$S'_\theta = p + \frac{1}{3}\int_{q_o}^{q} \frac{1+2r^{*2}}{\sqrt{1+r^{*2}+r^{*4}}}\,dq - p_o + S'_{\theta o} \qquad (b)$$

$$S'_z = p + \frac{1}{3}\int_{q_o}^{q} \frac{r^{*2}-1}{\sqrt{1+r^{*2}+r^{*4}}}\,dq - p_o + S'_{z_o} \quad . \quad (c) \qquad (6.29)$$

Since S'_R, S'_θ and S'_z have been found, the pore pressure p_f can be obtained from equation (6.19a) which reduces to

$$\frac{\partial}{\partial R}\left(\frac{R\,S'_R}{r^*}\right) - \frac{\partial}{\partial R}\left(\frac{R\,p_f}{r^*}\right) - r^*\,S'_\theta + r^*\,p_f = 0 \quad . \qquad (6.30)$$

This is the only equation that cannot be solved analytically.

6.3 THE SOLUTION

6.3.1 Numerical Implementation

In order to compute the numerical values of the stresses and pore pressures during the expansion, it is necessary to assign numerical values to the material constants. The material used for this purpose is Kaolin. The values of the material constants for Kaolin (Roscoe et al., 1968) are given in Table (6.1).

TABLE 6.1

λ	κ	M
0.27	0.0405	0.90

The strain components are defined in terms of the non-dimensional radius r^* as given by equations (6.26a), (6.26b) and (6.26c). The strain-space variables e and ε are given by equation (6.27). From these

variables, the effective pressure p, and the effective shear stress q, can be found with the aid of equations (6.28a) and (6.28b). From p and q the effective stresses S'_R, S'_θ and S'_z can be evaluated using equations (6.29a), (6.29b), and (6.29c). Finally, the pore pressure can be obtained from the equilibrium equation which is given in a simplified form by equation (6.30). Equations (6.28) and (6.29) require the initial values of p and q while equation (6.30) requires boundary values of S'_R, S'_θ and p_f.

The initial conditions are taken as follows,

$$\begin{aligned} S'_R(R,0) &= S_o \\ S'_\theta(R,0) &= S_o \\ S'_z(R,0) &= S_o \\ p_f(R,0) &= p_{fo} \quad . \end{aligned} \tag{6.31}$$

Equation (6.31) implies that

$$\begin{aligned} p(R,0) &= S_o, \quad \text{and} \\ q(R,0) &= 0 \quad . \end{aligned} \tag{6.32}$$

Further, define some non-dimensional variables as follows.

$$S'^{*}_R(R,t) = \frac{S'_R(R,t)-S_o}{S_o} \quad ; \quad S^{*}_R = S'_{R+1}$$

$$S'^{*}_{\theta}(R,t) = \frac{S'_{\theta}(R,t)-S_o}{S_o} \quad ; \quad S^{*}_{\theta} = S'^{*}_{\theta}+1$$

$$S'^{*}_{z}(R,t) = \frac{S'_{z}(R,t)-S_o}{S_o} \quad ; \quad S^{*}_{z} = S'^{*}_{z}+1$$

$$p^{*}(R,t) = \frac{p(R,t)}{S_o}$$

$$q^{*}(R,t) = \frac{q(R,t)}{S_o}$$

$$p^{*}_{f}(R,t) = \frac{p_f(R,t)-p_{fo}}{S_o} \quad . \tag{6.33}$$

The boundary conditions are chosen at a point infinitely far away from the cavity wall. It is assumed that

$$f(R,t) = f(R,0) = f_o \qquad \forall t \in (0,T) \text{ and } \forall\ R > R_\infty \quad , \tag{6.34}$$

where f may refer to any of the variables considered in this chapter. There are two implications made by equation (6.34). One is that before the expansion the stresses, strains and displacements are uniform over the entire space under consideration. The other is that during the time under consideration, the variables do not change their values from their respective initial values at points sufficiently far away from the cavity wall.

It has been shown that the strain tensor and hence all the components of the stress tensor and the pore pressure depend only on r^*. This implies

$$f(R,t) = r^* \quad .$$

But

$$r^* = \sqrt{1 + \frac{(r_o/R_o)^2 - 1}{(R/R_o)^2}} \quad . \tag{6.36}$$

Therefore,

$$r^* = r^*(R/R_o, r_o/R_o) \quad .$$

This in turn implies that

$$f(R,t) = f(R/R_o, r_o/R_o) \quad . \tag{6.37}$$

The variables are evaluated by a simple computer code developed using the finite difference method. The non-dimensional radius R/R_o represents the radial coordinate. For numerical computation this variable has to be discretized. From equations (6.24) and (6.26) it is seen that the strains are high at points near the cavity wall and that they decrease rapidly at points farther away from the wall. For this reason, the stresses and pore pressure will also vary rapidly in the vicinity of the cavity wall. Therefore, it is necessary to choose more points of computation close to the cavity wall than away from the wall. This is achieved by uniformly discretizing $\log_{10}(R/R_o)$. The discretized non-dimensional radius array (R_i/R_o) is defined as

$$(R_i/R_o) = (R_\infty/R_o)^{i/N} \quad ,$$

where

R_∞ the largest value of R to be considered, and

N number of computation points .

The code was tested with different choices of R_∞ and N. The comparisons were made on the pore pressure predictions as the pore pressure is the final variable calculated. The errors in all other variables would be reflected in the pore pressure as it contains, in its calculation, all variables except S_z^*. The values of the pore pressure corresponding to the different sets of values considered for R_∞ and N are shown in Table (6.2). For this test run, the value of the expansion ratio r_o/R_o was taken to be 1.1.

TABLE 6.2

N	R_∞/R_o	p_f^*
1,000	10	0.76667
2,000	100	0.78597
3,000	1,000	0.78616
5,000	100,000	0.78616
4,500	1,000	0.78616
900	1,000	0.79197
600	1,000	0.79500

It can be seen from Table 6.2 that increasing N beyond 3,000 or increasing R_∞/R_o beyond 1,000 does not change the value of p_f^* expressed to five significant places. Since five significant places are considered sufficiently accurate for the prediction, N and R_∞/R_o are taken to be 3,000 and 1,000, respectively, in the computations that follow.

The computations are made for values of r_o/R_o varying from 1.0 to 1.5. The value of r_o/R_o equal to 1.0 corresponds to the initial state with no expansion. Hereafter, this state is referred to as the reference state and the values of all the variables corresponding to the reference state are referred to as the reference values.

6.3.2 Model Predictions

The stresses and pore pressure calculated are graphically presented in this section. The variables are shown as functions of the non-dimensional reference radius R/R_o. Each function is plotted for several values of the expansion ratio r_o/R_o. The values of r_o/R_o used here are 1.01, 1.02, 1.05, 1.1, 1.2 and 1.5. Expansion ratios more than 1.5 are not shown as they induce strains larger than 50% around the cavity wall and most experimental data used in the model are valid only for strains up to 20%.

Figure (6.2a) shows the variation of the non-dimensional effective pressure p^*. The value of p^* is 1 for all values of R/R_o during the reference state. When r_o/R_o is 1.01, p^* drops below 1 in the vicinity of the cavity, but the effect is not felt beyond distances of three times the cavity radius. As the expansion ratio increases, the value of

p^* drops at the cavity wall and the effect propagates farther. When r_o/R_o reaches a value of 1.2, p^* at the cavity wall reaches its critical state value of 0.55 and remains at that value thereafter.

Figure (6.2b) shows the variation of the non-dimensional effective shear stress q^*. The value of q^* is zero for all values of R/R_o in the reference state. The behavior of q^* during the subsequent deformation is similar to that of p^* except for three main differences. The first difference is that the value of q^* changes very rapidly at the initial stages of expansion. This is to be expected because of the very high value of shear modulus at the inception of loading.

The second difference is that q^* reaches its critical state value of 0.50 at the cavity wall for an expansion ratio of about 1.05. This expansion ratio is much smaller than that corresponding to p^*, which is 1.20. Such an observation is consistent with experimental observations. From the data presented in Chapter IV for undrained expansion it is seen clearly that q^* reaches its critical state value faster than p^*. The fact that q^* reaches its critical state value faster than p^* can also be seen from the stress trajectory shown in Figure (6.3).

Finally, q^* increases as the expansion progresses, while p^* decreases.

Figure (6.4) shows the variation of the non-dimensional effective radial stress S'^*_R as a function of the non-dimensional radius R/R_o. S'^*_R

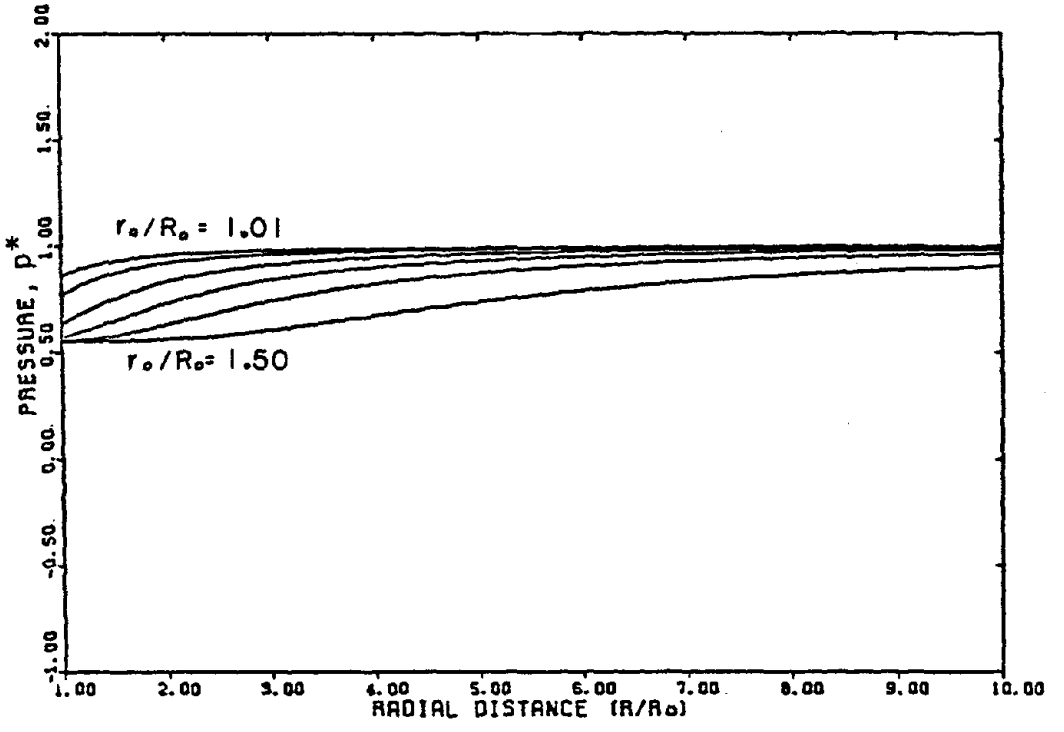

FIGURE 6.2a VARIATION OF THE NON-DIMENSIONAL PRESSURE

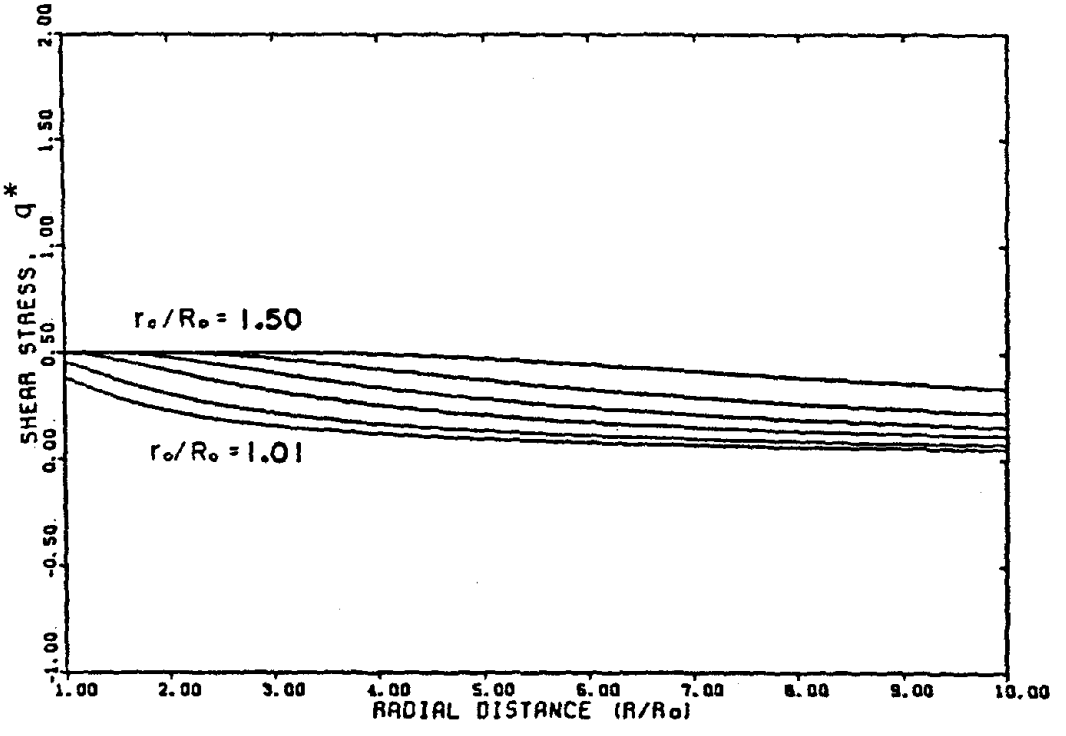

FIGURE 6.2b VARIATION OF THE NON-DIMENSIONAL SHEAR STRESS

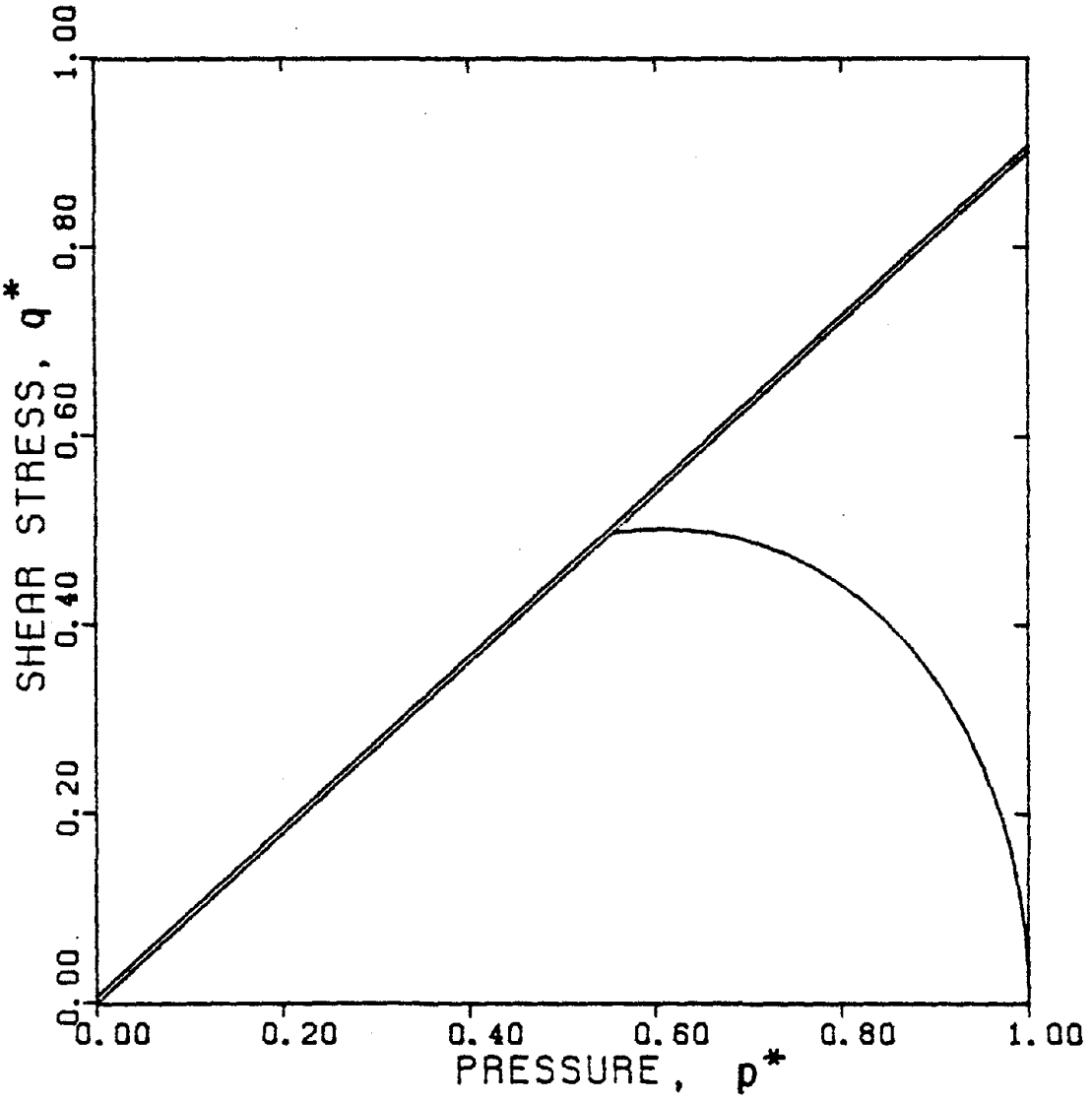

FIGURE 6.3 STRESS TRAJECTORY AT THE WALL

can be expressed in terms of p^* and q^* as follows,

$$S'^{*}_{R} = p^* + \frac{1}{3}\int_{o}^{q^*} \frac{2+r^{*2}}{\sqrt{1+r^{*2}+r^{*4}}}\, dz^* \qquad (6.38)$$

where,

$$z^*(r^*) = q^*(r^*) \quad .$$

It is seen from Figures (6.2a) and (6.2b) that p^* decreases and q^* increases as r_o/R_o increases. Further, it is also found that the rate of increase of q^* is much higher than the rate of decrease of p^* for values of r_o/R_o close to 1. It is hence clear that for values of r_o/R_o close to 1, S'^{*}_{R} will increase.

But q^* reaches its critical state value at expansion ratios much smaller than those corresponding to p^*. For this reason, as the expansion proceeds S'^{*}_{R} will begin to reduce, finally reaching a steady value.

These effects seen from the equation defining S'^{*}_{R} are found in Figure (6.4). S'^{*}_{R} is zero in the reference state, namely, for $r_o/R_o=1$. As r_o/R_o increases to 1.01, it is seen that the value of S'^{*}_{R} at the cavity wall has become positive. For the value of $r_o/R_o = 1.02$, S'^{*}_{R} is still positive at the cavity wall, but is smaller than the value corresponding to $r_o/R_o=1.01$. For values of $r_o/R_o=1.05$, and 1.1, the value of S'^{*}_{R} at the wall is negative and decreasing. Beyond $r_o/R_o=1.1$ the value of S'^{*}_{R} at the wall remains constant at its critical state

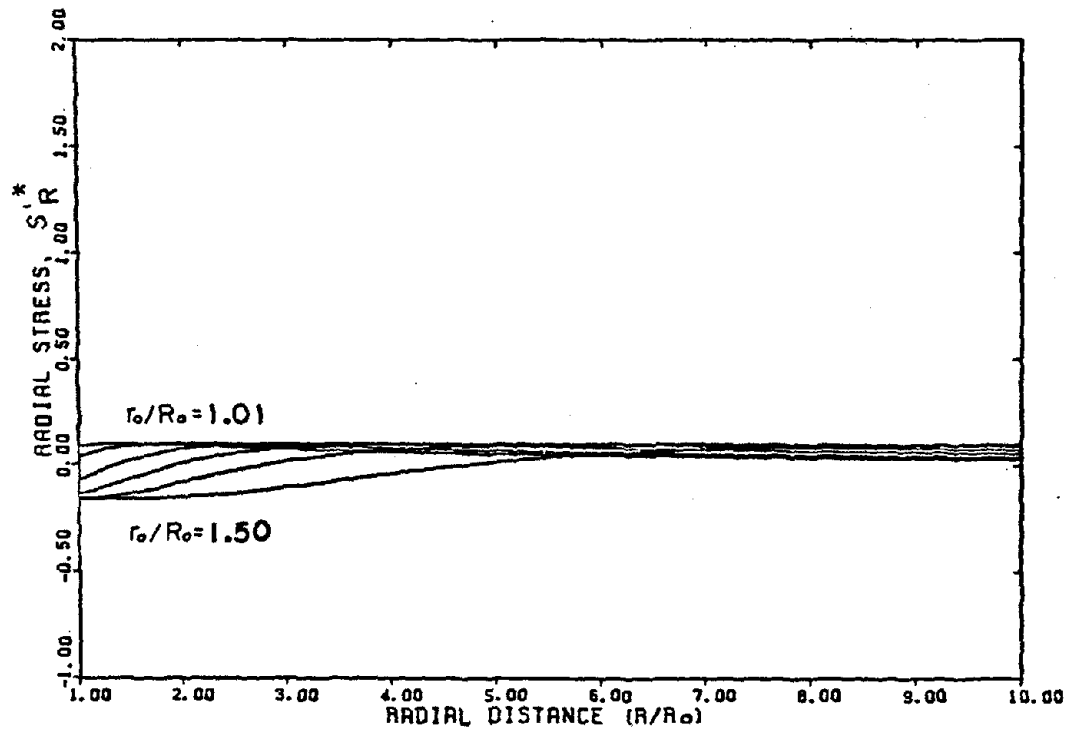

FIGURE 6.4 VARIATION OF THE NON-DIMENSIONAL RADIAL STRESS

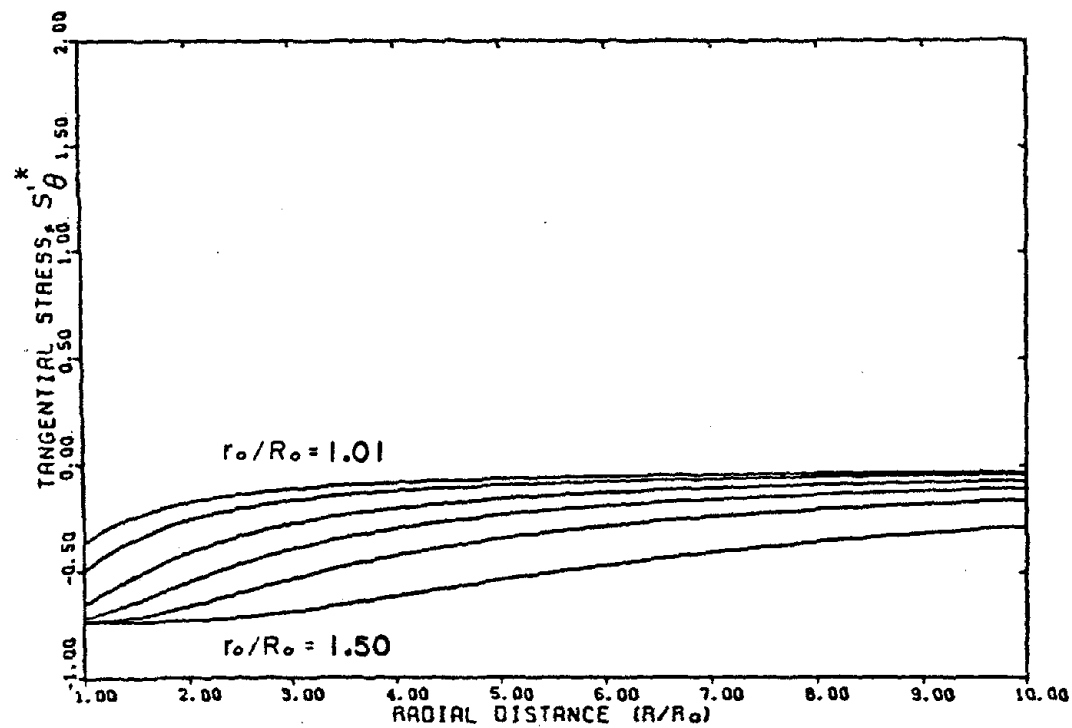

FIGURE 6.5 VARIATION OF THE NON-DIMENSIONAL TANGENTIAL STRESS

value of -0.15. Also, the positive values of S'^{*}_{R} propagate away from the cavity wall as the expansion proceeds.

Figure (6.5) shows the variation of the non-dimensional effective tangential stress S'^{*}_{θ}. Unlike the case of S'^{*}_{R}, S'^{*}_{θ} decreases from its reference value of zero during all stages of expansion. The value of S'^{*}_{θ} at the wall also reaches its critical state value of -0.75 at an expansion ratio of about 1.1.

The reason that the behavior of S'^{*}_{θ} is different from that of S'^{*}_{R} can be seen by taking a closer look at the equation defining S'^{*}_{θ}. From equation (6.29b),

$$S'^{*}_{\theta} = p^{*} - \frac{1}{3}\int_{0}^{q^{*}} \frac{1+2r^{*2}}{\sqrt{1+r^{*2}+r^{*4}}}\, dz^{*} \quad , \tag{6.39}$$

where,

$$z^{*}(r^{*}) = q^{*}(r^{*}) \quad .$$

Although p^{*} decreases while q^{*} increases, the coefficient of the term containing q^{*} is negative. Therefore, S'^{*}_{θ} would be always decreasing.

Figure (6.6) shows the variation of the non-dimensional effective axial stress S'^{*}_{z}. Here again it is found that S'^{*}_{z} always decreases from its reference value of zero. The value of S'^{*}_{z} at the wall reaches its critical state value of -0.45 for an expansion ratio of about 1.1.

The reason for the monotonic decrease of S'^{*}_{z} is more subtle than

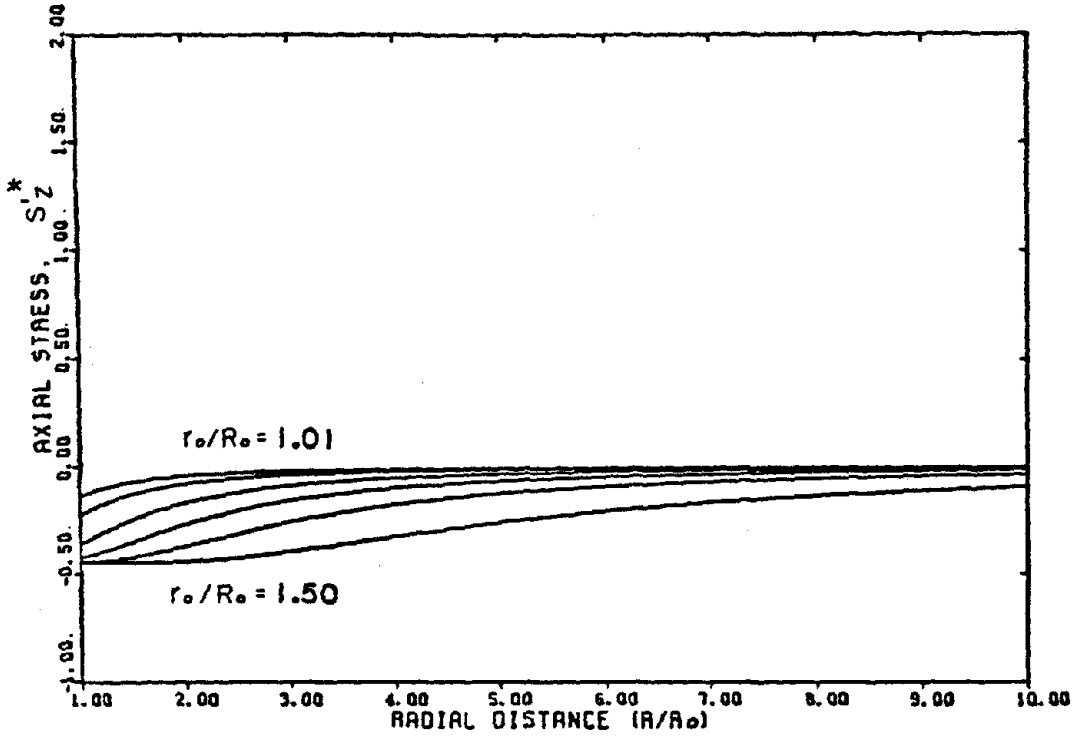

FIGURE 6.6 VARIATION OF THE NON-DIMENSIONAL AXIAL STRESS

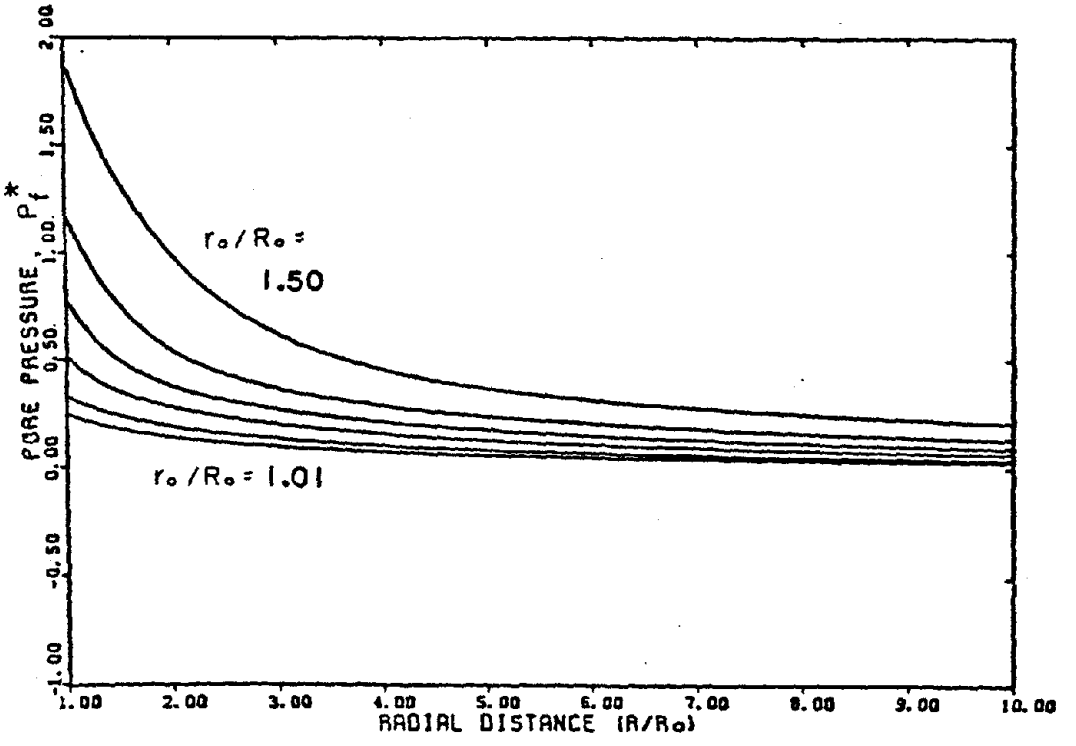

FIGURE 6.7 VARIATION OF THE NON-DIMENSIONAL PORE PRESSURE

that for S'^{*}_{θ}. The stress S'^{*}_{z} is defined as

$$S'^{*}_{z} = p^{*} + \frac{1}{3}\int_{0}^{q^{*}} \frac{r^{*2} - 1}{\sqrt{1+r^{*2}+r^{*4}}} \cdot dz^{*} \quad , \qquad (6.40)$$

where

$$z^{*}(r^{*}) = q^{*}(r^{*}) \quad .$$

At the reference state, r^{*} is unity. As the deformation proceeds r^{*} increases. Let

$$r^{*} = 1 + \mu \, , \qquad \mu \geq 0 \quad .$$

Then, it can be seen from equations (6.28a) and (6.28b), that, for values of μ very much smaller than 1,

$$p^{*} \sim (1-\mu) \quad \text{and,}$$
$$q^{*} \sim \mu \quad .$$

This, in turn, implies that

$$S'^{*}_{z} \sim 1 - \mu + c\mu^{3/2} \quad .$$

Therefore, S'^{*}_{z} will reduce initially. As the deformation progresses, q^{*} will reach its critical state value, while p^{*} is still decreasing. When this occurs it can be seen from equation (6.40) that S'^{*}_{z} will behave like p^{*}, thereby decreasing in value. For this reason, S'^{*}_{z} decreases monotonically.

Figure (6.7) shows the variation of the non-dimensional pore pressure $\bar{p}_f^*$ with R/R_o for different values of r_o/R_o. The non-dimensional pore pressure decreases monotonically. It is seen from the figure that even after the stresses reach their critical state values at the wall, the pore pressure at the wall keeps increasing. This occurs because the pore pressure depends on the equilibrium of the soil mass. The equilibrium equation corresponding to a state where the stresses, S'^*_R, S'^*_θ have reduced to their respective critical state values S'^*_{Rc}, $S'^*_{\theta c}$ reduces to

$$\left(\frac{r^{*2}-1}{r^{*2}}\right)\frac{dp_f^*}{dy^*} \approx r^*(S'^*_{\theta c}-p_f^*) - \left(\frac{2r^{*2}-1}{r^{*3}}\right)(S'^*_{Rc}-p_f^*) \quad . \qquad (6.41)$$

Although the stresses remain constant at the critical state, the deformation proceeds. Hence r* would not remain a constant. For this reason, the slope of p_f^* would be changing even after the stresses reach their critical state value.

6.4 COMPARISON WITH OTHER RESULTS

6.4.1 Experimental Results

Figure (6.8) shows the model prediction for the non-dimensional pore pressure as a function of the non-dimensional deformed radius r/r_o along with some experimental results. The model prediction shown corresponds to an expansion ratio of 1.5. The experimental results are

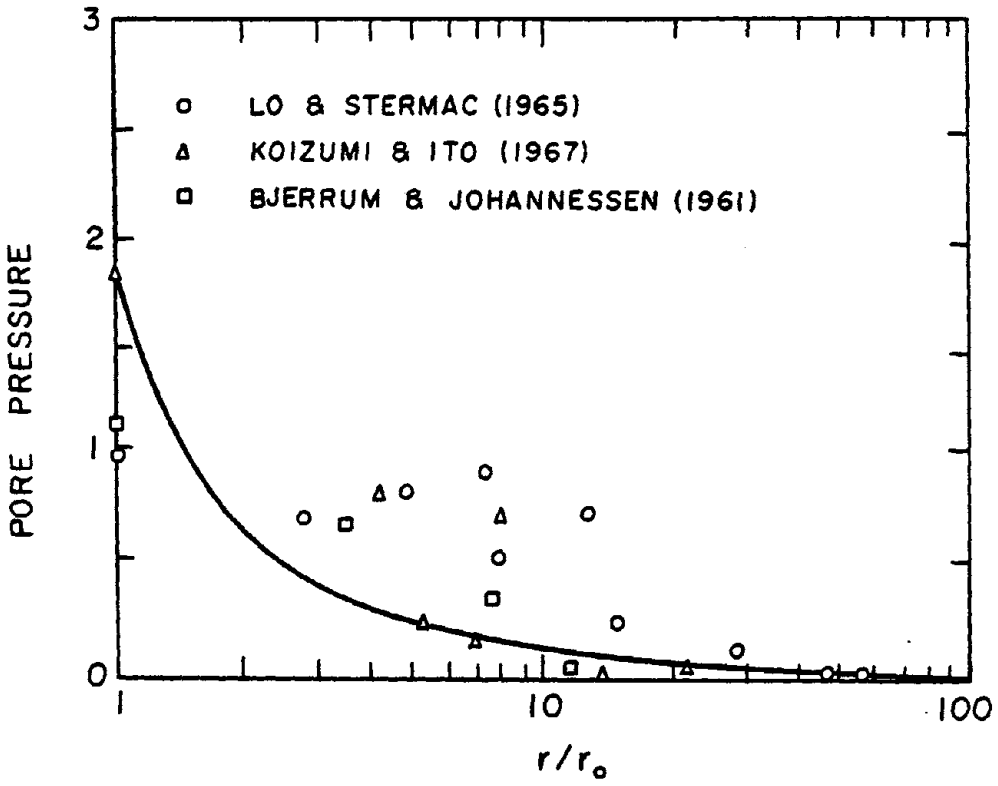

FIGURE 6.8 COMPARISON OF THE MODEL PREDICTIONS WITH EXPERIMENTAL DATA

those of Lo and Stermac (1965), Koizumi and Ito (1967), and Bjerrun and Johannessen (1961).

From the figure it is clear that the experimental results shows a very large scatter. The scatter is due to the influence of reaction piles, disturbance of the stress field by the measuring devices and inaccuracies involved in device location. Given such a scatter, the model prediction is close to the mean of the experimental observations.

6.4.2 Ladanyi's Calculations

In this section, the strain-space model prediction is compared with Ladanyi's calculations (Ladanyi, 1963). Ladanyi observes that an undrained plane strain triaxial test produces stress states similar to those produced by an expanding cylindrical cavity. Using this similarity, he directly calculates the components of stresses induced during the expansion of a cylindrical cavity, from the triaxial data.

There are three main differences between the strain-space model calculations and Ladanyi's calculations. First, Ladanyi's calculations are based on test data for Drammen clay. Since consolidation test results were not available from his paper it was not possible to obtain the material constants λ, K and M necessary for calculations, using the strain-space model. For this reason the strain-space model results correspond to Kaolin. However, both clays are similar in structure and mechanical behavior.

The second difference is in the stresses and strains employed. Ladanyi uses Eulerian strains and Cauchy stresses whereas the strain-space model uses Lagrangian strains and second Piola-Kirchoff stresses.

Finally, Ladanyi's calculations imply that the results are only a function of the non-dimensional deformed radius r/r_o. The results of the strain-space calculations indicate that the independent variables are r/r_o and r_o/R_o. Ladanyi's results would imply that the stresses at the wall do not vary with the degree of expansion, but that is not the case in reality.

Figures (6.9a) and (6.9b) show the strain-space model prediction and Ladanyi's results, respectively. Taking into account the differences mentioned above, the two results are qualitatively very similar. Both show critical state is reached close to the wall, that is, $r/r_o \simeq 1$. The calculations made by Ladanyi indicate that critical state is attained approximately for $r/r_o \leq 3$, while the strain-space calculations indicate that it occurs for $r/r_o \leq 1.5$. This is mainly due to the difference in the material properties.

From the undrained shear stress strain curve used in Ladanyi's calculations it is seen that q reaches 0.9 times its critical state value for an axial strain of about 0.4%. From the data on Kaolin presented in Figure (4.2) it is seen that this value is about 2%. This would clearly result in the Drammen clay reaching critical state at strains much smaller than those for Kaolin. This, in turn, implies that

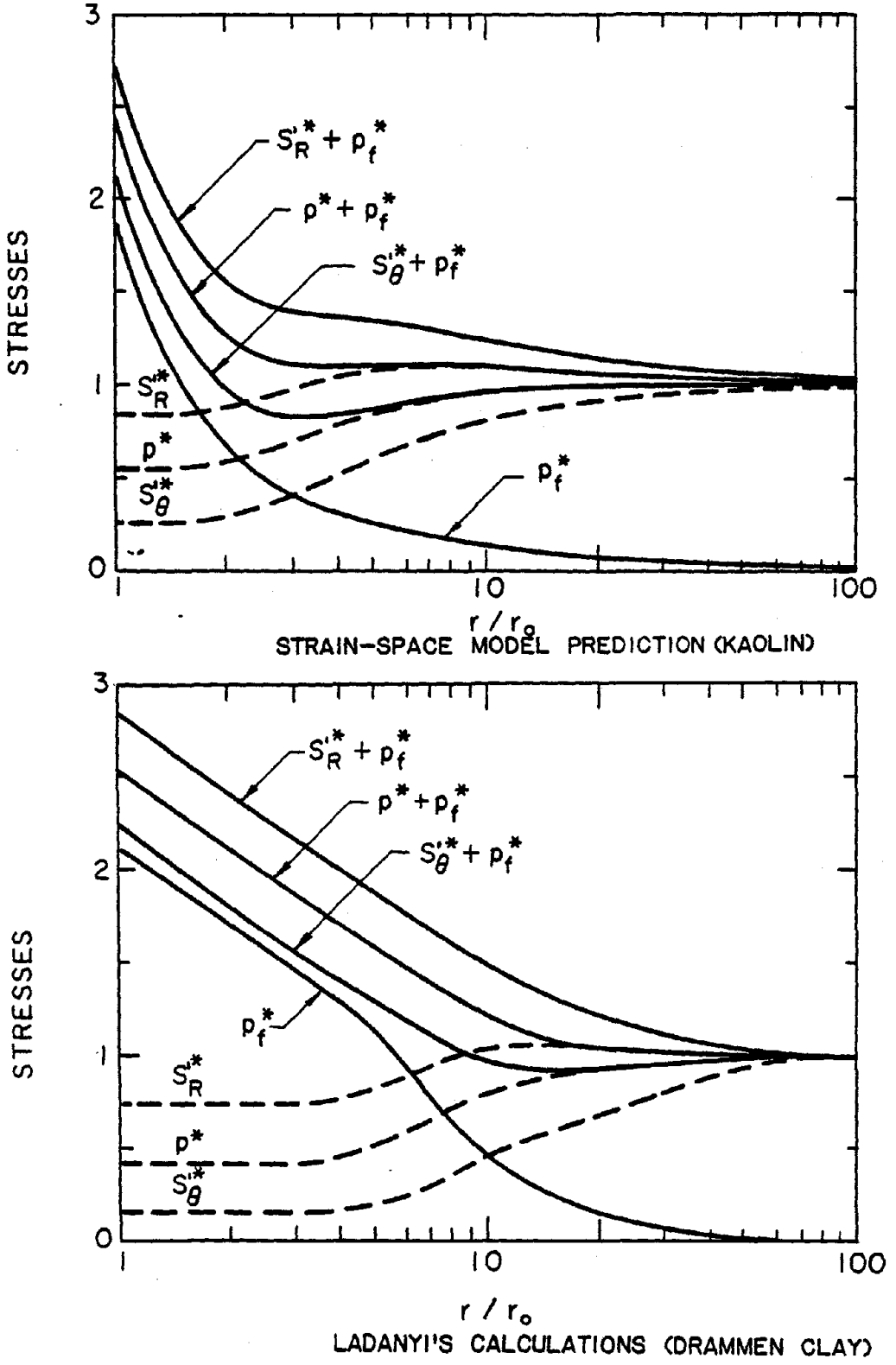

FIGURE 6.9 COMPARISON OF STRESS DISTRIBUTIONS

any prediction using Drammen clay data will show critical state behavior for values of r/r_o larger than those based on Kaolin.

Consider the variation of the normalized effective radial stress S_R^*. As r/r_o decreases from 100, S_R^* increases, initially reaching a maximum value of about 1.10 and 1.05 in the cases of the strain-space prediction and Ladanyi's calculations, respectively. The strain-space prediction of S_R^* reaches a maximum for $r/r_o = 7$, while Ladanyi's calculations reach this maximum for $r/r_o = 15$. In both cases S_R^* becomes negative at the cavity wall, namely, at $r/r_o = 1$.

The normalized effective pressure p^* and the normalized effective tangential stress S_θ^* increase monotonically in both cases.

The variation of the normalized pore pressure, p_f^*, is quite different between the two predictions. In the case of the strain-space prediction, the pore pressure increases as r/r_o decreases and the slope of the curve also increases monotonically. But in the case of Ladanyi's prediction, although p_f^* increases monotonically with decreasing r/r_o, the slope increases and then decreases, reaching a constant value. This discrepancy is mainly due to the different types of strains employed in the two methods. The Lagrangian strain increases much faster than the Eulerian strain as r/r_o decreases. This results in very large Lagrangian strain components around the cavity wall. This makes the pore pressure gradient steeper in the vicinity of the cavity wall.

6.4.3 Predictions of a Rate Type Model

The model used for comparison is a rate type model developed by Davis and Mullenger (1984). The model uses among other constants a shear modulus denoted by μ. The value taken for μ is 6.4 times the critical state pressure. The critical state pressure is of the same order of magnitude as the initial pressure. The values commonly used for clays are an order of magnitude higher than those used by Davis and Mullenger. Davis and Mullenger did not use material constants corresponding to any specific material. Therefore, the materials are different between the two predictions.

Figure (6.10a) shows the strain-space model prediction while Figure (6.10b) shows the Davis and Mullenger prediction. Both predictions are for quantities at the cavity wall. Qualitatively the two results are similar. The main differences arise from that fact that Davis and Mullenger use a constant shear modulus while the shear modulus of the strain-space model is infinite at the inception of the expansion and reduces rapidly thereafter. The stress components are ordered in the same way for both predictions

$$S'^{*}_{R} \geq S'^{*}_{z} \geq S'^{*}_{\theta} \quad .$$

But the prediction of S'^{*}_{R} is quite different between the two models quantitatively. Both the values of maximum S'^{*}_{R} and the expansion ratio corresponding to it are different between the two models. Table 6.3 shows these values for the two model predictions along with those from Ladanyi's calculations.

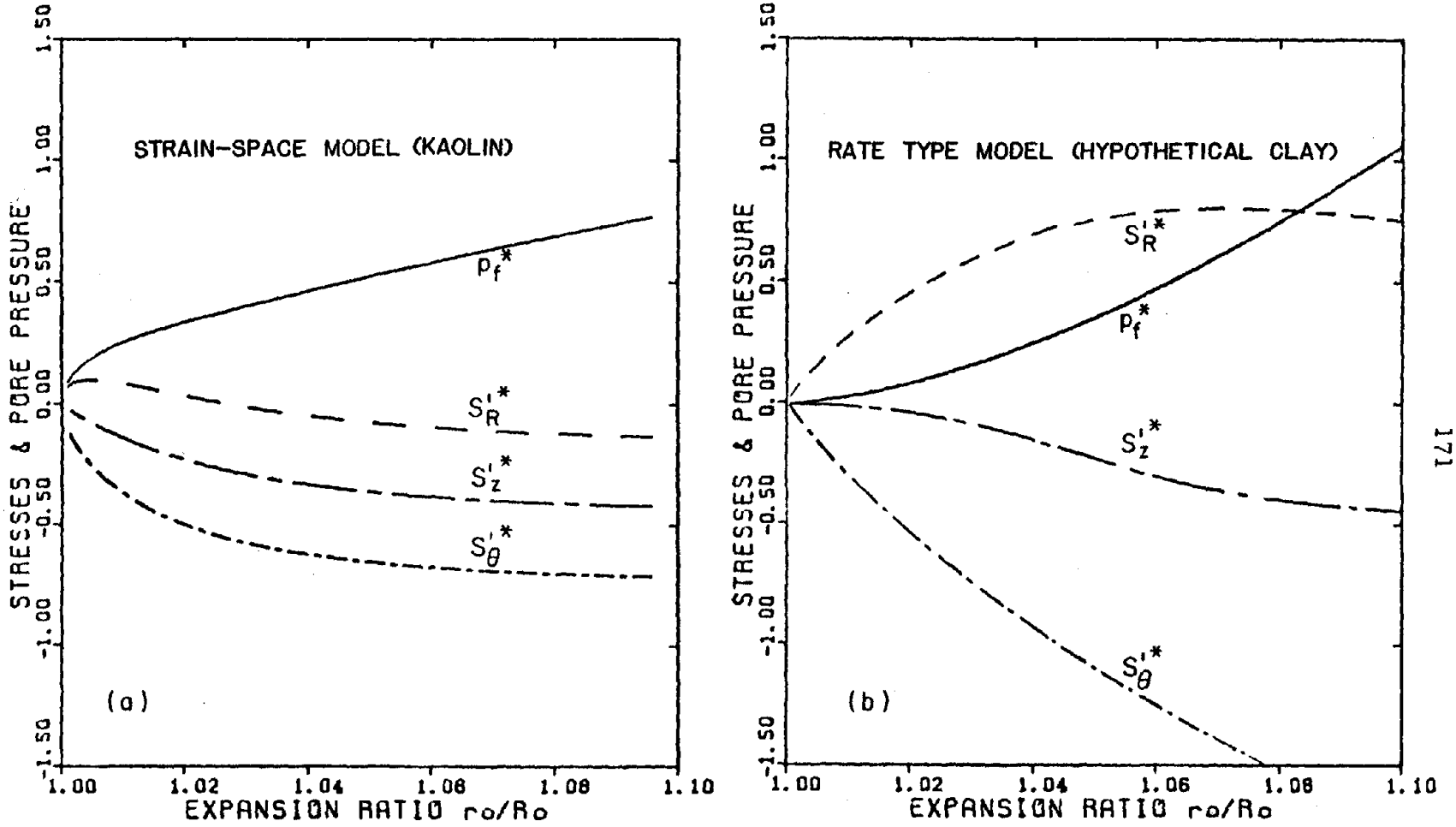

FIGURE 6.10 VARIATION OF THE CAVITY WALL STRESSES

TABLE 6.3

	S'^{*}_{R} maximum	r_o/R_o at S'^{*}_{R} max
Strain-space Model	0.1	1.005
Rate Type Model	0.05	1.005
Ladanyi's Calculations	0.8	1.07

The pore pressure predictions differ quite significantly in character between the two models. In both cases the pore pressures increase monotonically with increasing r_o/R_o. But the gradients of pore pressure differ. In the case of the strain-space prediction, the gradient of the pore pressure is high for low values of r_o/R_o and reduces monotonically reaching a constant positive value for the range of strains considered. The prediction made by Davis and Mullenger shows that the pore pressure begins with a zero gradient at $r_o/R_o = 1$ and then increases, subsequently reaching a positive constant higher than that of the strain-space prediction.

Ladanyi's calculations show a deviation from the strain-space prediction, but the deviation is in the opposite direction to that shown by Davis and Mullenger. At large strains, which correspond to smaller values of r_o/R_o, Ladanyi's calculations show that the pore pressure increase is lower than that predicted by the strain-space model.

6.4.4 Elastic Solution

Finally, a comparison is made with an elastic solution. Since such a solution is only valid for small strains, a linear elastic model is used to predict solutions for expansion ratios up to 1.01. There were two options available for elastic modeling. These were - using a compressible material with volume preserving deformation or using an incompressible material. The former was chosen because the latter requires that the effective pressure be specified independently. The material constants E and ν were taken to be 100 S_o and 0.3, respectively.

Figure (6.11) shows the elastic solution along with the strain-space model prediction for the variables p_f^*, S'^*_R and S'^*_θ as functions of r_o/R_o. For the material constants and range of expansions considered, the two results are reasonably close. For the range of expansion ratios considered the strain depends linearly on the expansion ratio and hence the elastic solutions are linear. Further, unlike Davis and Mullenger prediction, the pore pressure increases from the onset of the expansion. The strain-space prediction shows infinite slopes at $r_o/R_o = 0$ because of the infinite shear modulus at the inception of loading.

6.5 SUMMARY AND CONCLUSIONS

In this chapter the strain-space model is applied to a problem of an expanding cylindrical cavity. It has been seen that the effective pressure and the effective shear stress can be obtained in closed form. The stress components and the pore pressure can be obtained after some

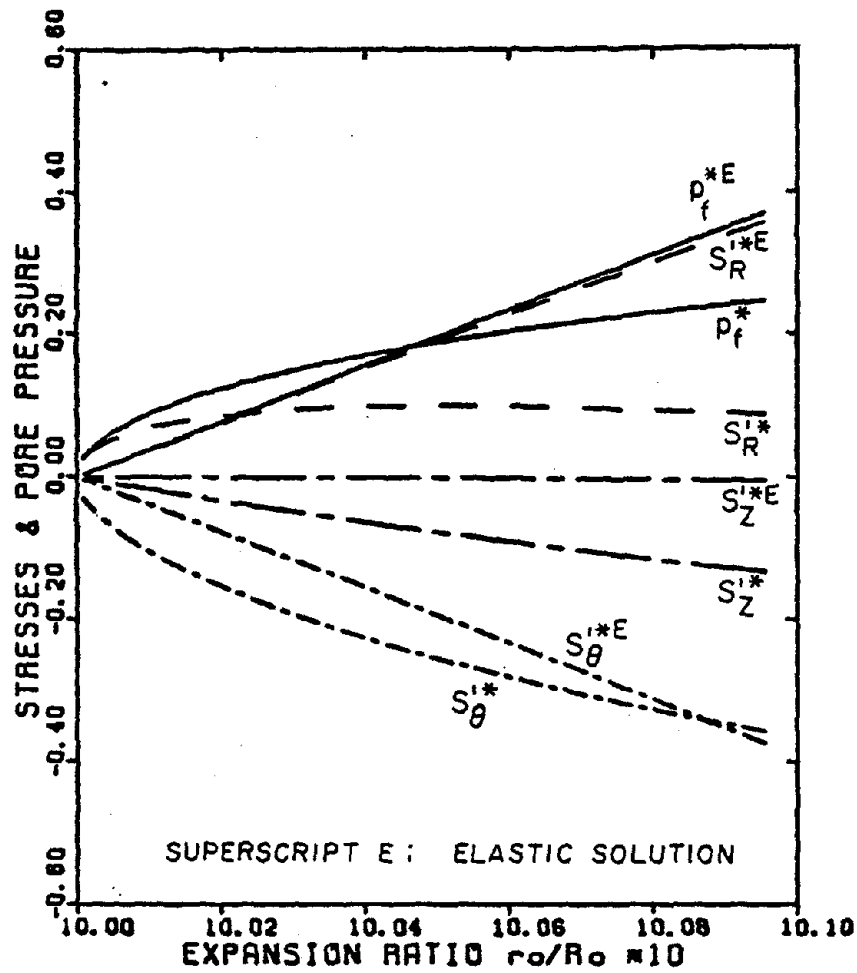

FIGURE 6.11 COMPARISON OF THE STRAIN-SPACE AND LINEAR ELASTIC SOLUTIONS AT THE WALL

simple numerical integration. The simple nature of the model makes possible such a straightforward solution process.

The solutions obtained from the model are compared with;

i) available experimental results,

ii) calculations made by Ladanyi directly from the results of experiments bearing some similarity to the expanding cavity, and

iii) the prediction made by Davis and Mullenger using a rate type soil model, and

iv) the elastic solution.

The experiments show results with very large scatter. The scatter is due to several reasons. Usually in pile experiments the loading is performed by introducing reaction piles and these piles are about 5 to 10 diameters away from the pile under experimentation. It is clear that this would affect the pressure distribution around the experimental pile. Therefore, the reliable readings are only those obtained very close to the experimental pile.

Secondly, the measurement of stress greatly depends upon the flexibility of the pressure transducers. Since soil is a soft medium, the measuring devices itself can easily affect the stress fields. Finally, the measurements must be made at depths sufficiently below the free surface of the soil so as to eliminate heaving effects and local failure. Hence, instruments have to be placed a few meters below the ground level. This is achieved by driving the instruments into the

ground with smaller tubes. A slight inclination of these tubes will cause large errors in locations at a few meters' depth.

In spite of all the potential sources of error in the experiment, the solutions obtained by the simple strain-space model predict pore pressures reasonably close to those observed from the experiments.

The second set of results used for comparison are those from Ladanyi's calculations. The simple strain-space model prediction is in good agreement with Ladanyi's prediction, although the material constants are somewhat different.

The third set of results are those from the prediction of a rate type soil model and once again qualitatively reasonable agreement is found.

It is evident from the comparisons made in this chapter that the simple strain-space model is capable of predicting general soil behavior. The simplicity of the model yields simple solutions. Hence, the strain-space model can be applied to other soil problems with certain simplifying assumptions made to facilitate analytic solutions.

CHAPTER VII

SUMMARY AND CONCLUSIONS

A simple strain-space constitutive model is developed herein for wet clays. Despite the large number of soil constitutive models available, the linear elastic solution is still popular in soil practice mainly because of its simplicity. With the aim of simplicity in mind, the model developed herein was based on a few physical characteristics of soils rather than on fitting extensive experimental data. From the past theories and experimental observations it was observed that the plastic behavior of clays would depend upon a nondimensional quantity defined herein as the over compression ratio. By defining the stresses to be functions of strains and this over compression ratio, it has been found that very simple functions are capable of predicting clay behavior quite accurately. The identification and use of this key variable greatly simplifies the formulation. Furthermore, as the model is developed in the strain-space, the solution process is also simpler. These two effects together make it possible to obtain closed form analytic solutions for a wider class of problems.

The model was initially developed for undrained, monotonic, triaxial loading cases. A very simple generalization was used to relax the constant volume, or the undrained, constraint. The model that evolved from this simple generalization has been verified by analyzing its prediction for constant pressure triaxial tests. These verifications are seen to substantiate the model.

Having relaxed the undrained constraint, the model was modified to accommodate load reversals. This was achieved by introducing a Bauschinger-like effect in the relationship between the normalized shear stress and over compression ratio. First, the simplicity of the model is not adversely affected. Secondly, the model predicts the softening behavior commonly observed in soils under repeated cyclic loadings (shake down phenomena).

The generalized model was once again verified. The verification was made against two independent sets of test data and the prediction of a few other well-accepted constitutive models. The simple strain-space model not only gives simpler solutions but also predicts the experimental observations more closely than other models.

Finally, the model was generalized to three-dimensional stress-strain states. The stress and strain tensors were defined from the basics along the lines of nonlinear elasticity. The concept of effective stresses was presented mathematically and the model was generalized in a simple manner within the framework of these definitions. The generalized model was then tested by using it to solve the problem of an expanding cylindrical cavity. The model prediction was compared with two other predictions, with a linear elastic solution and with some data obtained from pile tests. The prediction of the simple model agrees qualitatively quite well with the other models. A quantitative comparison is not possible because of insufficient data on the materials used in the other predictions. However, all the

predictions are for normally consolidated clays. The pile test data are also predicted quite well by the model.

In summary, a simple model to predict the constitutive behavior of wet clay has been developed herein. The model is sufficiently general to handle any loading and has been tested for validity against experimental data. In order to use the model, the numerical values of three common material constants, λ, K and M are necessary. These constants are obtained from a simple undrained or constant pressure shear test and from a one- or two-dimensional consolidation test. Such straightforward derivation of the constants renders the model very attractive in solving engineering problems.

In the strain-space formulation the undrained problems turn out to be a simple case. The stress under general circumstances depends upon the current void ratio, shear strain and a memory variable. When the deformation takes place under undrained conditions, one of the three independent variables, namely, the void ratio, remains constant and hence the problem is greatly simplified. Most clays have permeabilities of the order of 10^{-8} cm/sec. The normal head gradients are of order 1 m/m, thus resulting in pore fluid flow rates of the order of 10^{-8} cm/sec. For soil deformations that take place at rates of a few orders of magnitude higher than this value, the deformation is well approximated by an undrained deformation. For this reason, the undrained deformation assumption is quite common for transient solutions. The final steady-state solution will, of course, depend upon the drainage properties and must be solved in all its generality. The

problem of the pore pressure diffusion subsequent to the initial expansion of the cylindrical cavity is currently under investigation. The only solution currently available (Randalph and Wroth, 1979)for this diffusion problem is based on linear elasticity theory.

If it is desired to improve the accuracy of the model, a few simple changes may be made. However, a word of caution is in order here. It is not desirable to demand high accuracies from a model until the input constants can be determined to the same or slightly higher accuracy. With the current state of experimental technology, it is believed that the model is sufficiently accurate as it is. Nevertheless, the accuracy can be improved by taking more terms for the hardening functions given in equation (3.14) or for the shear stress response function given in equation (3.26). At this stage only a single term approximation is used in both cases.

Another place for improvement is in the load reversal formulation. Some experiments indicate that the shear stress-shear strain relationships do not remain symmetric when loading is applied in opposite directions, from an isotropically consolidated state. Such a behavior can be incorporated into the model by defining two values for the critical state constant M. One value corresponds to tensile loading; the other corresponds to compressive loading. In the current model these are taken to be equal.

The model can now be applied to solve any problem involving wet clays. It is only through such repeated applications and the subsequent analysis of the solutions that the advantages of this model can be

established. The model has been formulated with simplicity in mind. From the starting point of determining the material constants to the end of obtaining the solution, the model has been kept as simple and as accurate as possible, thereby making its usage straightforward.

REFERENCES

Biot, M.A., and D.J. Willis, "The elastic coefficients of the theory of consolidation," Journal of Applied Mechanics, Vol. 24, p. 594, 1957.

Bjerrum, L., and I. Johannessen, "Pore pressure resulting from driving piles in soft clay," in Pore Pressure and Suction in Soil, Butterworth, London, 1961.

Brace, W.F., and R.J. Martin III, "A test of effective stress law for crystalline rocks of low porosity," International Journal of Rock Mechanics and Mineral Science, Vol. 5, p. 415, 1968.

Burland, J.B., "The yielding and dilatation of clay," correspondence, Geotechnique, Vol. 15, pp. 211-214, 1965.

Burland, J.B., "Deformation of soft clay," Ph.D. Thesis, Cambridge, 1967.

Casey, J., and P.M. Naghdi, "On the characterization of strain hardening plasticity," Journal of Applied Mechanics, Vol. 48, pp. 285-296, June 1981.

Casey, J., and P.M. Naghdi, "Strain hardening response of elastic plastic materials," Mechanics of Engineering Materials, Eds. C. Desai and R.H. Gallagher, John Wiley and Sons Ltd., 1984.

Dafalias, Y.F., and E.P. Popov, "Plastic internal variable formalism of cyclic plasticity," Journal of Applied Mechanics, Vol. 98(4), pp. 645-650, 1976.

Dafalias, Y.F., and L.R. Herrmann, "A bounding surface soil plasticity model," Proceedings of the International Symposium on Soils under Cyclic and Transient Loadings, Swansea, pp. 335-345, 1980.

Dafalias, Y.F., L.R. Herrmann, and J.S. DeNatale, "The bounding surface plasticity model for isotropic cohesive soils and its application at the Grenoble workshop, 1982," in press.

Davis, R.O., and G. Mullenger, "A rate type constitutive model for soil with a critical state," International Journal for Numerical and Analytical Methods in Geomechanics, Vol. 2, pp. 285-292, 1978.

Davis, R.O., and G. Mullenger, "Some simple boundary value problems for dilatant soil in undrained conditions," International Journal for Numerical and Analytical Methods in Geomechanics, March 1984.

DiMaggio, F.L., and I.S. Sandler, "Material model for granular soils," Journal of the Engineering Mechanics Division, ASCE, pp. 935-950, June 1971.

Garg, S.K., and A. Nur, "Effective stress laws for fluid-saturated porous rocks," Journal of Geophysical Research, Vol. 78, No. 26, pp. 5911-5921, Sept. 1973.

Geertsma, J., "The effect of fluid pressure decline on volumetric changes of porous rocks," Transactions of AIME, Vol. 210, p. 331, 1957.

Glossop, R., "The rise of geotechnology and its influence on engineering practise," Eighth Rankine Lecture, Geotechnique, Vol. 18, pp. 105-150, 1968.

Handin, J., R.V. Hager, Jr., M. Friedman, and J.N. Feather, "Experimental deformation of sedimentary rocks under confining pressure: pore pressure tests," Bulletin of the American Association of Petroleum Geologists, Vol. 47, p. 717, 1963.

Houlsby, G.T., C.P. Wroth, and D.M. Wood, "Prediction of the results of laboratory tests on a clay using a critical state model," International Workshop on Constitutive Behavior of Soils, Grenoble, Vol. 2, pp. 88-133, Sept. 1982.

Hvorslev, M.J., "On the physical properties of disturbed cohesive soils," Ingeniorvidenskabelige Skrifter, A., No. 45, p. 159, 1937.

Iwan, W.D, "On a class of models for the yielding behavior of continuous and composite systems," Journal of Applied Mechanics, ASME, Vol. 34, No. E3, pp. 612-617, Sept. 1967.

Iwan, W.D., and P.J. Yoder, "Computational aspects of strain-space plasticity," Journal of Engineering Mechanics Division, ASCE, Vol. 109, No. 1, pp. 231-243, Feb. 1983.

Ko, H.Y., "Static stress-deformation characteristics of sand," Ph.D. Thesis, California Institute of Technology, 1966.

Koizumi, Y., and K. Ito, "Field tests with regard to pile driving and bearing capacity of piled foundations," Soils and Foundations (Japan), Vol. 7, No. 3, 1967.

Ladanyi, B., "Expansion of a cavity in a saturated clay medium," Journal of the Soil Mechanics and Foundations Division, Proceedings of ASCE, Vol. 89, No. SM4, pp. 127-161, July 1963.

Lade, P.V., "Elastoplastic stress-strain theory for cohesionless soil," Journal of the Geotechnical Engineering Division, Proceedings of ASCE, Vol. 101, pp. 1037-1053, Oct. 1975.

Lade, P.V., "Elastoplastic stress-strain theory for cohesionless soil with curved yield surfaces," International Journal of Solids and Structures, Vol. 13, pp. 1019-1035, 1977.

Lo, K.Y., and A.G. Stermac, "Induced pore pressures during pile driving operations," Proceedings of the 6th International Conference on Soil Mechanics and Foundation Engineering, Montreal, Vol. 2, 1965.

London, P.A., "Some deformation characteristics of Kaolin," Ph.D. Thesis, Cambridge University, 1967.

Mroz, Z., and V.A. Norris, "Elastoplastic and viscoplastic constitutive models for soils with applications to cyclic loading," Soil Mechanics - Transient and Cyclic Loads, Eds. G.N. Pande, and O.C. Zienkiewicz, John Wiley & Sons, 1982.

Murrell, S.A.F., "A criterion for brittle fractures of rock and concrete under triaxial stress, and the effect of pore pressure on the criterion," in Rock Mechanics, Ed. C. Fairhurst, p. 563, Pergamon, New York, 1963.

Nur, A., and J.D. Byerlee, "An exact effective stress law for elastic deformation of rock with fluids," Journal of Geophysical Research, Vol. 76, p. 6414, 1971.

Naghdi, P.M., and J.A. Trapp, "The significance of formulating plasticity theory with reference to loading surfaces in strain space," International Journal of Engineering Science, Vol. 13, No. 9/10, pp. 785-797, Sept./Oct., 1975.

Pender, M.J., "A model for the behaviour of overconsolidated soil," Geotechnique, Vol. 28, No. 1, pp. 1-25, 1978.

Prevost, J.H., "Plasticity theory for soil stress-strain behaviour," ASCE, Journal of The Engineering Mechanics Division, pp. 1177-1194, October 1978.

Randalph M.F., and C.P. Wroth, "An analytical solution for the consolidation around a driven pile," International Journal for Numerical and Analytical Methods in Geomechanics, Vol. 3, pp. 217-229, 1979.

Robinson, L.H., Jr., "The effect of pore pressure and confining pressure on the failure process in sedimentary rock," Colorado School of Mines Quarterly, Vol. 54, p. 177, 1959.

Roscoe, K.H., A.N. Schofield, and C.P. Wroth, "On the yielding of soils," Geotechnique, Vol. 9, pp. 22-53, 1958.

Roscoe, K.H., and H.B. Poorooshasb, "A theoretical and experimental study of strains in triaxial compression tests on normally consolidated clays," Geotechnique, Vol. 13, pp. 12-38, 1963.

Roscoe, K.H., A.N. Schofield, and A. Thurairajah, "Yielding of clays in states wetter than critical," Geotechnique, Vol. 13, pp. 211-240, 1963.

Roscoe, K.H., and J.B. Burland, "On the generalised stress-strain behaviour of wet clay," Engineering Plasticity, Eds. J. Heyman and F.A. Leckie, Cambridge University Press, 1968.

Skempton, A.W., "Effective stress in soils, concrete and rock," in Conference on Pore Pressure and Suction in Soils, pp. 4-16, Butterworth, London, 1961.

Suklje, L., "Rheological aspects of soil mechanics," Interscience, New York, p. 123, 1969.

Terzaghi, K., "Die berechnung der durchlassigkeitsziffer des tones aus dem verlauf der hydrodynamischen spannungserscheinungen," Sitzungsber. Akad. Wiss. Wien, Vol. 132, p. 125, 1923.

Thurairajah, A., "Some shear properties of Kaolin and of sand," Ph.D. Thesis, Cambridge University, 1961.

Valanis, K.C., and H.E. Read, "A new endochronic plasticity model for soils," Soil Mechanics - Transient and Cyclic Loads, Ed. G.N. Pande and O.C. Zienkiewicz, John Wiley and Sons Ltd., pp. 375-417, 1982.

Walker, A.F., "Stress-strain relationships for clay," Ph.D. Thesis, Cambridge University, 1965.

Yoder, P.J., "A strain-space plasticity theory and numerical implementation," Ph.D. Thesis, California Institute of Technology, 1981.

Yoder, P.J., and W.D. Iwan, "On the formulation of strain-space plasticity with multiple loading surfaces," Journal of Applied Mechanics, Vol. 48, pp. 773-778, December 1981.

BIBLIOGRAPHY

Fung, Y.C., Foundations of solid mechanics, Prentice Hall, 1965.

Hill, R., The mathematical theory of plasticity, Oxford University Press, 1956.

Knowles, J.K., "Mathematical elasticity theory," class notes, California Institute of Technology, 1981.

Knowles, J.K., and E. Sternberg, "Advanced mathematical elasticity theory," class notes, California Institute of Technology, 1984.

Prager, W., "Recent developments in mathematical theory of plasticity," Journal of Applied Physics, Vol. 20, No. 3, pp. 235-241, March 1949.

Prager, W., An introduction to plasticity, Addison Wesley, 1959.

Scott, R.F., Principles of soil mechanics, Addison Wesley, 1963.

Scott, R.F., and J.J. Schoustra, Soil: mechanics and engineering, McGraw Hill, 1968.

Scott, R.F., "Soil mechanics," class notes, California Institute of Technology, 1982-84.

Sokolnikoff, I.S., Mathematical theory of elasticity, McGraw Hill, 1946.